A Model for Predicting the Fatigue Life of Functionally Graded Additively Manufactured Metal Components

Un modèle pour prédire la durée de vie à la fatigue des composants métalliques à gradation fonctionnelle fabriqués de manière additive.

A Thesis Submitted to the Division of Graduate Studies
of the Royal Military College of Canada
by

Francis Pantuso, CD, MEng, rmc
Captain

In Partial Fulfillment of the Requirements for the Degree of
Master of Applied Science in Aeronautical Engineering.

May, 2023

© This thesis may be used within the Department of National Defence but
Copyright for open publication remains the property of the Author.

Abstract

A model of the crack initiation and life of a functionally graded material using additive manufacturing is developed using conventional fatigue-life analysis. A specimen geometry, an additive manufacturing process, materials, and loadings are selected. A review of literature provides data to permit the development of a fatigue model. A framework is presented on how to link the design of a specimen to the predicted fatigue performance. Functional gradings of material properties are specified by mapping a potential function to crack growth rates of two materials and interpolating between the crack growth rates to estimate the properties of the graded material. A Matlab application was created that implemented the developed fatigue model to reduce iteration time for the purposes of this thesis. The application was verified by comparing results to manual calculation and those obtained from commercial software. A case of a specimen with functionally graded Ti-6Al-4V alpha laths is analyzed. It was estimated that the crack growth life of the designed specimen with a functional grading of Ti-6Al-4V alpha lath size could be increased by 3% at a maximum gross stress of 400 MPa, by 18% at a maximum gross stress of 350 MPa, by 46% at a maximum gross stress of 300 MPa, by 93% at a maximum gross stress of 250 MPa, and by 138% at a maximum gross stress of 200 MPa. A second case is analyzed, where an ungraded 7075-T6 specimen is compared to a replacement specimen that is functionally graded from Ti-6Al-4V to 7075-T6 aluminium. It was estimated that the total fatigue life could be increased by approximately two to three orders of magnitude for a range of maximum gross stresses between 100-300 MPa. Several additional examples were presented on how the developed fatigue model and Matlab application could be improved. The results demonstrated that total fatigue life of functionally graded, additively manufactured materials can be modelled without the use of finite element analysis software, assuming a stress intensity solution is available for the geometry.

Un modèle d'initiation de fissure et de durée de vie d'un matériau à gradation fonctionnelle utilisant la fabrication additive est développé à l'aide d'une analyse conventionnelle de la fatigue et de la durée de vie. Une géométrie d'échantillon, un processus de fabrication additive, des matériaux et des charges sont sélectionnés. Une revue de la littérature fournit des données permettant le développement d'un modèle de fatigue. Un cadre est présenté sur la façon de lier la conception d'un spécimen à la performance de fatigue prévue. Les gradations fonctionnelles des propriétés des matériaux sont spécifiées en mettant en correspondance une fonction potentielle avec les taux de croissance des fissures de deux matériaux et en interpolant entre les taux de croissance des fissures pour estimer les propriétés du matériau gradé. Une application Matlab a été créée pour mettre en œuvre le modèle de fatigue développé afin de réduire le temps d'itération dans le cadre de cette thèse. L'application a été vérifiée en comparant les résultats aux calculs manuels et à ceux obtenus à l'aide de logiciels commerciaux. Le cas d'un spécimen avec des lattes alpha en Ti-6Al-4V à gradation fonctionnelle est analysé. Il a été estimé que la durée de vie de la croissance des fissures de l'échantillon conçu avec un classement fonctionnel de la taille des lattes de Ti-6Al-4V alpha pouvait être augmentée de 3% à une contrainte brute maximale de 400 MPa, de 18% à une contrainte brute maximale de 350 MPa, de 46% à une contrainte brute maximale de 300 MPa, de 93% à une contrainte brute maximale de 250 MPa et de 138% à une contrainte brute maximale de 200 MPa.

Un deuxième cas est analysé, dans lequel un échantillon 7075-T6 non calibré est comparé à un échantillon de remplacement fonctionnellement calibré de Ti-6Al-4V à l'aluminium 7075-T6. Il a été estimé que la durée de vie totale en fatigue pouvait être augmentée d'environ deux à trois ordres de grandeur pour une gamme de contraintes brutes maximales comprises entre 100 et 300 MPa. Plusieurs exemples supplémentaires ont été présentés sur la manière dont le modèle de fatigue développé et l'application Matlab pourraient être améliorés. Les résultats ont démontré que la durée de vie totale en fatigue des matériaux à gradation fonctionnelle fabriqués de manière additive peut être modélisée sans l'utilisation d'un logiciel d'analyse par éléments finis, en supposant qu'une solution d'intensité de contrainte soit disponible pour la géométrie.

Acknowledgments

To my thesis advisors Dr. Diane Wowk and Dr. David DuQuesnay, thank you for your support, mentorship, and guidance throughout this research. Your many insights and questions contributed greatly to enhancing my understanding and enriching this wonderful academic journey.

To Mr. Yvan Caron, the program champion from the Director of Technical Airworthiness and Engineering Support (DTAES), thank you for supporting a deviation from the typical academic program to afford me the opportunity to conduct this research. Without your support this thesis would not have been possible.

To Mr. Brendan Freeman, the RMC Machine Shop Supervisor, and the entire Machine Shop team, thank you for the numerous hours of support providing feedback on my ideas, helping with equipment, and for being available to work through problems with me.

Finally, thank you to the Canadian Armed Forces for supporting and funding my academic endeavours in additive manufacturing for almost five years. These opportunities have greatly enhanced my engineering knowledge and development as a military officer.

Table of Contents

List of Tables

List of Figures

List of Acronyms

AM	additive manufacturing
BCC	body-centered cubic
CT	compact tension
DED	directed energy deposition
EBM	Electron Beam Melting
E-PBF	electron beam powder bed fusion
FEA	finite element analysis
FGM(s)	functionally graded material(s)
HCP	hexagonal close packed
HIP	hot-isostatic pressing
L-PBF	laser powder bed fusion
PBF	powder bed fusion
PSPP	Process-Structure-Properties-Performance
RCAF	Royal Canadian Air Force
RMC	Royal Military College of Canada
SF	speed function
SMART	Separating Morphing and Adaptive Remeshing Technology
SWT	Smith-Watson-Topper
UMM	unstructured mesh method
VED	volumetric energy density
XFEM	extended finite element method

Nomenclature

a	crack length
b	fatigue strength exponent
c	fatigue ductility exponent
d	specimen hole diameter
h	hatch spacing
m	Paris exponent
q	fatigue notch sensitivity
r	specimen hole radius
v	scan speed
C	Paris coefficient
D	depth of an elliptical notch
E	elastic (Young's) Modulus
I	beam current
K	stress intensity
ΔK	stress intensity range
L	layer thickness
L	length of grading
N	fatigue cycles
P	value of potential function
R	stress ratio
S	applied stress
V	beam voltage
W	specimen gross width
Y	geometry parameter
ε	strain
ρ	notch root radius
σ	stress
n'	cyclic strain hardening exponent
K'	cyclic strength coefficient
a_0	initial crack length
l_t	transition crack length
F_N	geometry parameter adjustment for specimen of finite width
K_f	fatigue notch factor
K_{tn}	net section stress concentration factor
N_f	cycles to failure
$2N_f$	reversals to failure
N_g	cycles from crack initiation to fracture
N_i	cycles to initiate a crack
N_{total}	total cycles to failure
ε_f'	fatigue ductility coefficient
σ_f'	fatigue strength coefficient
ε_a	strain amplitude
ε_e	elastic strain
ε_p	plastic strain
σ_{max}	maximum applied stress
$\sigma_{nocthed}$	notched specimen stress
$\sigma_{unnocthed}$	unnotched specimen stress
φ_N	geometry parameter for specimen of infinite width

1. Introduction

The invention of additive manufacturing technologies has afforded new possibilities for advanced engineered materials. The layer-by-layer buildup of material offers the opportunity to manufacture materials and geometries unattainable through conventional manufacturing methods. A material created by the localized control of properties is called a functionally graded material (FGM), a term first described in 1984 by a team in Japan [1]. Functionally graded materials are similar to conventional composites but are distinct as properties can vary within the entire volume of the component and are not limited to discrete material boundaries. The localized control of material properties within a complex geometry is a unique blend of the two capabilities whereby a functional grading design may only be possible using additive manufacturing.

State-of-the-art fatigue analysis has progressed towards the use of finite element analysis (FEA) to predict total fatigue life. The increasing complexity and capabilities of FEA software makes it difficult for engineers and designers to understand the inherent assumptions that are built into software by the software developers. This has sometimes led to an overconfidence in the results of FEA software resulting in disastrous structural failures, like the collapse of the Hartford Civic Center (XL Centre) roof in 1978 [2]. Specific to the application of functionally graded components, the most current methods using FEA software requires writing custom scripts that are implemented in an ad-hoc fashion [3]. This approach can often increase the complexity and analysis time for results, while also limiting availability to those with the necessary coding knowledge. The goal of this research is to design a model for estimating the total fatigue life of functionally graded, additively manufactured components without custom scripting in FEA software. The vision is that any engineer or designer with a basic understanding of additive manufacturing technology and conventional fatigue analysis could apply the developed model. By this approach a user can understand all underlying assumptions associated with results and reduce the effort required to analyze the fatigue life of functionally graded components.

A functional grading emanating from a notch in a specimen allows a designer to specify material properties that increase component fatigue life from crack initiation to crack growth. The practical significance of this capability is that conventional components may be replaced with functionally graded components, achieving greater fatigue life than the original, while maintaining the same form and function. Similarly, new components could be designed that outperform ungraded components. In both cases the maintenance burdens; e.g., time between replacement and inspection requirements, are reduced resulting in a cost savings and an increase in operational availability of the system.

As a member of the Royal Canadian Air Force (RCAF), selection of an AM process and feedstock material with foreseeable applications in aerospace was carefully considered. The design of custom replacement aerospace components with improved fatigue resistance using functionally graded additive manufacturing supports the Sustain function of the RCAF as outlined in Royal Canadian Air Force Doctrine [4]. By replacement of components with greater fatigue resistance the RCAF could operate aircraft for longer periods without maintenance or logistical support. This would increase available flying hours during operations, while reducing the costs associated with managing supply and

repairs in the field. Additionally, the longer service life of the improved components would require less stock compared to that required for conventional components. The use of additive manufacturing is also a cost savings opportunity for small runs of parts compared to retooling or establishing a manufacturing line for a run of conventionally manufactured components. This research demonstrates a fatigue model for analyzing engineered components of improved total fatigue life with the intent of realizing these opportunities.

The developed fatigue model was integrated into a Matlab application strictly for the purposes of design studies and iteration while doing research for this thesis. This step is neither necessary nor linked to the results of using the fatigue model, as demonstrated by comparison to the commercially available fatigue life analysis software AFGROW. It could be argued that the coding of the Matlab application could have been created as a subroutine for FEA software like Ansys. This research is tailored to accessibility of the model rather than detailed analysis and results. The developed model is, therefore, best suited for preliminary design studies and academic exercises with results demonstrating design potential rather than detailed estimates of component performance. To move from preliminary design to a detailed design phase the use of FEA or other advanced modelling techniques would be necessary. Nonetheless, the developed model provides a simple method for analyzing and predicting the fatigue performance of functionally graded additively manufactured metal components.

2. Literature Review

2.1. Additive Manufacturing

According to ISO/ASTM 52900 [5], additive manufacturing (AM) is defined as the “process of joining materials to make parts from 3D model data, usually layer upon layer, as opposed to subtractive manufacturing and formative manufacturing methodologies” The ISO/ASTM 52900 standard groups all current and future AM processes into seven categories: material extrusion, binder jetting, sheet lamination, directed energy deposition (DED), material jetting, vat polymerization, and powder bed fusion (PBF). The use of standardized terminology and groupings is important as it avoids confusion in communication, particularly when considering corporations often assign trademarked names for their individual processes when their technology fits within those defined by the ISO/ASTM 52900 standard. Terminology within this thesis will conform to the ISO/ASTM 52900 standard for clarity. Additionally, one AM process, electron beam powder bed fusion, is selected as the primary example for analyzing the fatigue life of a functionally graded component. The analysis method developed for this example was designed so that any other AM process or feedstock material could be analyzed using the same method. This is important because extensions from the primary example case are also presented in this thesis using other combinations of AM technology and material.

For conventional materials, physical properties like strength, hardness, ductility, fracture toughness and fatigue life are typically determined by experimentation using bulk material specimens. Results are therefore a statistical representation of physical properties that may be achieved and provide a basis of comparison between stocks of material. Unfortunately, the lack of current standards for manufacturing, testing, and evaluation of parts made by additive manufacturing complicates comparison. This challenge is exacerbated when bulk properties are no longer applicable in the case of functionally graded materials. The path forward has therefore been to invest in the development of standard practices, led largely by the ASTM Committee F42 on Additive Manufacturing Technologies [6], along with international efforts to test, evaluate, and certify additive machines, processes, and materials. Until such time that international standards are established current adopters of additive technologies must define their own standard for testing, modelling, and analyzing additive manufactured components.

2.2. Electron Beam Powder Bed Fusion (E-PBF)

Electron Beam Powder Bed Fusion (E-PBF) is an additive process where an electron beam is directed at a surface of powdered material feedstock. The material is melted by the thermal energy transferred to the powder from the impact of electrons on the surface. Solidified components result from natural cooling in the build environment during and after processing. The process was developed by Arcam AB (a subsidiary of General Electric) [7] and is known in the industry as Electron Beam Melting (EBM). Electron beam additive processes are typically used in the manufacturing of metal components. A schematic of a typical E-PBF machine is shown in Figure 1. A metal filament, typically made of tungsten, is supplied with input power that supports the emission of electrons in a continuous beam. The beam is controlled in a manner synonymous to electro-optics by

passing the beam through a series of focussing and deflection coils. The coils are supplied with an electrical current that generates a magnetic field which affects the beam properties. By actively controlling the currents to the filament, focussing, and deflection coils, the beam power, surface scanning speed, and the scanning pattern are controlled. An electron beam melting machine operates under a vacuum to reduce the scatter of the electrons and to prevent undesirable chemical interactions from occurring during processing. An image of a typical E-PBF machine is shown in Figure 2.

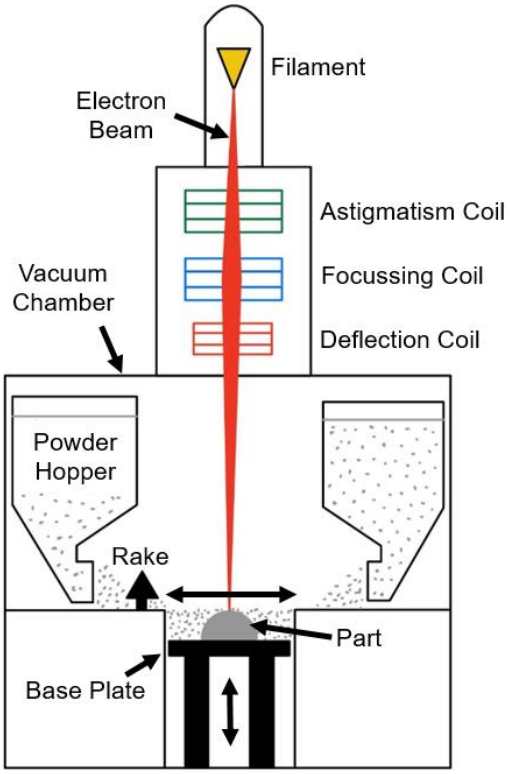

Figure 1. Schematic of an electron beam melting machine.

Figure 2. "Arcam A2" by William Sames, licenced under CC-BY-SA-4.0 [8].

A manufacturing cycle for a single layer occurs in four steps, as shown in Figure 3. Firstly, a thin layer of powder feedstock is spread over the current layer by use of a rake that gathers powder from feedstock hoppers. The layer is then preheated by a rapid pass of the electron beam over an area larger than the required layer pattern (layer slice). The preheating significantly reduces the electron beam power requirements for melting the material. The electron beam is then scanned across the layer surface in a predetermined pattern according to algorithms in the slicing software. The impact of the electrons on the powder particles generates the heat required to create a pool of molten metal. The solidification of the layer occurs by natural cooling in the machine during processing. Finally, the build plate is lowered by the predetermined layer height and the manufacturing cycle resumes for the next layer. Upon completion of all layers, the machine is allowed to cool and the part is removed for post processing. Minimum post-processing steps include removal of excess powder and support material to reveal the final part.

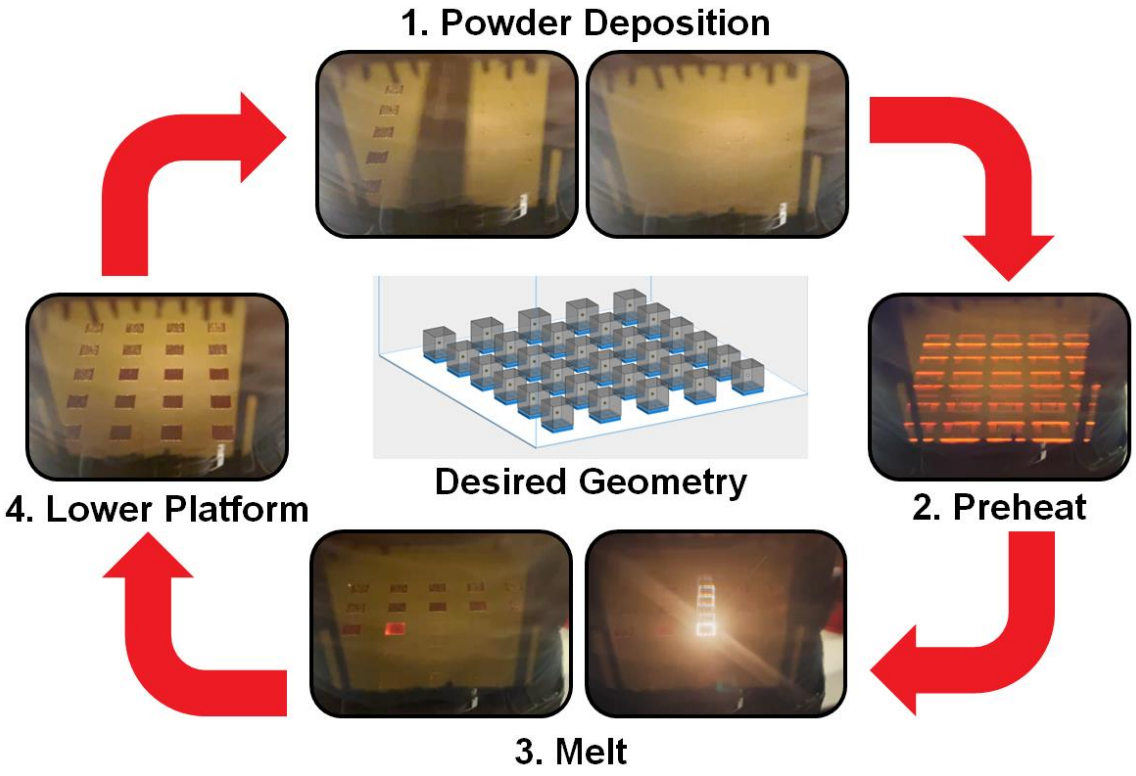

Figure 3. Electron Beam Melting processing cycle.

2.3. E-PBF Process Parameters

The effects of variations in the electron beam parameters are described in a convenient formulation known as the Volumetric Energy Density (VED) written as:

$$VED = \frac{IV}{vhL} \tag{1}$$

Where I is the current, V is the voltage of the electron beam, v is the scan speed of electron beam, h is the hatch spacing between scans of the electron beam, and L is the layer thickness. Volumetric energy density is typically specified in units of J/mm^3. A visual representation of the VED relationship is shown in Figure 4. VED does not fully characterize the transfer of energy into the powder material during processing. Another key parameter is the focus offset. The focus offset is controlled by the focussing coil of the E-PBF machine and sets the spot size of the electron beam on the powder bed surface. As the focussing coil current in increased, the focus offset increases and so too does the spot size. For a given beam power the focus offset adjusts the distribution of the electron beam within the powder bed. Representative examples of a small, moderate, and large focus offset for a gaussian irradiance electron beam are shown in Figure 5. Although other beam modes like the flat-top (top-hat) may be used, the gaussian beam remains a common mode for E-PBF.

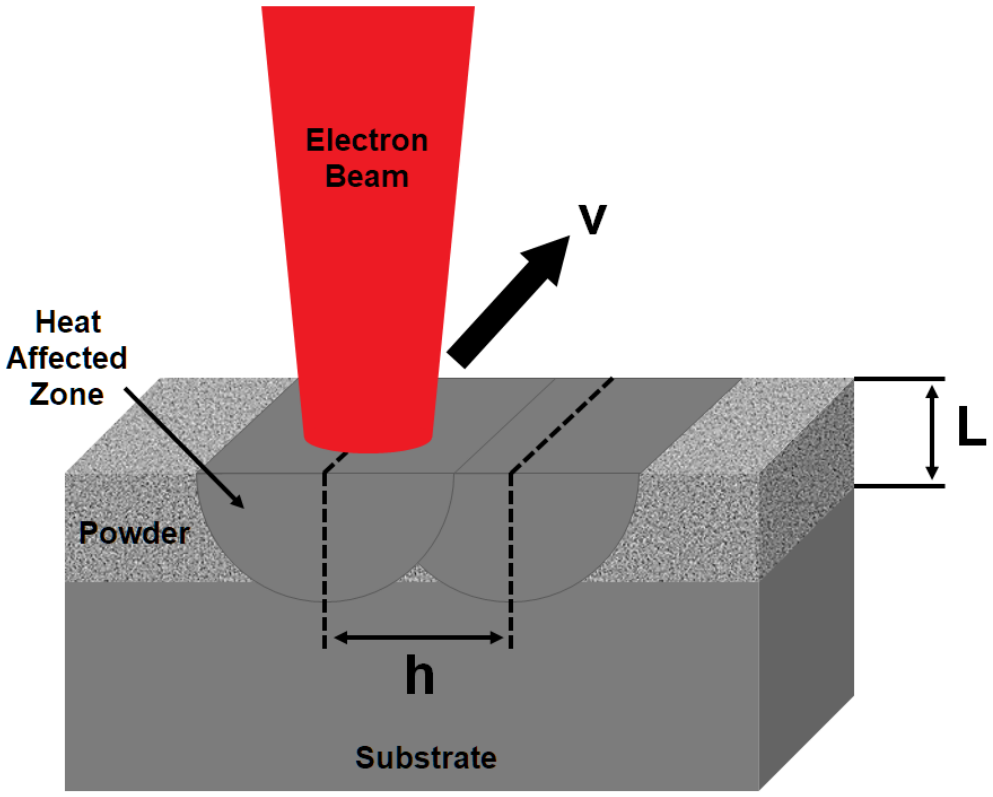

Figure 4. Definition of volumetric energy density.

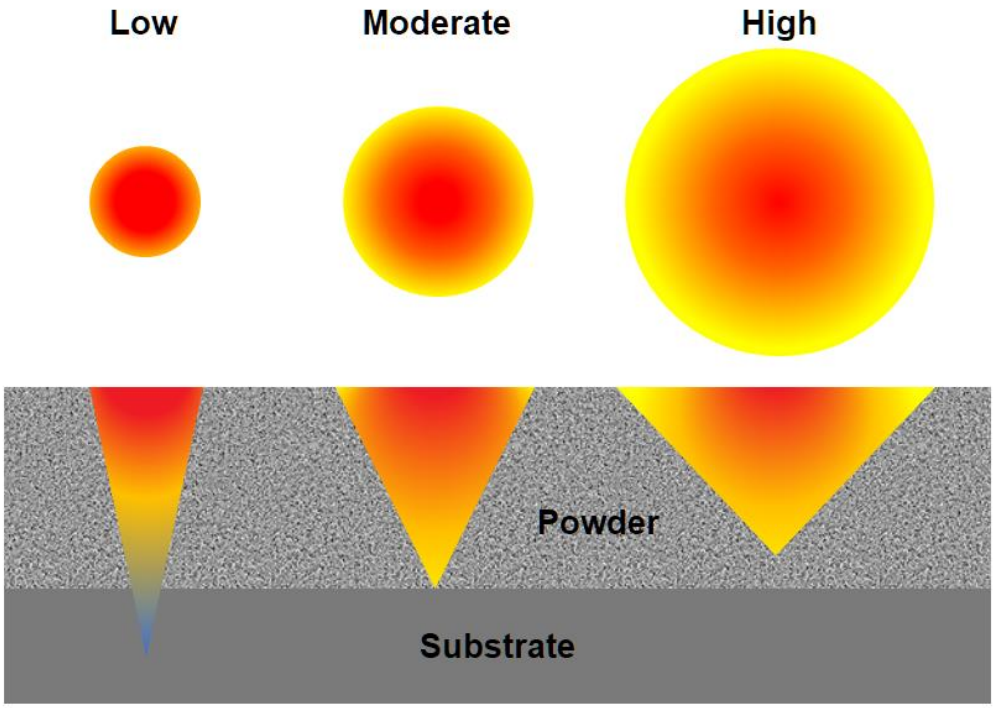

Figure 5. Focus offset effect on gaussian mode electron beam. The distribution of energy is indicated by the colour of the beam with orange being greatest energy, yellow moderate, and blue lowest.

The variables within the VED relationship and the focus offset are important process parameters because they are controlled by the input settings of the E-PBF machine. The heating and cooling rates, melt pool dynamics, and properties of the solidified material are therefore directly related to the input parameters.

2.4. E-PBF Ti-6Al-4V Processing Window

Regarding current E-PBF machines, most notably those manufactured by the largest manufacturer Arcam (General Electric), machine parameters are defined by algorithms proprietary to the manufacturer. Specifically, Arcam EBM machines use build themes that are preprogrammed into the machine and are applied for different use cases. A built-in speed function (SF) automatically adjusts the properties of the electron beam and the scanning speed to maintain acceptable melt pool characteristics. It is possible to provide user defined inputs for machine parameters on Arcam EBM machines, however this capability requires specific training and authorization from the manufacturer. At the date of writing of this thesis only one organization in Canada, the University of Waterloo, had the capability for manual input of their Arcam A2X EBM machine. This reality hampers the ability to investigate the impact of different process parameters on final properties of a component and the sensitivity of properties to each parameter by experimentation.

Fortunately, several studies on the optimization of E-PBF Ti-6Al-4V process parameters were found in the literature that estimated the processing windows for E-PBF Ti-6Al-4V.

Figure 6 to Figure 8 were created by outlining process windows using a dashed black line defined by surrounding the data generated through testing in each reference. Data points were extracted from each reference using the free software WebPlotDigitzer [9]. In all three studies the layer thickness L was 50 µm and the hatch spacing h was 100 µm. Kircher et al. [10] used an Arcam A2X machine across a range of beam currents and scanning speeds to develop a process window using beam current as the dependant variable (Figure 6). Pobel et al. [11] used an in-house developed machine called ATHENE [12] to develop a process window with the beam power as the dependant variable (Figure 7). Scharowsky et al. [13] used an ARCAM machine to develop a process window with VED as the dependant variable. Although all three references developed process windows in different ways, the VED relationship allows lines of equivalent volumetric energy density to be included in each plot to permit comparison. The coloured lines of equivalent VED in Figure 6 to Figure 8 were plotted manually to fit within all three estimated process windows. Reviewing the estimated process windows, discrepancies appear to exist across the three experiments. Possible explanations for the discrepancies are the use of different machines in the manufacturing of test specimens, different specimen geometries, stochastic variabilities, and the lack of identification of the focus offset setting in two of the three cases. Additionally, there are other process parameters like shape of the beam, the locations of the specimens in the build plate, and preheating settings that were not provided in each reference. The process windows, however, do generally agree on acceptable process settings for E-PBF Ti-6Al-4V. From this analysis, it was assumed that any parameter settings that were within all three process windows would result in components without significant flaws following manufacturing.

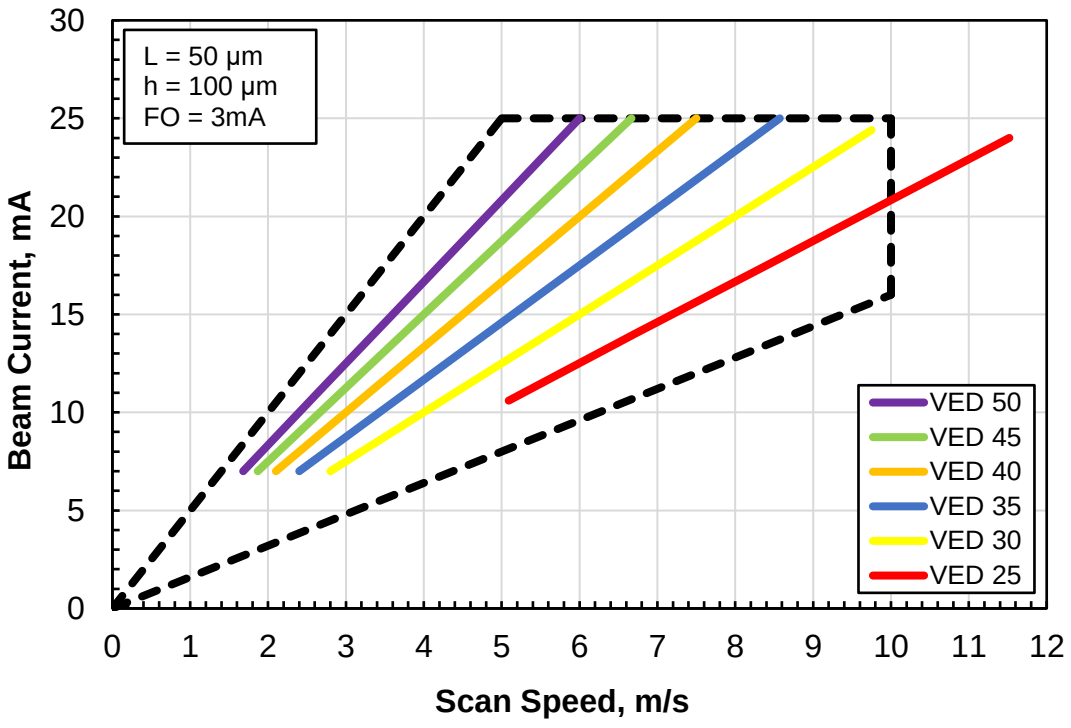

Figure 6. E-PBF Ti-6Al-4V process window by beam current. Adapted from [10].

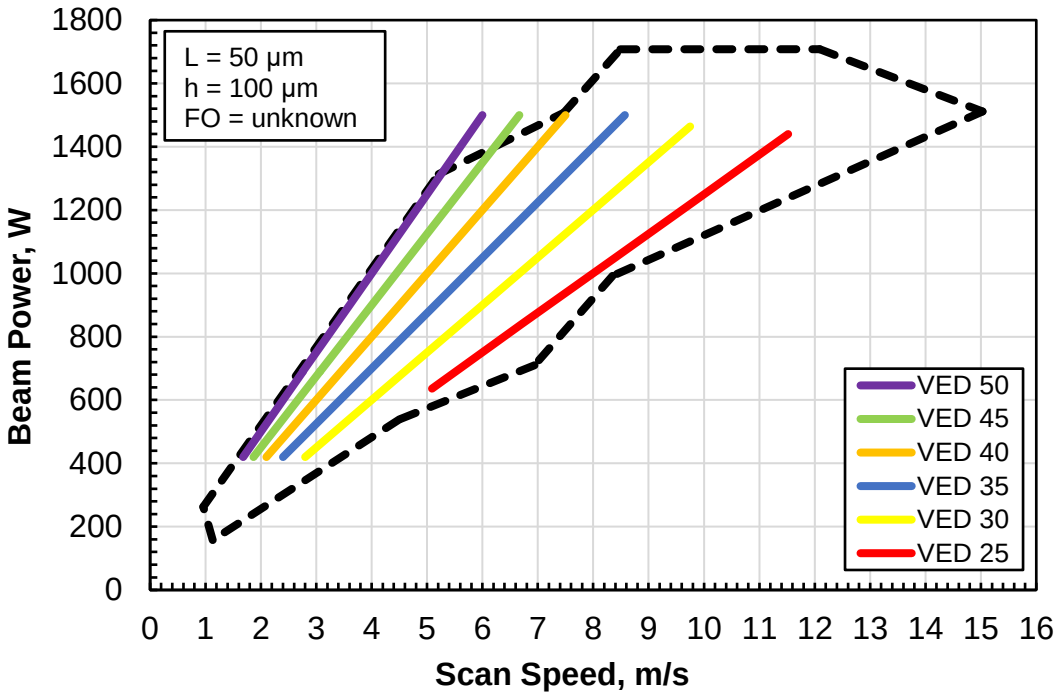

Figure 7. E-PBF Ti-6Al-4V process window by beam power. Adapted from [11].

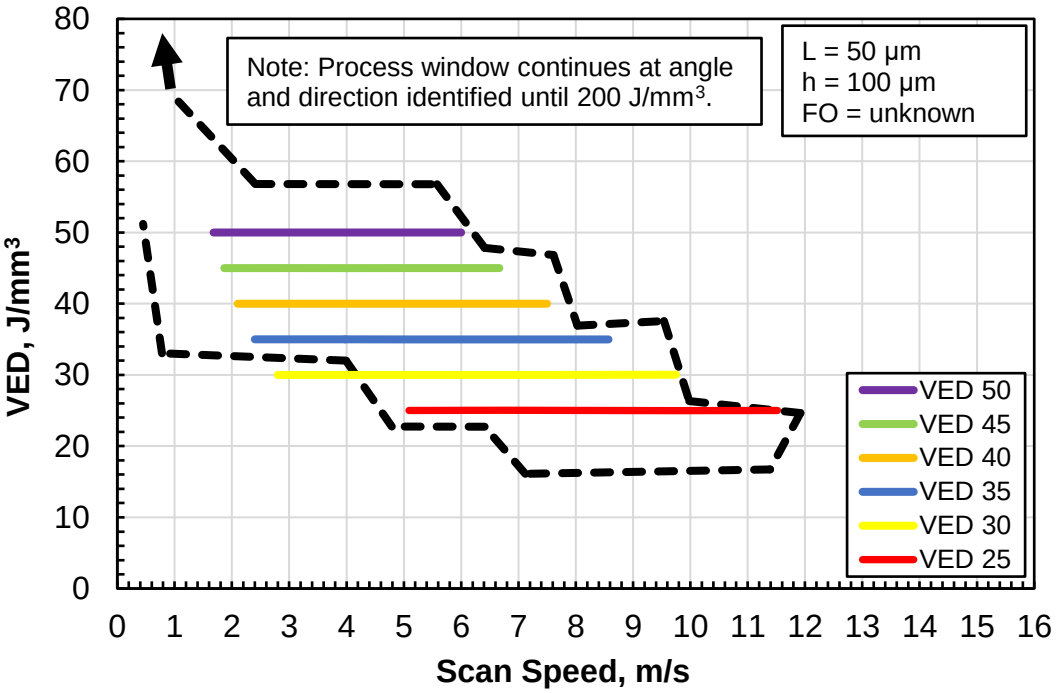

Figure 8. E-PBF Ti-6Al-4V process window by VED. Adapted from [13].

2.5. E-PBF Ti-6Al-4V Microstructure

The Ti-6Al-4V alloy typically exists in two distinct unit cell crystal structures or phases. The alpha phase is characterized by a hexagonal close packed (HCP) crystal structure and the beta phase by the body-centered cubic (BCC) crystal structure. The general microstructure of E-PBF Ti-6Al-4V has been observed to take a relatively consistent form following processing. From preheating at approximately 650 °C, the material is heated above the beta transus temperature of approximately 980 °C by passing of the electron beam. The melt pool is then subsequently cooled in a vacuum environment. There exists partial reheating of lower layers as the build continues, however the temperature achieved near the heat affected zone of the current layer is below the temperature required to maintain a melt pool. Following processing, the build chamber must be returned to room temperature for removal of the specimens. From this heating cycle the microstructure of E-PBF Ti-6Al-4V is typically described as a Widmanstätten or basket weave or needle-like. A phase diagram for Ti-6Al-4V with the unit cells for the two phases and a depiction of the typical microstructure is shown in Figure 9. Although it is possible to obtain variations of the microstructure with post-process heat treatment, the E-PBF Ti-6Al-4V materials analyzed in this thesis were considered in the as-built condition. Additionally, the AM processing of Ti-6Al-4V introduces some anisotropy of the material due to the build direction and scanning pattern of the machine. To mitigate this challenge all material properties were considered for builds in the XY direction. Builds in the Z direction are provided for comparison purposes only and were omitted form analysis.

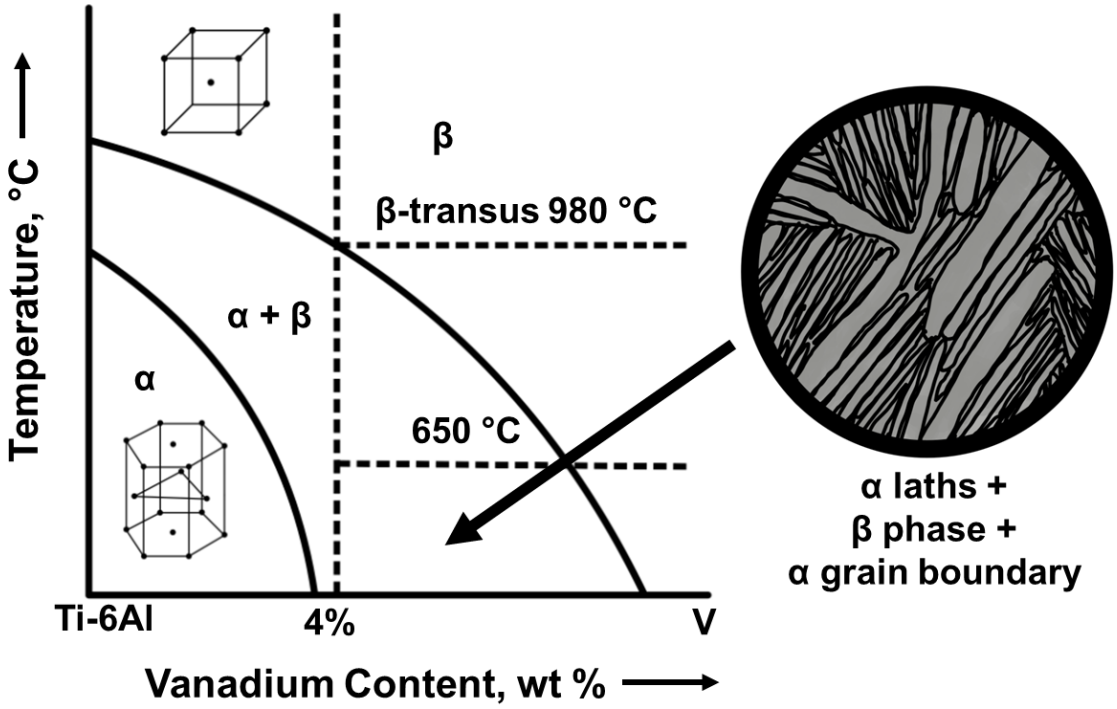

Figure 9. Typical microstructure of E-PBF Ti-6Al-4V with black representing the β phase and grey representing the α phase.

2.6. E-PBF Ti-6Al-4V Hall-Petch Relationship

It has been shown that the microstructure of metals is the main property from which performance of a material is derived. More accurately, the sizes of microstructural elements are generally inversely proportional to the strength and hardness of a material. The relationship between the size of microstructural grains and the hardness or strength of a material is known as the Hall-Petch Relationship. The Hall-Petch relationship predicts, for many common metals, that as the grain size decreases the yield strength of the material increases in proportion. This effect is generally true for the range of grain sizes above 1 nm, below which further decreasing the grain size decreases the yield strength in proportion. Establishing that the Hall-Petch relationship is true for E-PBF Ti-6Al-4V is critical to controlling the performance of a material by adjustment of the microstructure. A review of the literature revealed numerous references for material yield strength from tensile testing of standard specimens manufactured using E-PBF Ti-6Al-4V. It was noted during review of the literature that the methods for measuring the alpha lath size from micrographs was inconsistent as several different software programs with unknown setups were used. To improve the consistency in measurement of lath size, micrograph images from each reference were taken and evaluated using MIPAR Image Analysis Software [14]. For this reason, the alpha lath sizes estimated in each reference is likely to differ from those calculated in MIPAR. The yield strength data from each reference was extracted from a stress-strain curve using the free software WebPlotDigitizer [9] if it was not included in tabular form in the reference. The results are shown in Figure 10 with a fitted line so that the yield strength may be estimated for a given alpha lath size. It was not possible to include error bars for each data point from the information provided in the references. It is also important to recognize that significant scatter exists in the data. Nonetheless, for the range of grain sizes estimated using the micrograph images and the yield strength data from each reference, the Hall-Petch relationship is generally maintained for E-PBF Ti-6Al-4V.

Similarly, the alpha lath size can be related to the material hardness. A comparison to tested specimens and literature values by Sharma et al. [15] demonstrated good agreement with the Hall-Petch relationship for various condition of E-PBF Ti-6Al-4V. Testing and analysis by Wanjara et al. [16] for two different specifications of powder (virgin and recycled) revealed a similar relationship between E-PBF Ti-6Al-4V alpha lath size and Vickers hardness; the data was collected and plotted in Figure 11 using WebPlotDigitizer [9]. The results show that as the lath size decreases the hardness tends to increase in proportion.

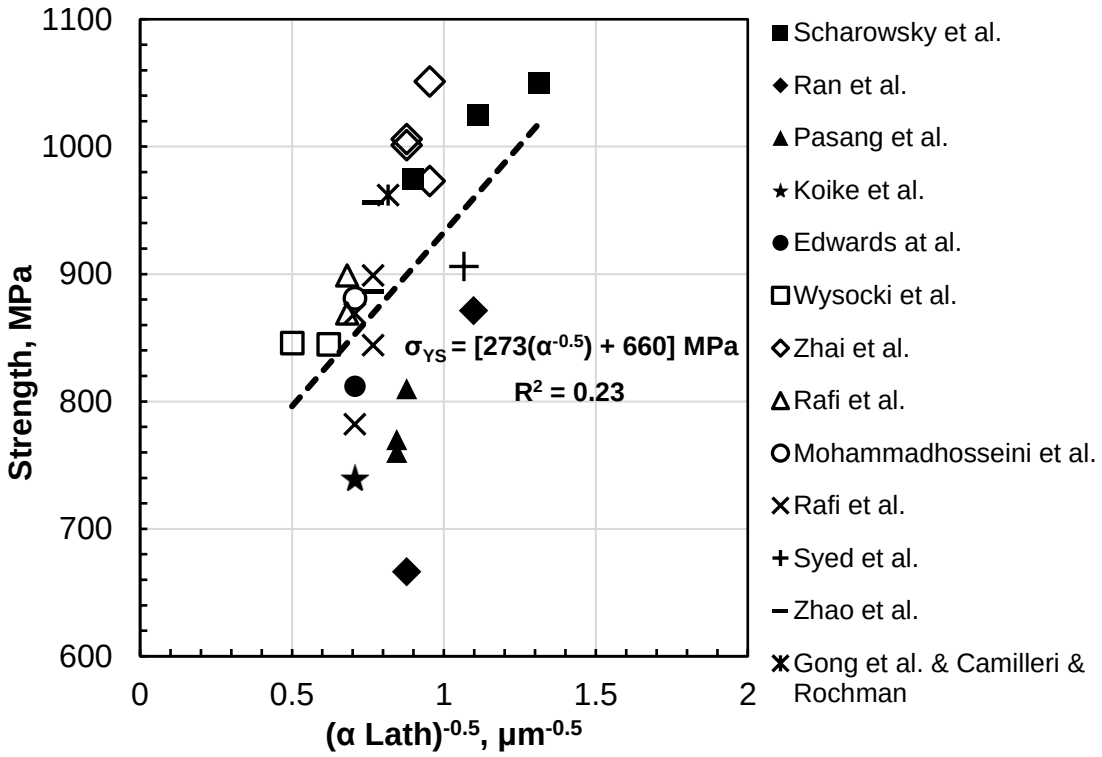

Figure 10. Hall-Petch relationship for E-PBF Ti-6Al-4V. Sources [13,17–29].

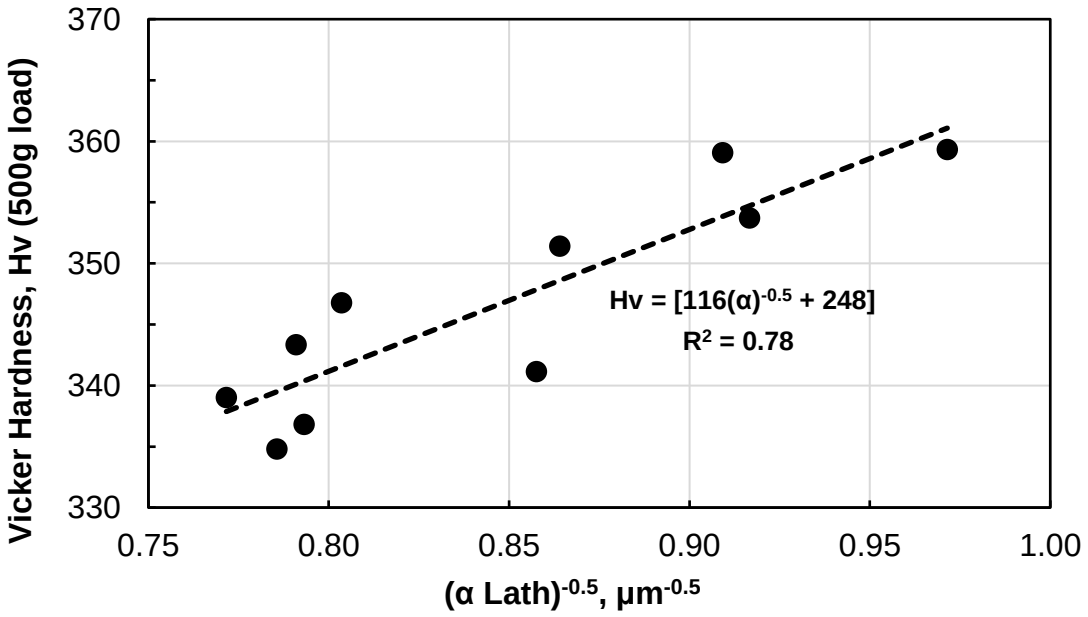

Figure 11. Relationship between alpha lath size and hardness for E-PBF Ti-6Al-4V. Source [16].

2.7. Crack Initiation of E-PBF Ti-6Al-4V

The fatigue cycles to initiate a crack is approached using a Strain-Life (ε-N) methodology for a notched geometry. The notch stress-strain relationship (notch response) may be determined by Neuber's rule outlined in Bannatine et al. [30] as:

$$\sigma\varepsilon = \frac{(K_t S)^2}{E} \tag{2}$$

where σ is the local notch stress, ε is the local notch strain, K_t is the notch stress concentration factor, S is the applied stress, and E is the elastic modulus of the material. The stress concentration factor is often estimated for various geometries for both the net and gross section areas of the specimen. Care should, therefore, be taken to ensure consistency in calculations. For crack initiation in this analysis, the net section area was used in estimating the stress concentration. It has been shown by Peterson [31] that the stress concentration factor does not fully characterize the effects of the notch on the fatigue life using a Strain-Life methodology. In this case, the fatigue notch factor K_f is used to estimate the effects of the notch by empirically relating the fatigue life of an unnotched specimen to that of the notched specimen:

$$K_f = \frac{\sigma_{unotched}}{\sigma_{notched}} \tag{3}$$

Through testing, it has been shown that fatigue life is sensitive to the geometry of the notch and the material. Considerable effort has been made to link the stress concentration factor to the fatigue notch factor and this is achieved by an empirically derived fatigue notch sensitivity, q, described as:

$$q = \frac{K_f - 1}{K_t - 1} \tag{4}$$

If a notch has no effect on the fatigue strength, then $K_f = 1$ and $q = 0$. Conversely, while K_f>1 and approaches K_t the notch sensitivity will increase to a maximum value when $K_f = K_t$ and $q = 1$. Therefore, as the notch sensitivity increases, the fatigue notch factor also increases. Notch sensitivity results depend on the geometry of the notch and the applied stress. A review of available literature revealed several studies aimed at estimating values of fatigue notch sensitivity for conventional and E-PBF Ti-6Al-4V specimens. Details of the tests and results are provided in Table 1. For several specimens of E-PBF Ti-6Al-4V the notch radius ρ was not explicitly provided and could not be inferred from the information in the reference. Reviewing the 90° angle flat specimens tested by Razavi et al. [32], the notch root radius for the specimen design is typically small, in the range of 1.0 mm to 0.1 mm. Comparing to the other specimens in Table 1, the notch root radii were all within this range. It was therefore assumed that the unknown values for notch root radius in Table 1 were also in the range of 1.0 mm to 0.1 mm.

Rearranging the relationship for fatigue notch sensitivity for the fatigue notch factor K_f provides a relationship that can be substituted into Neuber's equation:

$$K_f = 1 + q(K_t - 1) \tag{5}$$

$$\sigma\varepsilon = \frac{\left(K_f S\right)^2}{E} \tag{6}$$

The notch response can be expressed in terms of one variable by recognizing that the total strain ε can be written in terms of elastic and plastic strain as a function of the stress:

$$\varepsilon = \varepsilon_e + \varepsilon_p = \frac{\sigma}{E} + \left(\frac{\sigma}{K'}\right)^{1/n'} \tag{7}$$

$$\sigma\left[\frac{\sigma}{E} + \left(\frac{\sigma}{K'}\right)^{1/n'}\right] = \frac{\left(K_f S\right)^2}{E} \tag{8}$$

where K' is the cyclic strength coefficient and n' is the cyclic strain hardening exponent, with both material terms determined empirically through experimentation. The notch stress is then determined by iteration of the equation. The same analysis may be applied to determine the minimum stress and stress amplitude at the notch for each cycle.

A review of the available literature revealed several studies estimating the cyclic strength coefficient and cyclic strain hardening exponent for various conditions of E-PBF Ti-6Al-4V. For crack initiation, it was assumed that the machined XY build conditions would most likely be used for structural purposes. The number of cycles to crack initiation is then estimated using a strain-life equation. A prominent variation of the strain-life equation that adjusts for mean stress effects is the Smith-Watson-Topper (SWT) equation outlined by Bannatine et al. [30] as:

$$\sigma_{max}\varepsilon_a = \frac{\left(\sigma_f'\right)^2}{E}\left(2N_f\right)^{2b} + \sigma_f'\varepsilon_f'\left(2N_f\right)^{b+c} \tag{9}$$

where σ_{max} is the peak stress during a cycle, ε_a is the strain amplitude of the cycle, and $2N_f$ is the number of reversals to failure. The fatigue strength coefficient σ_f', the fatigue strength exponent b, the fatigue ductility coefficient ε_f', and the fatigue ductility exponent c, are all experimentally determined parameters. The SWT equation is solved by iteration of the number of reversals $2N_f$. Plots of strain-life for E-PBF Ti-6Al-4V using the SWT equation are shown in Figure 12 using the values from Table 2. The intersection of several cyclic strain-life curves for the machined XY conditions likely indicates differences in material hardness. For this reason, this thesis refers to two conditions of E-PBF Ti-6Al-4V, HARD and SOFT, with the naming convention being carried throughout.

Table 1. Notch sensitivities of conventional and E-PBF Ti-6Al-4V. R is the stress ratio and ρ is the notch root radius.

Build Condition	Heat Treatment	R	K_t	ρ (mm)	q	Ref.
Forged Bar	2 hrs, 705°C Annealed	0.1	2.78	0.127	0.51	[33]
Forged Bar	2 hrs, 705°C Annealed	0.1	2.78	0.329	0.79	[33]
Forged Bar	2 hrs, 705°C Annealed	0.5	2.78	0.127	0.39	[33]
Forged Bar	2 hrs, 705°C Annealed	0.5	2.78	0.329	0.57	[33]
Forged Plate	75 min, 932 °C Annealed	0.1	2.78	0.127	0.42	[33]
Forged Plate	75 min, 932 °C Annealed	0.1	2.78	0.203	0.37	[33]
Forged Plate	75 min, 932 °C Annealed	0.1	2.78	0.329	0.42	[33]
Forged Plate	75 min, 932 °C Annealed	0.5	2.78	0.127	0.44	[33]
Forged Plate	75 min, 932 °C Annealed	0.5	2.78	0.203	0.51	[33]
Forged Plate	75 min, 932 °C Annealed	0.5	2.78	0.329	0.51	[33]
E-PBF Sandblasted Notched Cylinder	HIP	0.1	2.5	0.85	0.40	[34]
E-PBF As-Built Notched Cylinder	*	0.1	3.0	*	0.14	[34]
E-PBF As-Built Notched Cylinder	HIP	0.1	3.0	0.85	0.40	[35]
E-PBF As-Built Notch Dogbone	*	0	2.34	*	0.39	[32]
E-PBF As-Built Notch Dogbone	*	0	2.41	*	0.34	[32]
E-PBF As-Built Notch Dogbone	*	0	2.43	*	0.33	[32]

* Data not provided in cited reference.

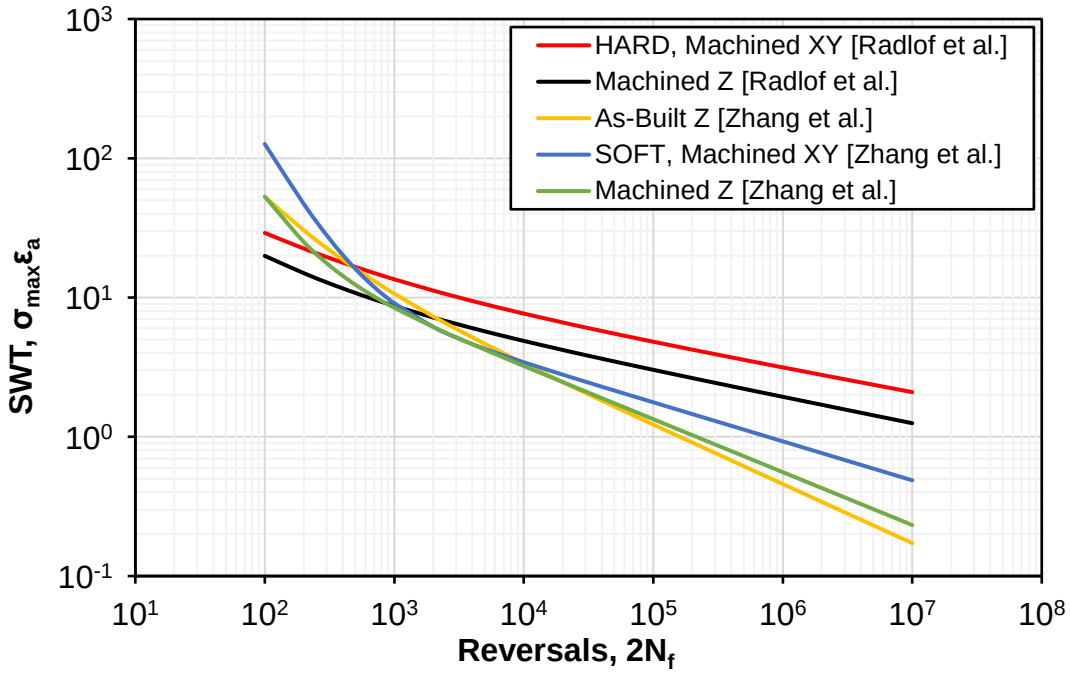

Figure 12. SWT mean stress corrected strain life for E-PBF Ti-6Al-4V. Adapted from [36–39].

Table 2. Cyclic strain-life parameters for E-PBF Ti-6Al-4V

Build	K' MPa	n' -	σ_f' MPa	b -	ε_f' -	c -	E GPa	σ_{yc} MPa	Ref.
Machined XY (HARD)	1710	0.11	1935	-0.087	0.13	-0.546	108.8	877*	[36]
Machined XY (SOFT)	1460	0.088	2327	-0.14	89.4	-1.49	122	757*	[38]
Machined Z	1700	0.098	1722	-0.094	0.158	-0.645	114.6	895*	[36]
Machined Z	1337	0.063	3600	-0.19	21	-1.48	122	1026	[39]
As-Built Z	2887	0.178	4436	-0.212	1.382	-0.943	123	982	[40]

*Values estimated from cyclic stress-strain curve.

2.8. Transition from Crack Initiation to Crack Growth

A longstanding challenge in estimating fatigue of metal components is defining when crack initiation ends and crack growth begins. In practice, crack growth analysis is undertaken by assuming an initial crack size based on either a crack observed in the field during inspection or by the detection limits of inspection equipment. This is problematic when most of fatigue life occurs in the initiation phase. Additionally, the strain-life approach to calculating crack initiation does not result in an estimation of the crack length and small cracks following initiation may not be within a detectable range for field detection methods.

Attempts have been made to understand when crack initiation ends and when crack growth begins. Theoretically, the transition should occur when the crack has reached a length such that the influence of the notch is no longer significant and the plasticity of material ahead of the crack tip is driving crack growth. The crack length at which this occurs is known as the transition crack length. A summary of several methods for estimating the transition crack are presented in Bannatine et al. [30]. The method proposed by Smith & Miller [41] was applied in this thesis for its simplicity and is denoted as:

$$l_t = 0.13\sqrt{D\rho} \tag{10}$$

where l_t is the transition crack length, D is the depth of an elliptical notch, and ρ is the notch root radius. The dimensions are described visually in Figure 13. For simplicity it was assumed that the initial crack size a_0 following crack initiation is the estimated transition crack length l_t.

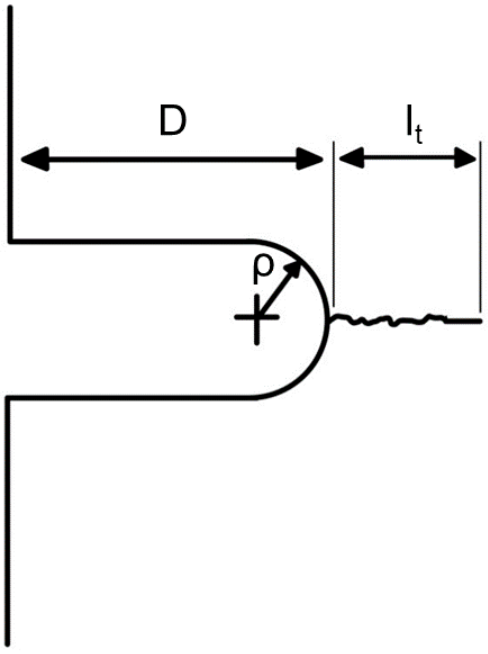

Figure 13. Definition of transition crack length.

2.9. Crack Growth of E-PBF Ti-6Al-4V

The analysis of fatigue crack growth is achieved by referencing an experimentally determined crack growth curve. A typical crack growth curve is split into three regions and is plotted with the logarithm of the crack growth rate da/dN, where a is the crack length and N is the number of cycles, versus the logarithm of stress intensity K or stress intensity range ΔK. The solution for the stress intensity factor is generalized by the equation:

$$K = Y\sigma\sqrt{\pi a} \quad or \quad \Delta K = Y\Delta\sigma\sqrt{\pi a} \tag{11}$$

where Y is an experimentally determined geometry parameter, which is a function of the crack length a, the shape of the crack front, and the component geometry. A representative crack growth curve is shown in Figure 14 with the distinctive "S" shape that is common for many materials. For metals, Region I is characterized by slow crack growth rates driven by properties of the microstructure and the applied loading. The lower limit of stress intensity by which crack growth is not expected to occur is the threshold stress intensity, K_{th}. Region II is characterized by moderate crack growth rates where the effects of microstructure, load, and component geometry have a limited impact. Region II, denoted the Paris region, may be fitted by a line on the log-log plot with the equation:

$$\frac{da}{dN} = C(K)^m \tag{12}$$

where C is the intercept of the line, denoted as the Paris coefficient, and m is the slope of the line, denoted as the Paris exponent. The fitting of the line permits convenient integration of the crack growth curve in the Paris region for several common cases with metals. Region III is characterised by high crack growth rates and where the growth is again sensitive to microstructure, loads, and geometry.

A review of available literature revealed crack growth curves for E-PBF Ti-6Al-4V of various conditions and stress ratios. Unfortunately, each of the assessed studies did not include enough data for a consistent analysis of total crack growth based on the functional grading of Ti-6Al-4V alpha lath size. Of the results, only three curves from Galagarra et al. [42], Seifi et al. [43], and Draper et al. [44] were available at the selected stress ratio of R = 0.1. Additionally, the data from Draper et al.[44] was for the machined and Hot Isostatic Pressed (HIP) condition while Galagarra et al. [42] and Seifi et al. [43] were in the as-built condition, an important consideration for maintaining a functional grading created during manufacturing. Crack growth curves for E-PBF Ti-6Al-4V with fitted Paris curve lines for Region II are shown in Figure 15. Data was extracted from each source graph using the free software WebPlotDigitzer [9].

It has been shown that softer materials tend to impede crack growth more than harder materials. This is largely due to softer materials absorbing greater strain energy ahead of the crack tip instead of the energy being applied to further open the crack. On this premise the crack growth curve in Figure 15 from Galagarra et al. [42] is denoted as SOFT material and the curve from Seifi et al. [43] is denoted as HARD material. The curve from Draper et al. [44] was included to show the impact of machining and HIP on crack growth for E-PBF Ti-6Al-4V.

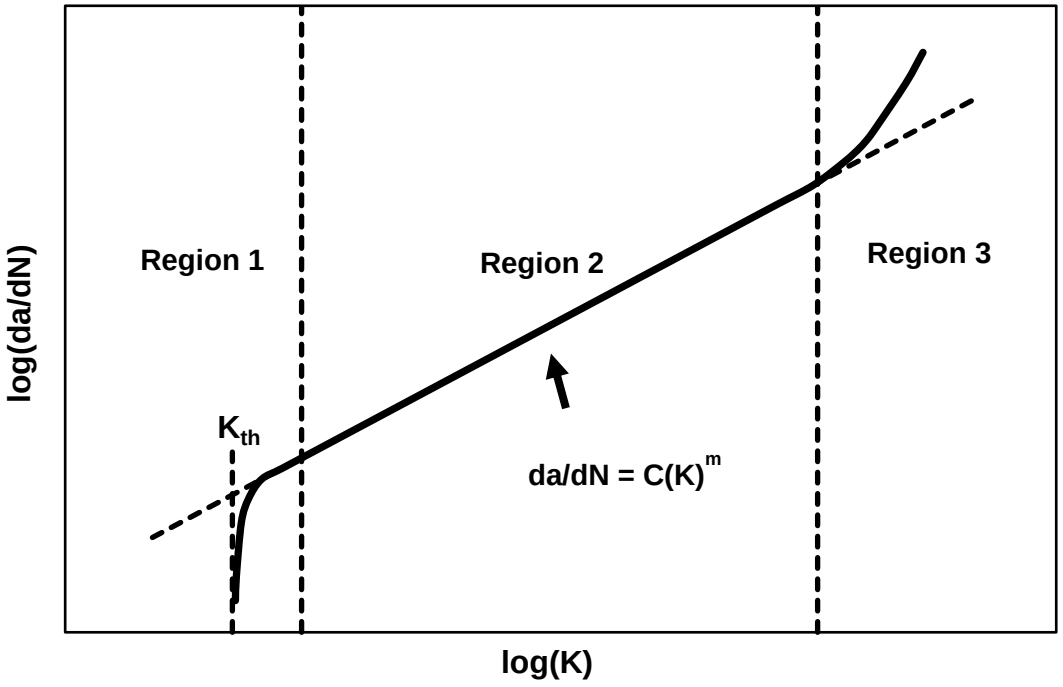

Figure 14. Typical crack growth curve for metals.

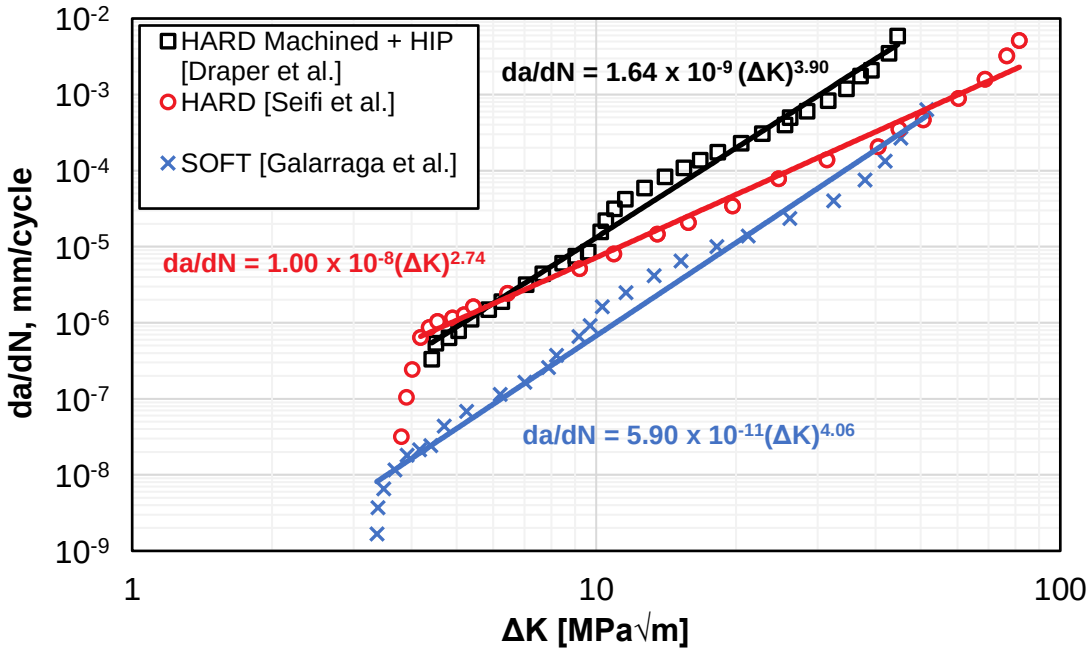

Figure 15. Crack growth curves for E-PBF Ti-6Al-4V. Sources [42–44].

Estimates of fatigue crack growth may be approached by assuming that only the Paris region is relevant and by integrating the Paris equation using analytical integration. This approach is often used because the value of the Paris exponent permits a relatively simple integral and because the scatter in crack growth data results is an approximation. Another common approach is to apply numerical integration methods for small increments of crack growth to estimate the crack propagation life. Either approach has advantages and disadvantages depending on the tools used for analysing crack growth. If using computer software, it is argued that the method of numerical integration is ideal as crack growth can be calculated quickly with a loop algorithm for small increments of crack growth, which limits the integration error. For this thesis the trapezoid rule for small increments of crack growth was used to numerically integrate crack growth curves. Crack growth is estimated from an initial crack length a_0 until failure by either net section yielding of the component or exceedance of the plane strain fracture toughness of the material K_{IC}. The total fatigue life of a component may therefore be expressed as:

$$N_{total} = N_{i_{(a \leq a_o)}} + N_{g_{(a > a_0)}} \tag{13}$$

where N_{tot} is the total cycles to failure, N_i is the number of cycles to initiate a crack of size a_0, and N_g is the number of cycles from a_0 to failure.

2.10. Functionally Graded Materials (FGMs)

Currently, a universal definition for a “functionally graded material” is not available, although various authors have provided definitions in their work. One definition provided by Zhang et al. [45] is that FGMs are: “materials whose properties change gradually with respect to their dimensions”. This definition is concise and was therefore selected for this thesis. The introduction of the term “functionally graded material” first appears in the literature in 1987 in a study by Niino et al. [1] who sought to improve the heat resistance of components for a spacecraft using functional grading. Although the term is relatively recent, the existence of FGMs have been prevalent in nature and history for thousands of years. A study of functionally graded materials that occur in nature was conducted by Liu et al. [46]. One common natural FGM is wood, where layer-by-layer properties and grain orientation are defined by the structural requirements of the tree trunk and branches [46]. Another common biological FGM are bones, in which the internal structure is made of combined hard and soft material whose localized properties are tuned to the structural requirements of the bones [46]. In many cases engineered FGMs are inspired by what has been achieved in nature.

A FGM may be conceptualized by splitting a component into smaller units of volume called voxels. The term “voxel” originates from the combination of the word volume and the word pixel, a word representing a unit area, typically on a screen [47]. Although originally invented to describe computer graphics, voxels are a fundamental concept in describing and analyzing functionally graded materials. An example of a component split in terms of voxels is shown in Figure 16. Various properties that might be considered by a designer are suggested for the voxel being considered. The idea is that a designer would specify properties for each voxel within the component. Assuming that the resultant component could be manufactured without challenges at the boundaries of voxels, a FGM would be

the result. Notably, there is some dichotomy between the discrete theoretical description of FGMs in terms of voxels and the continuous properties of some FGMs, whether in nature or engineered. This is largely due to the limitations of physics in creating a discrete boundary. Expanding on the definition provided by Zhang et al. [45], in the case of discrete volumes using voxels, an elaboration is that the size of voxels must be much smaller relative to the size of the overall component. This requirement is derived from the description by Zhang et al. [45] underlining that FGM properties be gradual. It is argued that the gradual change in properties is what separates FGMs from composite materials. Additionally, the location specific nature of FGMs contributes to the differences of FGMs compared to composites as the ability to manufacture some FGMs may only be possible with techniques like additive manufacturing. Although these elaborations on the definition by Zhang et al. [45] leaves some ambiguity they were adopted for clarity in lieu of a universal definition.

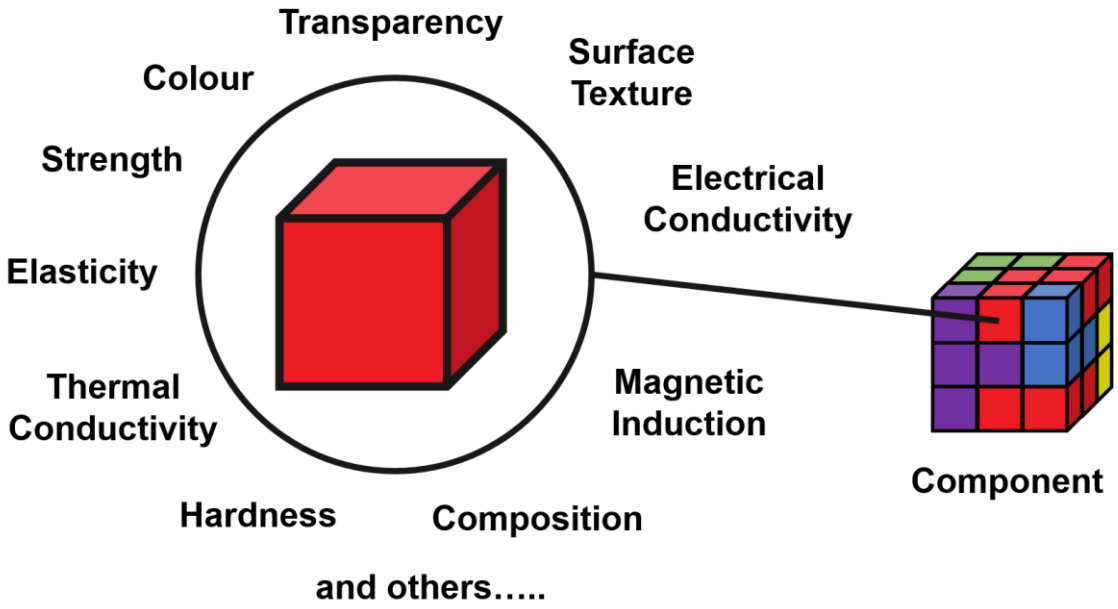

Figure 16. Example of a voxel and possible properties.

The advent of AM is one way to realize the potential of engineered FGMs. The layer-by-layer process inherent to AM provides the opportunity for specifying localized properties. The work by Liu et al. [46] identified two methods of functional grading: discrete and continuous, and six unique categories of functional gradings: composition, arrangement, distribution, dimension, orientation, and interface. Following the work by Liu et al. [46] several reviews of FGMs using AM were undertaken highlighting future potential. A review by Zhang et al. [48] highlighted examples of additive manufactured FGMs, mainly using metal AM processes. Tyangi & Manjaiah [49] reviewed available examples using laser-based AM to create FGMs using titanium alloys as the primary feedstock. The review demonstrated the feasibility of directed energy deposition and powder bed fusion AM in manufacturing functionally graded materials using several categories highlighted by Liu et al. [46].

El-Galy et al. [50] attempted to classify all functionally graded materials by proposing a comprehensive classification method that included conventional and additive processes with a broad range of materials by categorizing FGMs according to how they were made and the manufacturing cost and effort. In defining types of FGMs El-Galy et al. [50] outlined three categories: composition, microstructure, and porosity. These categories loosely relate to those proposed Liu et al. [46]. A review by Li et al. [51] sought to further examine and categorize all available examples of FGMs created using AM and demonstrated opportunities across a broader range of materials and applications. By this review it was found that FGMs using AM are possible using all seven AM categories with materials suitable for each AM process [51]. Interestingly the categories of functional gradings presented by Liu et al. [46] was referenced in both Zhang et al. [48] and Li et al. [51]. By this association it was concluded that the categories of functional gradings presented in Liu et al. [46] are representative of those possible by additive manufacturing. It is argued that the six categories presented by Liu et al. [46] may be simplified because the categories of composition and distribution are synonymous concepts and orientation may be built into the remaining categories. The six categories were therefore simplified into three: morphology (shape and size), distribution, and composition. A summary of the two methods and three categories of are shown in Figure 17.

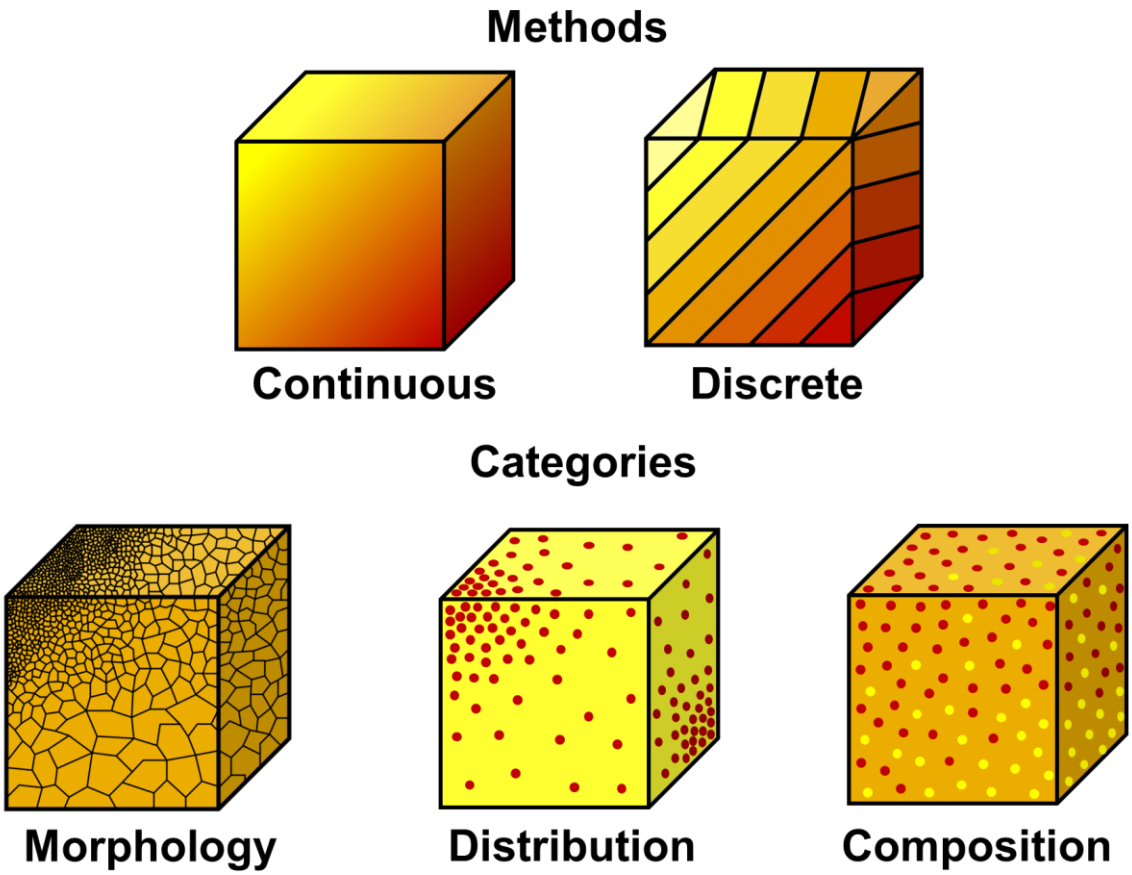

Figure 17. Examples of three dimensional functional gradings.

2.11. Potential Functions and Functional Grading

Following an understanding of FGMs, it is necessary to define a functional grading in mathematical terms. This is required to permit applying a functional grading to a model of a component. The simplest definition of a potential function is a function whose value defines a physical property. A use of potential functions for computer graphics and simulation was described by Gupta & Tandon [52] to define a distribution of colour in two or three dimensions. Examples of several two-dimensional potential functions and their associated material distribution is shown in Figure 18. The potential functions are defined such that both the length of a component and mixture between two materials are normalized between values of zero and one. Normalized potential functions are convenient because they can be applied to different shapes and can be represented graphically. A potential function in the graphical form may be defined by a continuous curve with a mathematical equation or in discrete intervals as shown in Figure 18. By assigning a potential function to a desired component geometry a functional grading can be designed with a single relationship. This relationship can then be used to map the properties of voxels within a FGM. A potential functional may also be described in three dimensions, resulting in gradings that are also in three dimensions. This was not considered for this thesis but is an area for future research.

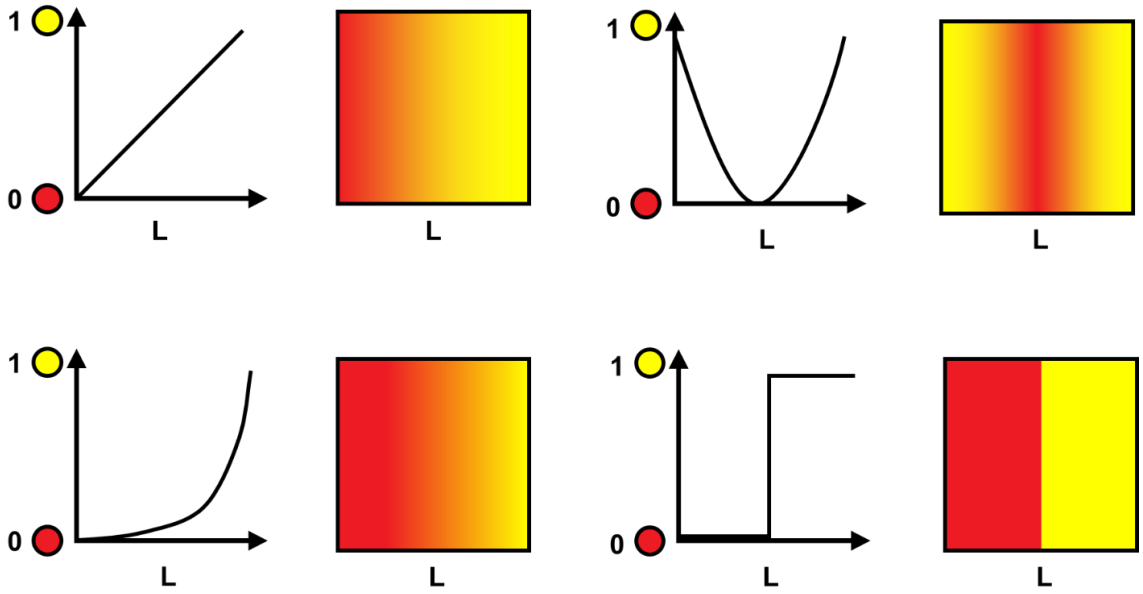

Figure 18. Examples of normalized potential functions.

2.12. Functionally Graded Ti-Al-4V Using Additive Manufacturing

The concept of FGMs has existed in the literature for almost 40 years, transcending beyond the invention of additive manufacturing technologies. A review of available literature is therefore complicated when seeking examples specifically related to additive manufacturing. Conveniently, numerous review papers since 2020 have assessed FGMs manufactured using AM. Many of the review papers included references that were ubiquitous, although the specific focus of each review paper varied. A historical look at FGMs over the past 30 years that included both conventional and additive manufacturing methods was completed by Saleh et al. [53]. This review provides comprehensive details on the conventions of identifying FGMs and their applications until the year 2020. In the review by Reichardt et al. [54] several older examples were found that were not included in the other references. The work focusses on material compatibility and generally considers composition type FGMs. A review by Yan et al. [55] focussed on laser-based AM technology providing details specific to those use cases. Ghanavati et al. [56] provided a holistic review of all FGMs manufactured using AM up to the year 2021. The review included numerical studies, although many of the material combinations have not yet been produced and tested experimentally. A more recent review by Tyagi & Manjaiah [57] considered laser-based AM FGMs using exclusively Ti-6Al-4V. Hasanov et al. [58] covered all materials, but most examples provided in the review were FGMs using compositions of polymers.

To avoid duplicating the efforts of previous works, a summary of FGMs using AM Ti-6Al-4V is presented in Table 3. The table was created by cross-referencing the information presented in the various review papers in the literature along with other noted examples not found in the reviews. An interesting observation from Table 3 is that the historical focus for AM FGMs using Ti-6Al-4V has been for laser-based DED, whereby powdered feedstock is fed into nozzles and sent as a stream of powder particles into a source beam. Additionally, the majority of gradings were achieved by mixing compositions of two metals. The few examples of functional grading of grain morphology used laser or electron beam PBF processes, which is the intent of this research.

To gain further substantiation for developing a FGM by grading grain morphology an additional review of recent works was completed to highlight recent examples regardless of whether they were employing E-PBF or Ti-6Al-4V feedstock. The intent of this review was to provide examples of machine parameters being controlled to achieve locally specified grain morphology. On grading material properties by controlling microstructure, Popovich et al. [59] and Popovich et al. [60] used a laser powder bed fusion (L-PBF) process and Inconel 718 feedstock to grade discrete zones along the length of a tensile specimen by manipulating the machine parameters for each zone. Similarly, Ghorbanpour et al. [61] graded single edge notched fatigue specimens using L-PBF and Inconel 718 with two discrete zones of grading; one zone included the notch and one zone was away from the notch. The combined examples of FGMs of grain morphology, along with the process windows determined by experiment, provided the substantiation that functional grading of Ti-6Al-4V grain morphology using E-PBF was feasible. The review also highlighted numerous opportunities for improving fatigue life by grading material composition using DED.

Table 3. Summary of Ti-6Al-4V FGMs using AM.

Year	AM Process	FGM Type	Refs.
2005	L-DED	Composition - Inconel 718	[62]
2008	L-DED	Composition - Co–Cr–Mo	[63]
2011	L-DED	Composition - Inconel 718	[64]
	E-PBF	Morphology	[65]
2012	L-DED	Composition - Al	[66]
2014	L-DED	Composition - $TiAl_{6.5}Mo_{3.5}Zr_{1.5}Si_{0.3}$	[67]
2015	L-DED	Composition - TiC	[68]
	L-DED	Composition - TiC	[69]
	L-DED	Composition - $Ti_{47}Al_2Cr_2Nb$	[70]
	L-DED	Composition - 316L SS	[71]
	E-PBF	Morphology	[72]
2016	L-DED	Composition - 304L SS	[73]
	L-DED	Composition - Invar	[74]
	L-DED	Composition - 316 SS	[75]
2017	L-DED	Composition - TiC	[76]
	L-DED	Composition - $AlSi_{10}Mg$	[77]
	L-DED	Composition - Mo	[78]
2018	L-DED	Composition - 304L SS	[79]
	L-DED	Composition - Al_20_3	[80]
	L-PBF	Morphology	[81]
	E-PBF	Morphology	[82]
2019	L-DED	Composition - 17-4PH SS	[83]
	L-DED	Composition - Inconel 625/316L SS	[84]
2020	L-DED	Composition - Inconel 625	[85]
	L-DED	Composition - Inconel 718	[86]
	L-DED	Composition – ZrO_2	[87]
	E-PBF	Morphology	[88]
2021	L-PBF	Morphology	[89]
	E-PBF	Composition – $TiAl_{48}Cr_2Nb_2$	[90]
2022	Wire Arc-DED	Composition - Inconel 625	[91]

2.14. Modelling of FGMs in Commercial Software

Before developing a novel fatigue model, it was deemed useful to review the capabilities of commercially available software in analysing FGMs. Two common software suites with different approaches to fatigue life estimation were used: AFGROW Fracture Mechanics and Fatigue Crack Growth Analysis software tool [92] and Ansys Mechanical 2023 [93]. Both software suites were selected based on general popularity in the literature. AFGROW applies an algorithmic approach using empirical data and historical fatigue life analysis methods, while Ansys mechanical applies knowledge of crack growth equations in a finite element method.

AFGROW and its preceding software suites have existed since the mid-1980s as a tool for fatigue analysis with a long history of use during major aircraft projects [94]. The historical prevalence and ongoing support of the software suite makes it a logical candidate for analysing FGMs. AFGROW version 5.4.1.25 was used to trial estimating fatigue crack growth in FGMs for a constant amplitude loading. A sample of the AFGROW GUI with a representative model is shown in Figure 19. Within AFGROW, many materials, simplified geometries, and loads are built-in but users may also specify their own material properties, complex geometries, or variable amplitude loadings. The software calculates fatigue crack growth using an algorithm to integrate the crack growth curve. Of significance to analyzing FGMs, AFGROW allows a user to input tabular crack growth data for analysis. Tabular data can be inputted for a single material at several stress ratios allowing for an interpolation of crack growth curves between stress ratios. Data may also be inputted and tagged for various temperatures, although the assigned temperature is a tag only and does not change the analysis parameters. By using the temperature tags as a placeholder for different gradings of a material it is possible to analyze crack growth over small discrete grading steps. This approach becomes time consuming but more accurate as the number of discrete gradings increases. For each discrete grading level, the crack growth curve for that layer must be manually selected. AFGROW then overwrites results preventing continuation of the simulation using the crack length from previous results. An alternative approach is to input a crack growth curve that accounts for the change in rate according to a functional grading. The advantage of this approach is that no further input manipulation would be required to estimate fatigue crack growth of continuous FGMs. This was attempted in the software but was unsuccessful as it appears the software has been designed such that both the input crack growth rate and stress intensity values must be increasing. This restriction in the software prevents the input of derived crack growth curves for FGMs and hampers analysis of FGMs using AFGROW.

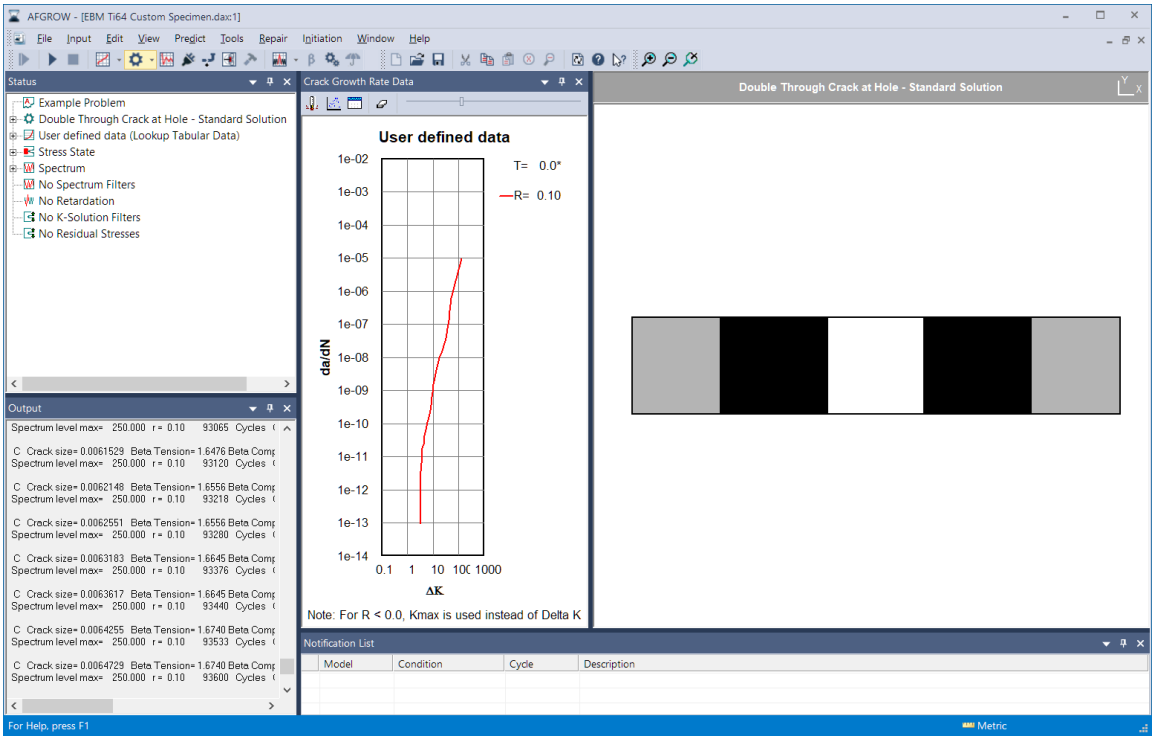

Figure 19. User interface with custom material inputs in AFGROW.

A package within Ansys Mechanical 2023 Student Edition was also trialed as a tool for estimating fatigue crack growth of FGMs. Within Ansys Mechanical exists a package called SMART Fracture [95]. The term “SMART” is an acronym for Separating Morphing and Adaptive Remeshing Technology (SMART), which describes an Unstructured Mesh Method (UMM) approach to simulating the propagation of cracks in a component [95]. Using the SMART package, crack growth is simulated incrementally by reforming of the mesh after each increment. The package allows a user to specify material properties in the same manner as any other FEA analysis in Ansys mechanical. Crack growth properties, however, are inputted by specifying the Paris coefficient and exponent for Region II of the crack growth curve. A user provides an initial crack by defining a crack front mesh and by setting boundary conditions to the model. When the model is initiated, the crack moves within the material and the remeshing is observed during calculation. In this way the crack path and cycles to failure are estimated. This method of estimating crack growth is relatively fast, requires no additional programming within Ansys, and offers the advantage of modelling crack propagation in three dimensions. A sample result from the SMART fracture package in Ansys mechanical for a structural steel material and a standard CT Fatigue specimen is shown in Figure 20. For a cyclic displacement of 0.002 mm the number of cycles to failure was estimated to be 1.1 x 10^6 cycles and the crack length at failure was estimated to be 10 mm.

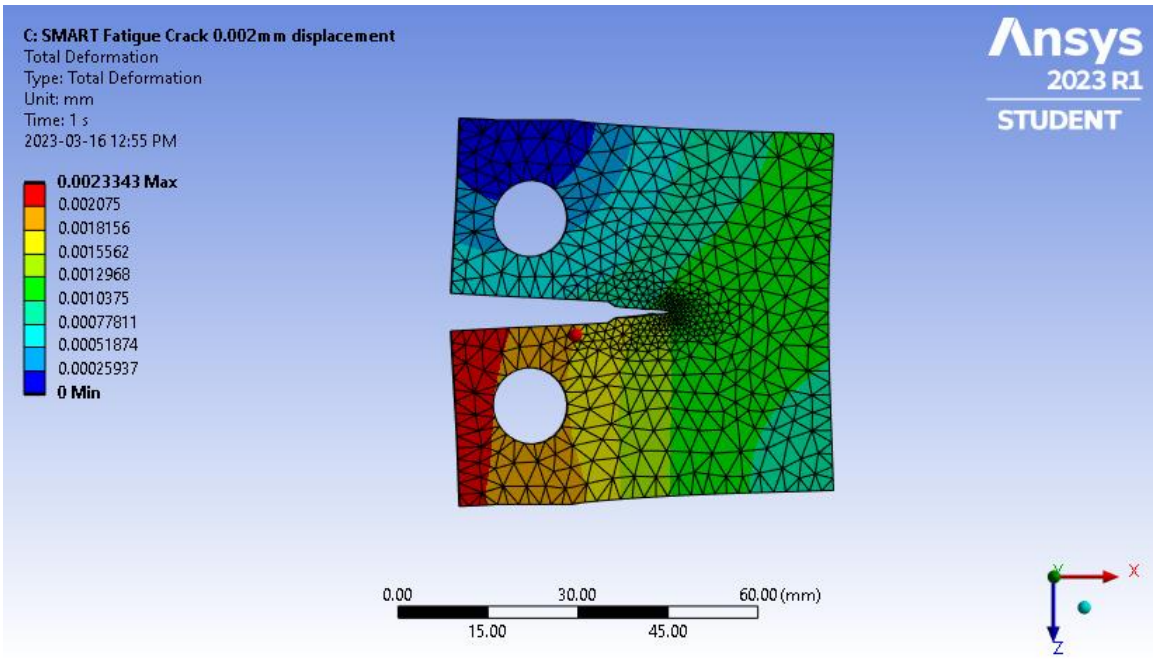

Figure 20. Example case using Ansys SMART Fracture solver.

The Ansys SMART Fracture method has significant limitations regarding modelling of FGMs. Firstly, the package operates with the assumption that a single crack growth curve is applied. This would not restrict the use of the software for FGMs except that there is no option to input a crack growth curve directly; the user must input the Paris exponent and coefficient. This is disadvantageous as it has been shown that many materials deviate from being linear in the Paris region. It could be argued that the restrictions could be overcome by splitting the material into discrete layers and accounting for the change in crack growth rate according to a functional grading. While technically feasible the effort and calculation time required in proportion to the number and thickness of the layers likely outweighs the use of this method. Additionally, this approach would result in a limited estimate of continuous FGMs. A similar approach to modelling FGMs in Ansys was discussed by Ashirbekov et al. [3] where a “dummy” thermal load is applied and material properties are changed in lieu of the temperature change. This option however results in the same restrictions as previously when calculating fatigue crack growth. Ashirbekov et al. [3] did, however, demonstrate that both strain (and therefore stress) of continuously graded FGMs could be modelled with this method. The analysis of the suitability of AFGROW and Ansys SMART Fracture contributed to the decision to analyze fatigue crack growth in FGMs manually.

2.15. A Novel Approach to Fatigue Analysis of FGMs

The intent of this work is to avoid the requirement to implement custom scripting within FEA software as it increases time and complexity in analysing crack growth in FGM components. A review of FGM modelling and analysis by Birman & Byrd [96], although providing limited information on modelling fatigue crack growth, did identify that FGM fatigue modelling up to 2007 was largely based on empirical relationships and finite element analysis. A recent review on modeling and analysis of FGMs by Kanu et al. [97] led to the same general conclusion but expanded that the extended finite element method (XFEM) is the state-of-the-art. The XFEM method was proposed in 1999 by Moës et al. [98] to permit the modelling of crack growth without needing to remesh the geometry after each iteration of calculation. A rigorous mathematical explanation of how this is achieved is beyond the scope of this thesis. The key concept is that material properties are defined by the stiffness matrix of each element in the mesh. A functional grading can therefore be applied by mapping the stiffness matrix of each element to the desired grading throughout the specimen. The XFEM approach then uses mathematics to estimate the incremental crack growth based on the stiffness assigned to each element. A recent example of the XFEM approach to model fatigue and fracture in common specimen geometries for ungraded L-PBF Ti-6Al-4V is highlighted by Verma et al. [99]. In the study the simulated crack growth curves agreed with the experimental results demonstrating the XFEM approach as a prediction tool for ungraded AM Ti-6Al-4V. In contrast, the fatigue model in this research maps experimentally determined crack growth rates for two materials to a potential function that defines the functional grading. This strategy has yet to be applied elsewhere in the literature and is the key contribution of this research.

From the literature review, it was not clear why FEA is the most common approach, although some hypotheses may be drawn from the characteristics of FEA models. The use of FEA permits analysis of crack growth in three dimensions, since the mesh of the specimen is in three dimensions. Assuming the FEA model can accurately account for different rates in crack propagation in three dimensions, this feature provides insight into the path of cracks as they move through the component material. Additionally, use of an FEA model permits direct analysis of complex geometries avoiding the requirement for simplifications to analyze the geometry using more traditional approaches. This could be beneficial in cases where no obvious geometrical simplifications would permit analysis using known stress concentration and stress intensity factor solutions. Direct analysis may also reveal interaction effects from the geometry that may not be revealed by analyzing the simplified case, like the impact of an edge that is away from the crack front but in the possible future path.

Regarding aerospace parts, it is argued that common components like spar caps, stringers, fittings etc., can be analyzed in fatigue by simplifying their geometry. Using an FEA analysis in these cases significantly increases the effort required to arrive at a fatigue life estimate. This is one reason traditional methods using empirical data and iteration remain relevant. For very complex geometries it may be difficult or impractical to model fatigue using this approach. However, it is argued that initial design studies could still be completed quickly using a simplified geometry and the proposed fatigue model.

Although there exist numerous examples of functional grading, as highlighted in Table 3, most do not analyze fatigue data, since their intent was to demonstrate feasibility in manufacturing FGMs. The closest experiment related to the goals of this research is the work by Ghorbanpour et al. [61] where a notched bending fatigue specimen was functionally graded in two discrete layers of Inconel 718 grain size by controlling of a L-PBF machine. The graded specimen was 80 mm in length and contained two 6 mm layers manufactured at different laser powers. The notch was created using electron discharge machining and is characterized as an edge notch with a depth of 0.30 mm and a radius of 0.20 mm. The first discrete layer that contained the notch was manufactured with a significantly smaller grain size than the second discrete layer. The material hardness was measured using graded and ungraded specimens to confirm that the smaller grain size resulted in harder material. A summary of the graded specimen manufactured in the horizontal orientation is shown in Figure 21. Based on the results of the study it could only be concluded that the crack growth rate reduced as it approached the interface region.

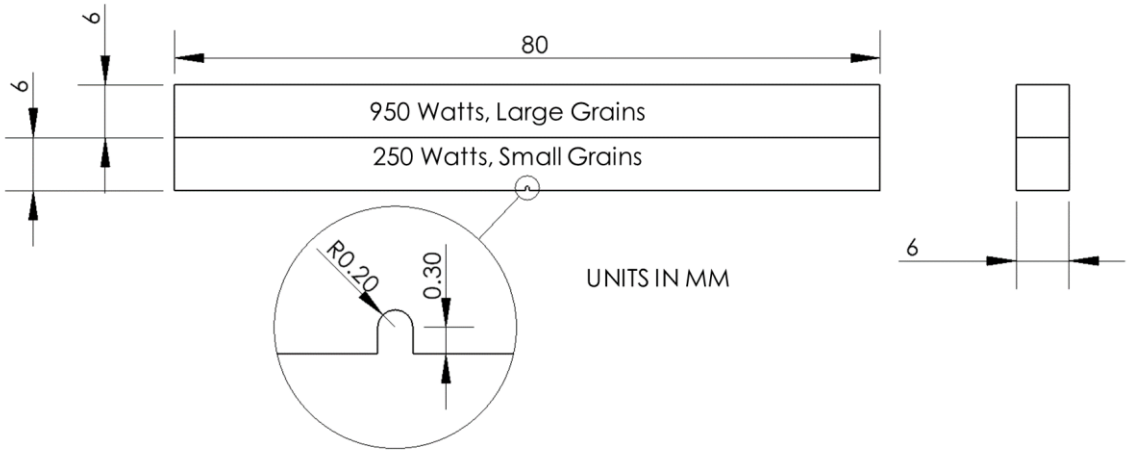

Figure 21. Functionally graded Inconel 718 geometry. Adapted from [61].

Several observations of the work by Ghorbanpour et al. [61] can be made to explain the results achieved. The experiment successfully demonstrated the ability to grade the Inconel 718 by controlling the process parameters of the L-PBF machine, as is expected to also be possible with E-PBF Ti-6Al-4V. Additionally, the harder material characterized by the smaller grain size is applied for the discrete layer that includes the notch. This grading design, however, is likely why there were limited changes in the crack growth rate measured for the horizontal specimen. Ghorbanpour et al. [61] attributed a slowing of the crack growth rate to a deflection at the interface of the discrete layers of grading. It is therefore argued that many smaller regions of discrete gradings would have a compounding effect on reducing the crack growth rate. A further improvement would be to apply a continuous grading that constantly slows the crack growth. Additionally, the notch is very small compared to the size of the discrete layer of hard material. It has been shown that microstructural slipping mechanisms characterize crack initiation while material plasticity characterizes crack growth. From this understanding, a large region of smaller grains ahead of an initiated crack would increase crack growth compared to applying a region of smaller grains just ahead of the crack tip. In summary, the size of the notch in comparison to the size of the discrete layer and the application of only two

discrete layers of relatively large thickness resulted in a specimen that performed like two materials stuck together with an interface. In contrast, the approach in the current research is to specify small grains in the region close to the notch and then smoothly control grain structure with a continuous grading. Based on the review of the literature smoothly controlling the grain structure this way using E-PBF and Ti-6Al-4V has yet to be undertaken.

3. Methodology

3.1. Conceptual Approach

To predict the total fatigue life of functionally graded AM components, a conceptual framework was adopted. The Process-Structure-Properties-Performance (PSPP) framework was used to guide the selection and design of test specimens from which total fatigue life could be modelled. An outline of the PSPP relationship for E-PBF components is shown in Figure 22. The PSPP framework may be used in the forward or reverse directions depending on the desired outcome. In the forward direction a user defines geometry and functional grading and determines performance outcomes as the result. In the reverse direction a desired performance outcome is specified and a user determines, through experimental data, optimization, or experience, what geometry, grading, and machine processing parameters are required to achieve the performance outcome. For this thesis the PSPP framework was considered in both directions to build a fatigue model. Component geometries, gradings, and machine processing parameters were selected with the intent of improving the total fatigue life of a component. Microstructural and material properties of the resultant components were gathered from available literature as input data for estimating the performance of the components in fatigue.

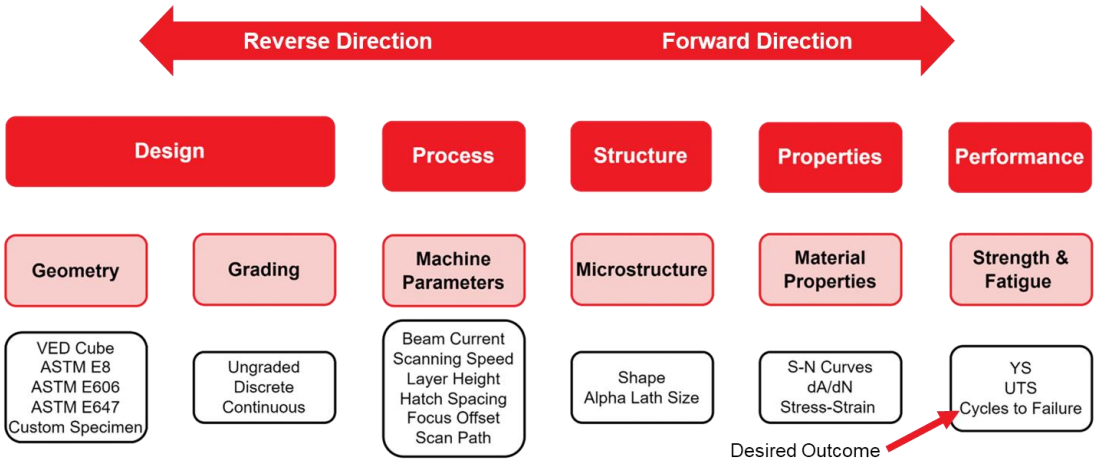

Figure 22. Process-Structure-Properties-Performance framework for E-PBF.

Applying the PSPP framework in the forward direction, the VED cubes are first used to gather information on the relationship between microstructure, VED, beam current, and scan speed. The specimen is designed to be cut into pieces so that the microstructure of the material can be analyzed using conventional metallographic techniques for Ti-6Al-4V. Using the predetermined E-PBF Ti-6Al-4V process windows, a range of VED settings are selected and tested. The goal is to test samples along lines of equivalent VED, like those shown in the process windows, with the hypothesis that as VED increases, alpha lath size decreases. This is expected because as VED increases, the melt pool receives greater energy in the form of heat, leading to a slower cooling rate and more time for the alpha laths to grow. To characterize error and scatter in the data it is ideal to manufacture numerous runs using the same VED settings. Additionally, for each run to be comparable

the focus offset, beam voltage, hatch spacing, and layer thickness must be constant for all specimens.
Once the relationship between VED and alpha lath is established the knowledge is used to define properties for the ASTM E8 Tensile, ASTM E606 strain controlled fatigue, and ASTM E647 compact tension (CT) specimens. The tensile specimens are used to determine the yield and tensile strength of the materials for a specific microstructure and for testing material hardness. This would provide further substantiation and improvement to the Hall-Petch relationship previously presented for the material, while also providing key information required in the equations of fatigue. The ASTM E606 specimens are used to link microstructure to the strain-life relationship providing data for estimating the crack initiation life for a specific microstructure. Finally, the ASTM E647 CT specimen is used to establish crack growth rate curves for each microstructure at the desired stress ratio. The resultant crack growth curves are then used to analyze crack growth life for any specimen design. In this way considering the PSPP framework in the forward direction the machine process parameters are linked to the resultant microstructure, which in turn reveals the properties of the material and the performance in terms of static and fatigue strength.

Following application of the PSPP framework in the forward direction, application in the reverse direction permits a designer to determine what is required to achieve a specific goal. For this thesis the goal is to improve the fatigue life of a component by functional grading. An ungraded, custom component geometry is assumed that represents a common geometry found in aerospace. Using the available data from the literature and an understanding of fatigue, the performance of the material in terms of crack initiation life and crack growth life are to be maximized. To achieve this performance, the material properties should be graded such that fatigue life during initiation is maximized and crack growth rate during crack growth is minimized. This requires a small alpha lath size for regions influencing crack initiation and a larger alpha lath size in regions influencing crack growth. The control of the alpha lath size is permitted by controlling the process, specifically the parameters of the VED relationship. From an understanding of the E-PBF process, a greater VED will generally lead to a larger alpha lath size. By considering the PSPP framework in the reverse direction the desired localized properties of the material for a custom specimen geometry can be specified.

The feasibility of completing the specimen testing described in the PSPP framework was limited, given the time and financial resources available for this thesis. The total number of specimens required to complete this effort is in the hundreds. This was the main consideration in the decision to create a total fatigue life model using available literature data instead of running the tests. There was, however, funds available to manufacture a limited run of specimens to be tested in future work with the goal of adding results to those obtained from the literature. Through a contract with the University of Waterloo, several test specimens identified in the PSPP framework were manufactured in Ti-6Al-4V material on an Arcam A2X EBM machine. A summary of specimens is provided in Table 4; all specimen geometries were defined as near-net-shape with the intent of final machining taking place after manufacturing on the AM machine. No CT specimens were manufactured as the project budget could not accommodate the cost. However, crack growth rates can be inferred using a custom designed notched specimen that models a typical feature found in aircraft structures. Using knowledge from the literature custom specimens were manufactured for three combinations of VED, beam current, and scan

speed predicted to result in a significant difference in alpha lath size. The intent is to test the crack initiation and growth properties at the three different lath sizes. Additionally, discrete graded specimens using the same custom geometry were manufactured with three zones of grading designated by VED, beam current, and scan speed. The intent is to determine if small regions of discrete functional grading near a notch could result in an improvement in fatigue life. In the future, when AM machine capabilities allow, the intent is to manufacture custom specimens with a continuous grading near the notch.

Table 4. E-PBF Ti-6Al-4V manufactured specimens summary.

Specimen	Geometry	Amount
VED Cube	15 mm^3	60
Rectangular Tension – Lath Size 1	Ref [100]	5
Rectangular Tension – Lath Size 2	Ref [100]	5
Uniform Gage Fatigue – Lath Size 1	Ref [101]	12
Uniform Gage Fatigue – Lath Size 2	Ref [101]	12
Custom Specimen – Lath Size 1	Figure 25	6
Custom Specimen – Lath Size 2	Figure 25	6
Custom Specimen – Discrete Grading	Figure 25	6

Note: beam voltage 60 kV, hatch spacing 0.1mm, and layer thickness 0.05mm.

In an unfortunate circumstance, the first run of 30 VED cubes had unacceptable porosity as the focus offset of the machine was set too high. This resulted in a lack of fusion of powder particles leading to internal voids and a poor surface finish of the specimens; an example is shown in Figure 23. A change in the focus offset to 3 mA resulted in significantly reduced internal porosity and improved surface finish. The failure of the first run of VED cubes means that only one data point is available for a specific VED, beam power, and scan speed setting and that more specimens will be required in the future to confirm the resultant alpha lath sizes. A portion of the VED cubes from the second run were polished and etched and micrograph images captured to be analyzed in the future. Several weeks were required to tune the polishing and etching procedures found in the literature to achieve acceptable micrographs of AM Ti-6Al-4V. This work will contribute to testing and analyzing the remaining VED cubes and any future AM Ti-6Al-4V specimens. Regarding the E8 tensile and E606 fatigue specimens, at the time of writing of this thesis practice machining runs were being conducted on samples of conventional Ti-6Al-4V with the intent of tuning post-process machining parameters. Concurrently, static and fatigue material test training was conducted in the lab using conventional Ti-6Al-4V specimens in anticipation of the specimens being ready for testing.

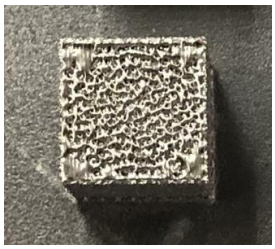

Figure 23. Failed 15mm^3 VED specimen with high porosity. E-PBF Ti-6Al-4V manufactured on an Arcam A2X EBM machine.

3.2. AM Process and Material Selection

The process by which a combination of AM machine and material was selected was pragmatic considering available information and resources. At the time of writing of this thesis, the Royal Military College of Canada (RMC) did not have direct access to an AM machine that could manufacture components using metal feedstock. Any future research required to test and verify the developed fatigue model would therefore require either the purchase of an AM machine or support from an outside contractor. For these reasons the selection of an AM process and material had significant future implications.

With the intent to analyze metal components, only AM processes that could manufacture with metal feedstocks were considered. This immediately excluded material jetting and vat polymerization AM processes, as they mainly work with polymer feedstocks. Material extrusion was also excluded because available feedstocks are composites of metal embedded in a polymer matrix. Binder jetting was rejected for a similar reason, as metal powder is adhered by a binding agent to create a green part, which is then fired in a kiln to sinter the material. The required sintering leads to greater porosity compared with the sheet lamination, directed energy deposition, and powder bed fusion AM processes. Sheet lamination would not be feasible because the process relies on sheets of metal being adhered and then cut to shape after the adhering process. This would significantly limit localized control of material properties and would permit only discrete functional grading. This initial analysis of options left either powder bed fusion or directed energy deposition processes.

The DED processes can be subdivided by energy source: laser, electron beam, plasma arc, or electric arc, and by feedstock: powder or wire [102]. A review of the literature was completed to verify what information was available on material properties and functionally graded materials using DED. It was noted that, although many examples could be found, there was not enough information about fatigue properties from which to build a model. Additionally, a wide variety of specimen geometries and material compositions were trialed in a limited capacity making comparison of results difficult. Lastly, from a pragmatic view, access to DED machines within North America was noted to be limited in comparison to PBF machines. For these reasons DED based AM processes were not the preferred option.

PBF processes can be roughly subdivided into two groups of technologies: laser or electron beam. A review of the literature revealed significant data with common metal materials like Ti-6Al-4V, stainless steels, and aluminum alloys. In general, feedstocks available for one technology were also available for the other so there was no significant difference in this respect. The key difference between the two technologies was that E-PBF manufactured components show no significant residual stresses compared to L-PBF processes. A comparison by Takase et al. [103] using Ti-6Al-4V feedstock on both a L-PBF and a E-PBF machine demonstrated this result. In the context of specifying and maintaining a functionally graded component this led to the selection of E-PBF.

The selection of material following the selection of process was less arduous. Ti-6Al-4V was the most referenced material with fatigue data using the E-PBF process. The feedstock is readily available as it is used in several conventional manufacturing processes. Conveniently Ti-6Al-4V is an aerospace material with both past uses and future expected applications. Additionally, Reichardt et al. [54] identified that Ti-6Al-4V is the most compatible metal in terms of mixing with other metals. This was not significant for this research but has future research implications. For these reasons Ti-6Al-4V was identified as the material of interest for this research.

3.3. Custom Specimen Geometry and Loading

The development of a model to predict the total fatigue life of functionally graded additively manufactured components is complicated by the interaction effects of geometry, material, loads, and functional grading. Within the scope of this thesis, it was not feasible to evaluate every interaction combination and therefore, initial assumptions were required. For this reason, a geometry representative of aerospace components was selected that was analyzed under constant amplitude loads with a single functional grading.

Common aerospace components like spar webs, stringers, skin panels, structural joints etc. may be simplified as sheets or plates with holes. Although these components are often loaded with fasteners in the holes, including the joint interactions in the analysis of fatigue life complicates the development of a model. Additionally, many aerospace components include unloaded or lightly loaded holes.

An example of a common aerospace component that might be improved by functionally graded AM is shown in Figure 24. The component is from a large, legacy military aircraft and is made from forged 7075-T6 aluminium. The fitting contributes to transferring loads from the aircraft wing to the fuselage and is a fatigue critical component. The fitting has several rows of bolted fasteners that secure it to the surrounding structure. From an analysis of the fleet a known location for fatigue cracks is shown in Figure 24. The crack is at the edge of a clearance fit threaded fastener so the hole is not loaded directly. To determine the load that passes through the material in the region near the hole a FEA analysis would be required using the maximum applied load experienced in flight. This would permit an estimate of the maximum applied gross or net stress for the material in the region closest to the identified hole. This component was not the focus of this research but merely demonstrates that holes in aircraft parts are a relatively common occurrence. Creating a custom specimen that approximates this common geometry, therefore, increases the applicability of this research.

A custom specimen geometry was designed that approximates holes like those found in the example component geometry. The custom geometry is described as a plate of finite dimensions with an unloaded fastener hole. A model of the specimen geometry is shown in Figure 25. Flat grip ends were added to permit fatigue testing of specimens in the future. The specimen length, width, hole diameter, and thickness are like those of the example component in Figure 24. The specific dimensions of the custom specimen were initially defined to keep the stress intensity solution within certain boundaries, while remaining true to modelling the example aircraft component. After sending the design for manufacturing, a better stress intensity solution that did not have the restrictions of the first solution was found and used for this work.

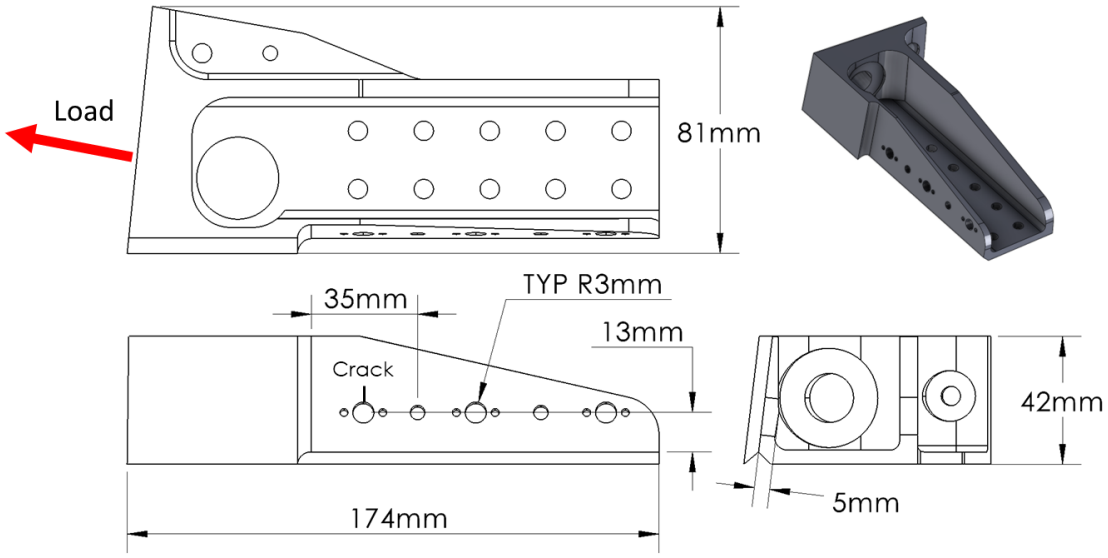

Figure 24. Example aerospace component from large military aircraft.

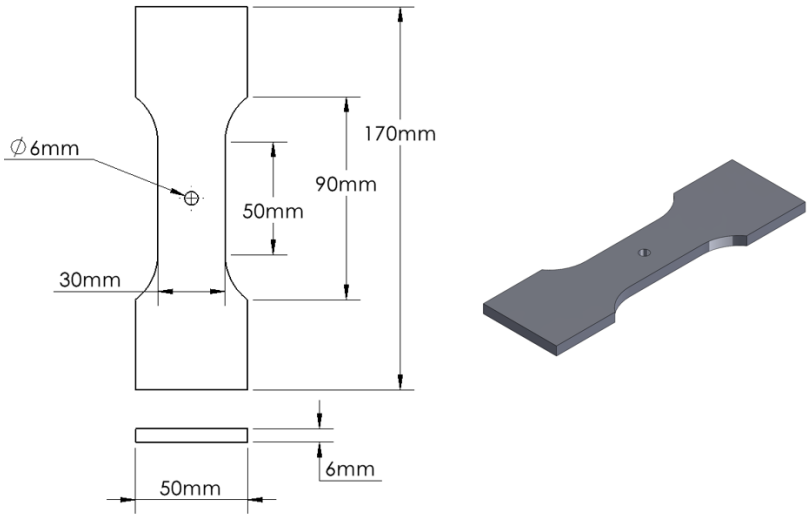

Figure 25. Custom specimen geometry.

Notably, for the example component in Figure 24 only one crack emanating from the edge of the hole was typically found. Careful examination of the geometry reveals that the localized region where a crack is found tapers in thickness and therefore less material exists to prevent crack initiation. This will not always be the case so it was decided to design the custom specimen with a single thickness and assume two cracks of roughly equal length would develop at the edge of the hole. For a specimen of finite dimensions with a center hole, a numerical fit for the net section stress concentration K_{tn} is given by Pilkey & Pilkey [104] as:

$$K_{tn} = 2 + 0.284\left(1 - \frac{d}{W}\right) - 0.600\left(1 - \frac{d}{W}\right)^2 + 1.32\left(1 - \frac{d}{W}\right)^3 \quad (14)$$

where d is the diameter of the hole and W is the gross width of the specimen perpendicular to a tensile stress. The general solution for the stress intensity for this specimen with two symmetrical cracks at the edge of the hole is provided in the ASM Handbook, Volume 19 [105] as:

$$K = \varphi_N F_N \sigma \sqrt{\pi a} \quad (15)$$

$$\varphi_N = \frac{0.6865}{\left(0.2772 + \frac{a}{r}\right)} + 0.9439 \quad (16)$$

$$F_N = \sqrt{\sec\left[\left(\frac{\pi}{2}\right) * \left(\frac{r + a}{W/2}\right)\right]} * \sqrt{\sec\left[\left(\frac{\pi}{2}\right) * \left(\frac{2r}{W}\right)\right]} \quad (17)$$

where φ_N is the geometry parameter for a specimen of infinite width, F_N is an adjustment to the geometry parameter for a specimen of finite width and r is the radius of the hole. The secant functions are evaluated in radians. In practice, it is inevitable that aerospace components will experience variable amplitude loading throughout their service life. Fatigue analysis under variable amplitude is typically addressed by a rainflow-counting algorithm. For this analysis using a variable amplitude loading was deemed unnecessary for developing a model, as results would be dependant on the selected loading spectrum and optimization of the functional grading to target a specific range of stress amplitudes in the spectrum. The model therefore assumes a constant amplitude loading. In aerospace it is common for fatigue modelling to be conducted with a stress ratio of R = 0.1 as many components experience tension only loading during their service life. The stress ratio of R = 0.1 was therefore adopted for this analysis to best represent an aerospace component.

3.4. Functional Grading Selection

In terms of fatigue, only variables that have an impact on the strain-life or crack growth rate of the material will influence the application of a functional grading. In selecting what properties of the E-PBF Ti-6Al-4V material to grade, the alpha lath size was identified

based on the literature references in Section 2.1 that demonstrated the capability to control machine process parameters during manufacturing. The definition of the potential function is arbitrary as it is normalized between 0 and 1. What is important is that whatever logic is used to define the potential function is consistent throughout the analysis. It was decided that one potential function would be used for analyzing the selected geometry to limit the number of variables in the analysis. The potential function and a depiction of the resultant grading of the component is shown in Figure 26. The potential function was defined at the tip of an initiated crack rather than at the edge of the hole or the center of the specimen so that if a different initial crack length is assumed then the potential function is offset according to the tip of the new initial crack size. Since initial cracks are often small and the material would likely be strengthened in the region of the notch, changes in material properties are likely to be minimal if a functional grading were applied along the length of the initial crack. The potential function in Figure 26 is defined with both the length of the grading L and the value of the potential function *P* between 0 and 1. By normalizing the length L, the value of the potential function can be recalculated if the specimen geometry is changed. Additionally, the value of the potential function can be determined as a percentage. The limits of the value of crack length are therefore between the initial crack a_0 and the edge of the specimen for the geometry shown in Figure 26. The value of the potential function was defined with 1 being the HARD material and 0 being the SOFT material as it was felt this mapping would provide an intuitive relationship between the physical scenario and the potential function when represented on a drawing of the specimen.

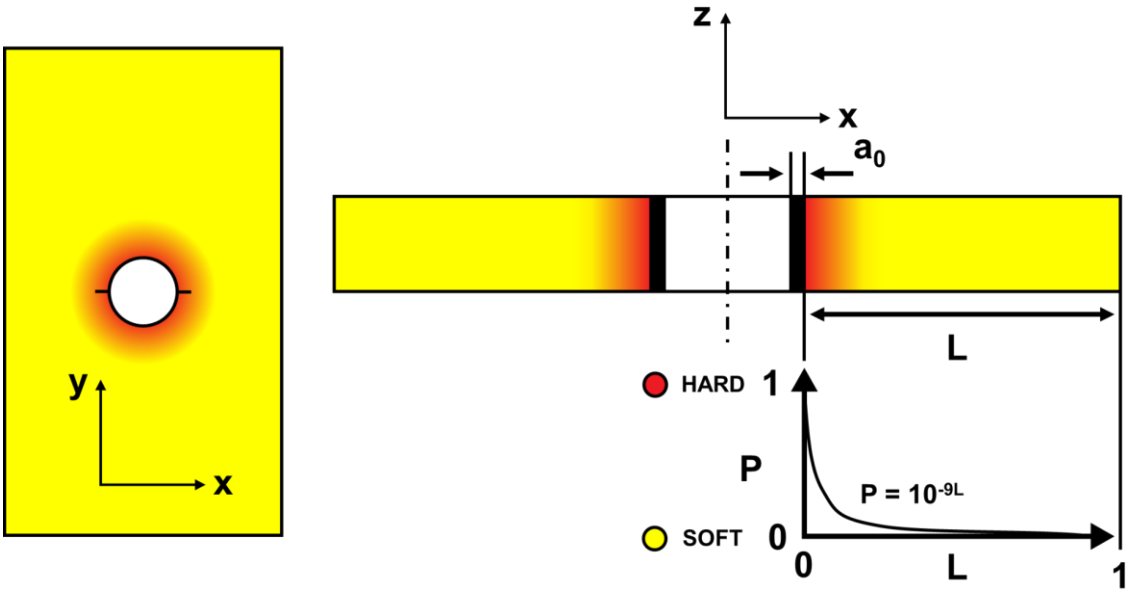

Figure 26. Custom graded specimen potential function.

The applied potential function was selected based on two pieces of knowledge; that harder materials tend to have greater fatigue crack initiation life but lesser fatigue crack growth life than softer materials (and vice-versa) and that at the transition crack length the influence of the stress concentration is generally minimized. From this insight, a design choice that likely maximizes the total fatigue life of the specimen is to grade from a hard

material until the transition crack length, followed by a transition to a softer material. This description may be characterized mathematically as a decaying function. For this work the equation $P = 10^{-9L}$ was chosen as the potential function. The function was established by setting a limit on the transition from HARD to SOFT E-PBF Ti-6Al-4V material. The limit was defined according to when the value of the potential function represents 10% HARD material and the location along the length L is between two to three times the transition crack length a_0. The 10% HARD material boundary was set because with a continuous grading it can be difficult to determine the exact location where the transition occurs. This offset ensures a clear delineation of the end of the grading while minimizing the variation in the change of the material boundary over a small distance. The two to three times transition length requirement was set because the transition length is an estimate based on empirical data. Tested specimens may result in slightly longer or shorter initiated cracks than the estimate. To ensure that the region around the notch in the specimen remains strengthened by the HARD material, the length of the grading in the direction of L provides a buffer to account for some variation. A plot of the selected potential function that shows how the resulting grading meets the established requirements is shown in Figure 27. The determination of how rapidly the change in properties should occur is an optimization challenge that requires more information and research.

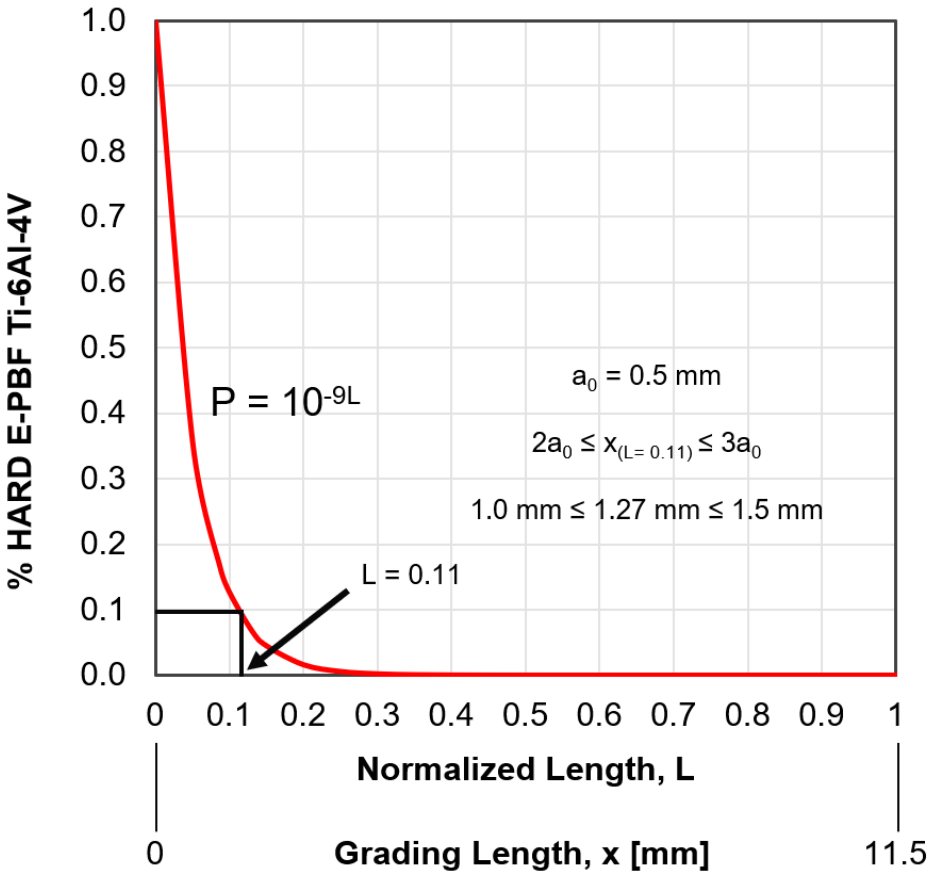

Figure 27. Potential function definition.

3.5. Mapping Potential Function to Stress Intensity

The key concept that permits a functional grading to be included in a fatigue crack growth model is the mapping of the potential function to the stress intensity for a given geometry. To permit the mapping there are a few criteria that must be met. First, for two materials to be graded each must have a distinct crack growth curve. Second, if a two-dimensional potential function is applied, then the component must accordingly be simplified to two-dimensional crack growth. Lastly, the geometry factor for the given specimen must be known and valid for the range of loadings to be applied. The process for mapping a potential function to a stress intensity and determining the graded crack growth rate is shown in Figure 28. At a given crack length the stress intensity is calculated for a given geometry factor and applied loading. Next, the crack growth rates for the two materials to be graded are determined using the calculated stress intensity. Starting at the tip of the initiated crack and extending a unit length L, the value of the potential function is found by observing that the crack length is along the length of L, or that $a = L$. The value of the crack growth rate for the functionally graded component is then determined by adding the value of the crack growth rate of the SOFT material to the difference in the HARD and SOFT material crack growth rates multiplied by the value of the potential function. Since the potential function was normalized between 0 and 1 this step can be thought of as the percentage of the crack growth rate between the HARD and SOFT material. The fatigue model for a different geometry would only require that a stress intensity solution exists. Any potential function can therefore be mapped to any crack growth rate using the same process.

An example of a crack growth curve created by mapping of the custom specimen from Section 3.3 and the potential function from Section 3.4 at an applied maximum load of 30 kN using the HARD and SOFT E-PBF Ti-6Al-4V materials is shown in Figure 29. The interpretation of Figure 29 is that the crack growth rate immediately after initiation begins where the graded curve starts and crosses the HARD material curve. The crack growth rate of the graded curve has a negative slope until it reaches the curve for the SOFT material. A physical interpretation to explain the negative slope is to visualize the crack growth curve for a discrete graded specimen of HARD and SOFT material. At the boundary of the HARD and SOFT materials the crack growth rate would be instantaneously slowed as the crack transits across the boundary. The graded material represents a smoothed slowing of crack growth. In this way the graded curve models the material crack growth response according to the change in material properties.

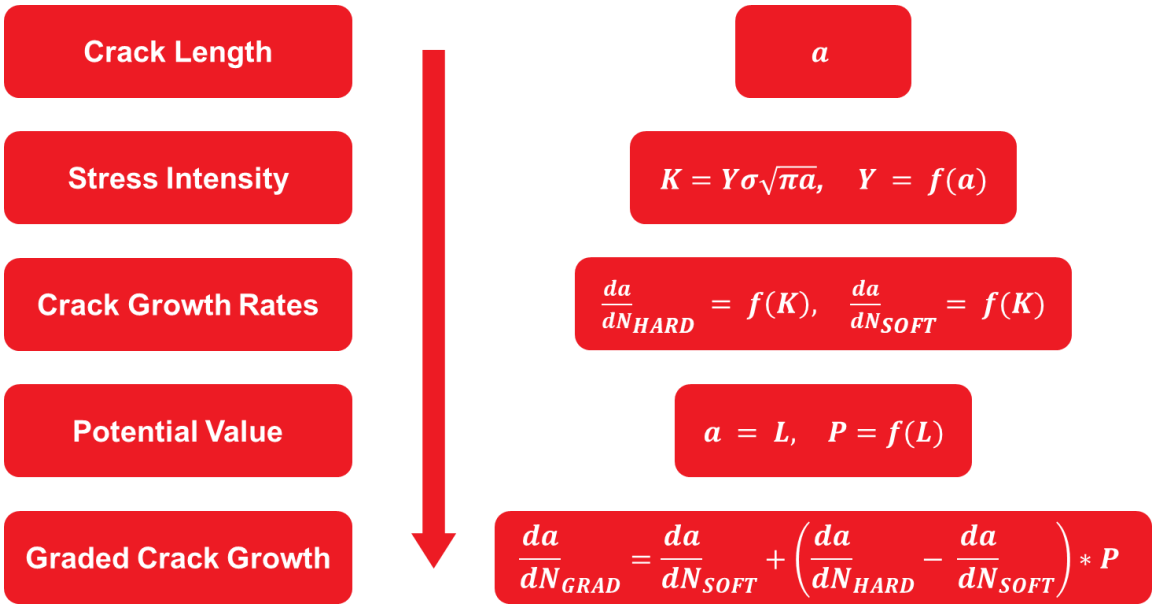

Figure 28. Process to map potential function to crack growth in a FGM.

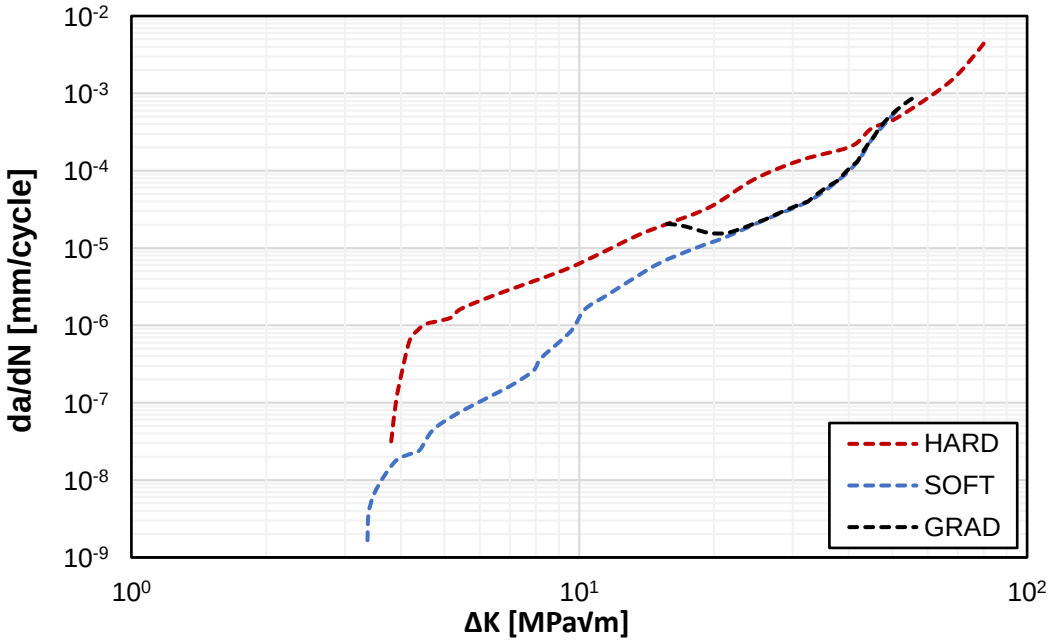

Figure 29. Example FGM crack growth curve, potential function P = 10^{-9L}.

3.6. Material Specifications

To create the desired functional grading two unique material specifications are required. For this thesis the two materials were labelled as HARD and SOFT. To permit a comprehensive understanding of the physical situation, all available information in the literature was used to specify as many variables within the PSPP framework as defined in Figure 22. A summary of the PSPP variables for the HARD and SOFT materials are shown in Table 5. Values with an asterisk indicate that either the value was assumed or calculated using information from the identified references. The key takeaway from Table 5 is that it is not possible to link all parts of the PSPP framework with the available information. A contributing factor to this challenge is the use of proprietary algorithms that manage machine parameters during the manufacturing of specimens. The given references identified which machine and build “theme” was used to manufacture specimens but since the parameters are varied live during the build, theme settings are of limited use. Without details of the machine algorithms or access to a readout of parameter data from the build, it is difficult to link process parameters to a specific grain morphology. From the perspective of the machine manufacturer and machine users, using the manufacturer’s recommended settings improves reliability and repeatability of final component properties and avoids voiding the machine warranty. The significant disadvantage is that the presented performance windows are of limited use when build themes are used. From a research perspective, full control and traceability of all parameters is preferrable because applying a functional grading of alpha lath size reliably using E-PBF Ti-6Al-4V depends on linking machine parameters directly to the resultant grain size. Recognizing the limitations in linking machine process parameters to grain size, the Hall-Petch relationship estimated from numerous sources was used to estimate alpha lath size from the material yield strength of the HARD and SOFT materials.

Table 5. HARD and SOFT Material Data, E-PBF Ti-6Al-4V

	Parameters		Material			
	Description	**Units**	**HARD**	**Ref.**	**SOFT**	**Ref.**
Process	E-Beam Current	mA	variable	[36,43]	variable	[38,42]
	E-Beam Voltage	kV	60*	[36,43]	60*	[38,42]
	E-Beam Scan Speed	m/s	variable	[36,43]	variable	[38,42]
	Layer Height	µm	50	[43]	50	[42]
	Hatch Spacing	µm	200*	[106]	220	[38]
	Focus Offset	mA	19*	[106]	19*	[106]
Structure	Alpha Lath Size	µm	1.6*	Figure 10	7.9*	Figure 10
Property	Cyclic Strength Coefficient, K'	MPa	1710	[36]	1460	[38]
	Cyclic Strain Hardening Exponent, n'	-	0.11	[36]	0.088	[38]
	Fatigue Strength Coefficient, σ'_f	MPa	1935	[36]	2327	[38]
	Fatigue Strength Exponent, b	-	-0.087	[36]	-0.14	[38]
	Fatigue Ductility Coefficient, ε'_f	-	0.13	[36]	89.4	[38]
	Fatigue Ductility Exponent, c	-	-0.546	[36]	-1.49	[38]
	Modulus of Elasticity, E	GPa	108.8	[36]	122	[38]
Performance	Cyclic Yield Strength, S_Y	MPa	877*	[36]	757*	[38]
	Plane Strain Fracture Toughness, K_{IC}	MPa$\sqrt{m}$	60* (avg)	[43]	56.6	[42]
	Crack Growth Rate, da/dN vs ΔK	mm/cycle vs. MPa$\sqrt{m}$	see Ref.	[43]	see Ref.	[42]

*Value assumed or calculated using information available in identified references.

3.7. Total Fatigue Life Analysis - Matlab Application

To permit quick analysis of total fatigue life in FGMs, the relationships for crack initiation, crack growth, and functional grading using a potential function were integrated into an application that can be run using Matlab. This application inevitably required scripting, which was established to be avoided at the outset of this thesis. However, the development of an application was strictly an academic exercise with the intent of conducting many runs at different maximum gross stresses and different material gradings. The program logic in the back-end of the app can be completed using manual methods like Microsoft Excel or pen and paper.

The Total Fatigue Life Analysis application allows a user to input component dimensions, apply a cyclic loading, input strain-life parameters, select crack growth data, and apply a functional grading. The application uses the conventional crack initiation and crack growth equations presented in the background section of this thesis. The application completes the calculations and provides an output of the gross section and notch properties and estimates the crack initiation, crack growth, and total crack life of the component. A screenshot of the Total Fatigue Life Analysis application is shown in Figure 30. Much of the data is integrated directly into the application and may be selected by drop-down menus. Some data like the strain-life curve parameters can be input manually. In the Total Fatigue Life Analysis application there are two drop-down menus for a “Primary Material” and “Secondary Material”. Below the menus is a toggle switch labelled “Graded Material” next to an indicator light that is greyed out when the toggle switch is “off” and shines green when the toggle switch is “on”. If the toggle switch is set to “off” all analysis will be completed with the primary material and the secondary material is ignored. When the switch is “on” then the potential function integrated into the back-end of the application applies a grading from the primary to the secondary material using the two crack growth curves. Crack initiation is always calculated using the selected primary material. The Specimen Geometry, SWT Strain-Life, and Crack Growth Curve figures are updated when the “Load” button located under the toggle switch is pressed. The Specimen Geometry figure will update every time the load button is pressed but the Crack Growth Curve figure will overlay all previous and current crack growth curves in different colours to permit easy comparison. To remove all previous crack growth curves the “Clear” button under the figure must be pressed. Finally, next to “Manual e-N Input” are a “Clear” and a “Load” button. These allow a user to input their own strain-life parameters for calculation. Clicking the “Clear” button sets all fatigue life parameter values to zero.

Although a user interface is not strictly necessary, since Matlab can handle and display the analysis within the main interface, there are several advantages in using one. Firstly, a visual representation of data is useful in ensuring model inputs are correct. From experience using hand calculations, MS Excel, AFGROW or Matlab to analyze total fatigue life, a questionable result could easily occur by forgetting to change an input buried in a long list of numbers, application menus, or lines of code. The visual feedback organized onto a single page offered by the Total Fatigue Life Analysis application helps to minimize these issues and makes incorrect inputs more obvious. Secondly, using back-end data inputs like the strain-life parameters and crack growth curves improves the speed at which different models can be analyzed. By comparison a single run to iterate the SWT crack initiation curve for the number of reversals can be calculated in a manner

of seconds using Matlab whereas the same analysis using the Goal Seek Function in MS Excel [107] took approximately 5-10 minutes. Finally, a visual interface permits an intuitive interpretation of inputs and results by demonstrating the impact on the crack growth curve from application of a functional grading and by displaying the crack length at fracture on the initial component in a single display window. The Total Fatigue Life Analysis application is one example of applying the fatigue model for FGMs; the application itself is not the model. A full copy of the application with back-end code is available upon request to the author.

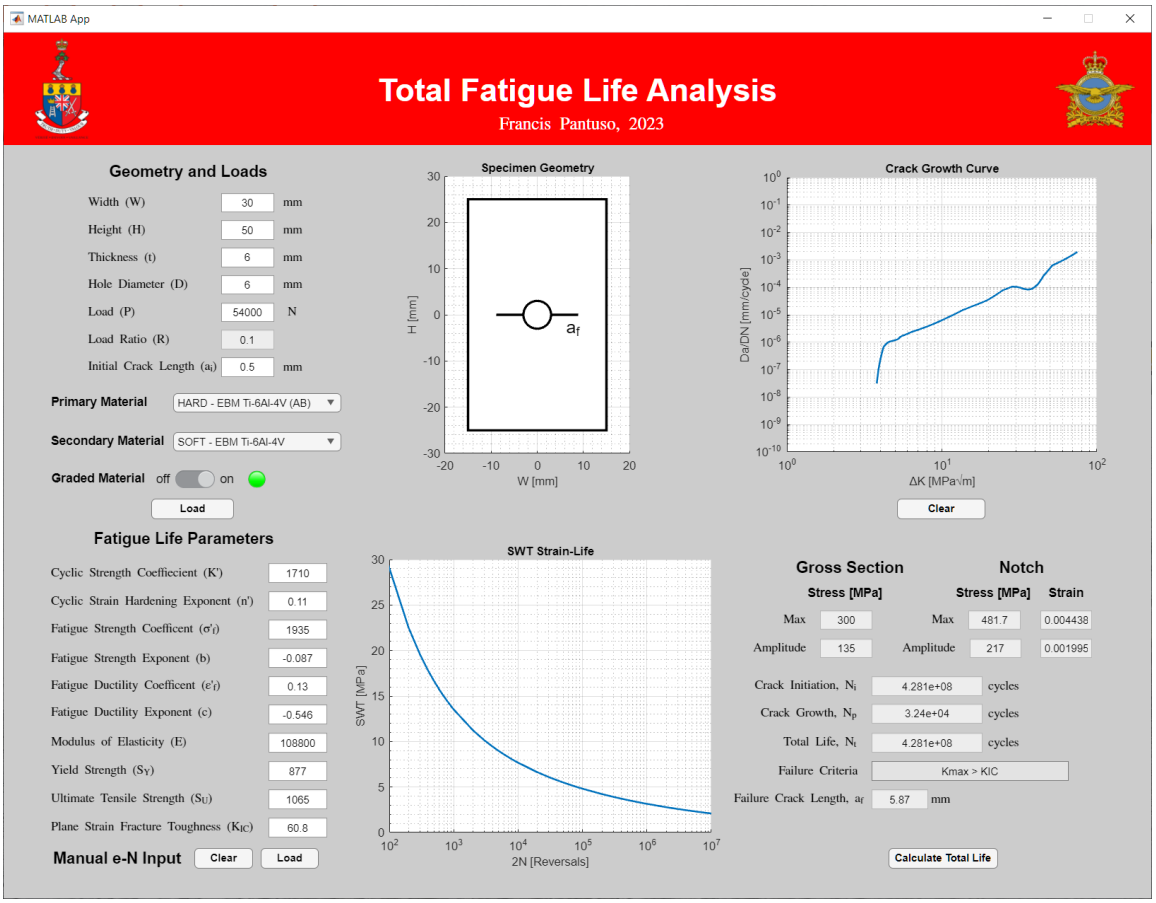

Figure 30. Screenshot of the Total Fatigue Life Analysis Matlab Application.

3.8. Fatigue Model Verification

To ensure that the model designed in Matlab reflects realistic estimates of fatigue life, a comparison of results was made to those from the commercial software AFGROW and by manual calculation using Microsoft Excel for an ungraded specimen. The use of Microsoft Excel is intended to demonstrate the simplicity and accessibility of applying the model using conventional methods. The use of a code in Matlab is to demonstrate that the model can be presented in an alternative format while still employing conventional fatigue life methods. The advantages of the Matlab code are the speed of calculation and flexibility in presenting the results. The basic code in Matlab was tested before the development of the Total Fatigue Life Analysis application.

Comparison of results was completed using the custom geometry and the HARD material properties for various values of maximum gross stress. The results from AFGROW were used as the baseline. A comparison of the estimated crack initiation life is shown in Figure 31. For all values of maximum stress, the initiation life using Microsoft Excel and Matlab were equivalent. The percentage difference between the Microsoft Excel and Matlab values and the baseline were underestimates of initiation life of between 2-5%. The percentage difference tends to increase as the maximum stress decreases. A comparison of the estimated crack growth life is shown in Figure **32**. The estimate using Microsoft Excel tended to underestimate the crack growth life compared to AFGROW, while the estimates using the Matlab script tended to overestimate the crack growth life compared to AFGROW. In general, crack growth life estimates were different by an average of 1200-1300 cycles. The discrepancies in the estimates are likely caused by the way the three approaches manage iteration in calculating the crack growth life. From this analysis, the Matlab script was confirmed to agree with the commercial software and was used as the basis for development of the Total Fatigue Life Analysis application. This exercise also demonstrated that, while a custom application was completed for convenience, the analysis can also be completed manually and provide results that agree with commercial software.

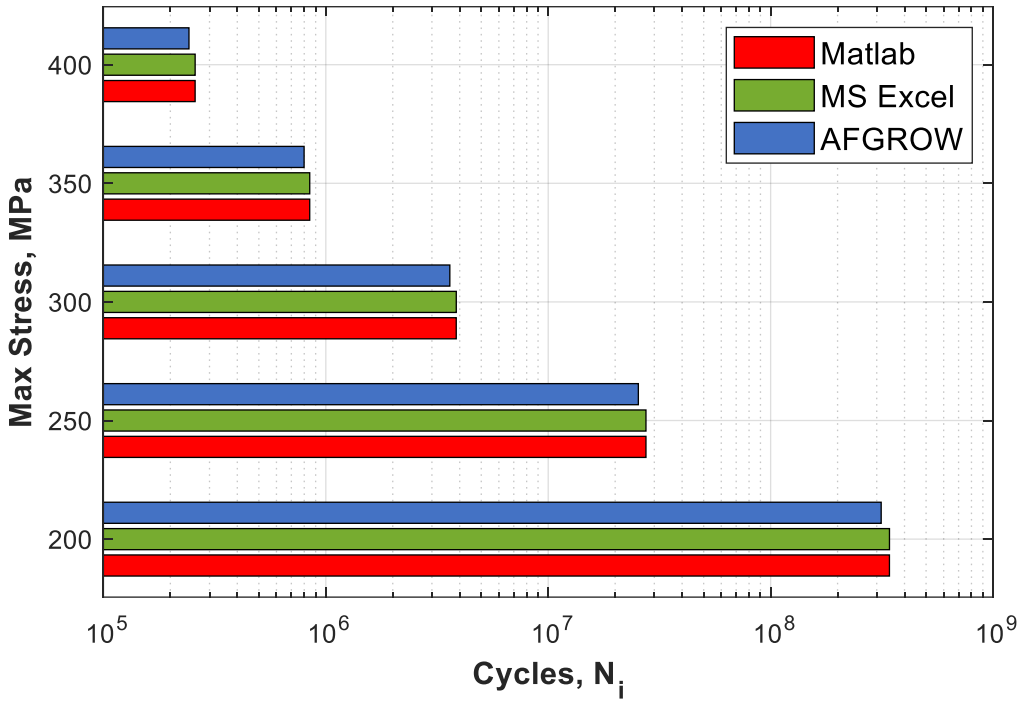

Figure 31. Comparison of cycles to crack initiation by software model.

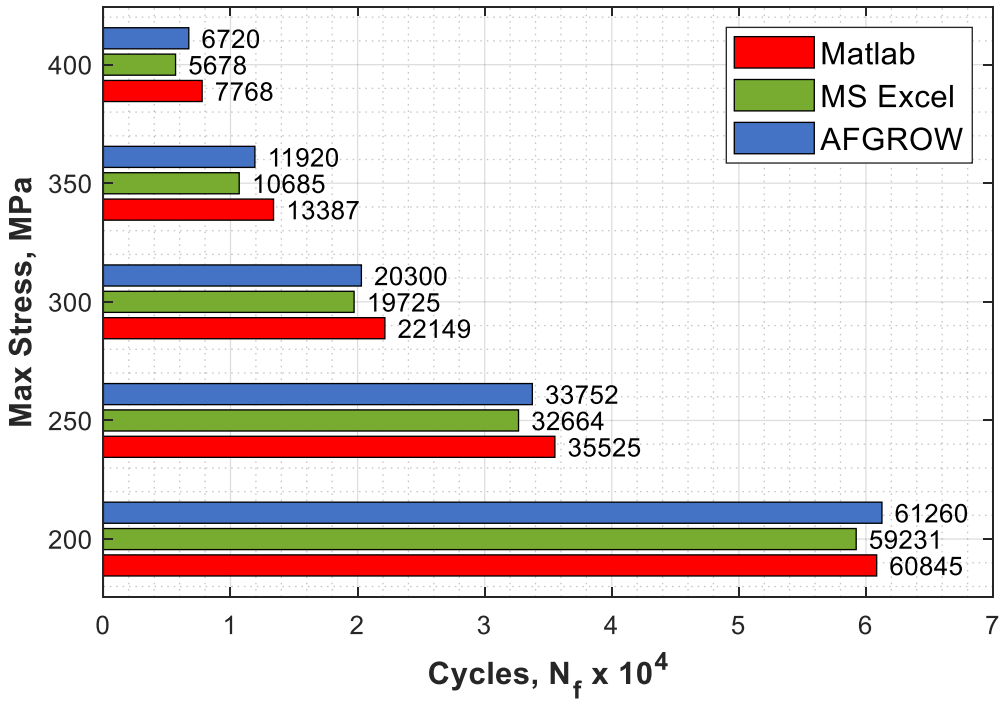

Figure 32. Comparison of crack growth cycles to failure by software model.

4. Results

4.1. Graded E-PBF Ti-6Al-4V Alpha Lath Case

Using the geometry from Figure 25, a stress ratio of R = 0.1, an applied maximum load of 54 kN, and a grading defined by the potential function of $P = 10^{-9L}$, the developed fatigue model was used to evaluate and compare the crack growth life of an ungraded and a graded specimen. This section provides an example calculation to demonstrate how the model is applied explicitly in the Total Fatigue Life Analysis application. For this analysis, crack initiation was ignored as the HARD material will be in the region from the notch to the initial crack length for both the ungraded and graded specimens. From a theoretical standpoint there would be no difference in the crack initiation life of the two specimens. First, the gross stress range is determined by considering the geometry of the component and the applied loading. The gross stress and gross stress range are calculated as:

$$\sigma_{max} = \frac{F}{A} = \frac{54000\ N}{30\ mm * 6\ mm} = 300 MPa$$

$$\Delta\sigma = \sigma_{max}(1 - R)$$

$$\Delta\sigma = 300\ MPa(1 - 0.1) = 270\ MPa$$

Next, the initial crack size is estimated by finding the transition crack length. Using the geometry of the specimen:

$$l_t = 0.13\sqrt{D\rho}$$

$$l_t = 0.13\sqrt{6\ mm * 3\ mm}$$

$$l_t = 0.55\ mm$$

Since the value is only an estimate the transition crack length was assumed to be 0.50 mm. This assumption is conservative in terms of total fatigue life as it implies that the initiated crack is still in the influence of the notch. The initial crack size a_0 inputted into the Total Fatigue Life Analysis application for analysis was therefore 0.50 mm. Estimation of the number of cycles to failure by analytical methods may be arduous in cases where the geometry parameter is a function of the crack length. A generalized form of the integral for the number of cycles to failure is stated as:

$$N_f = \int_{a_0}^{a_f} \frac{1}{C(\Delta K)^m} da = \int_{a_0}^{a_f} \frac{1}{C\left(Y\Delta\sigma\sqrt{\pi a}\right)^m} da$$

An alternative is to estimate the integral by numerical integration assuming a small increment of crack growth. For estimates using manual calculation increments of crack growth of 0.01 mm were used and it was assumed that this was a suitably small increment to avoid significant errors when using numerical integration. For estimates in the Total

Crack Analysis app a smaller increment of 0.001 mm was used as there was no significant impact to calculation time. The trapezoid rule for numerical integration was applied, which approximates the value of an integral as:

$$N_i = \int_{a_0}^{a_i} \frac{1}{da/dN} da \approx \frac{1}{2}\left(\frac{1}{da_o/dN} + \frac{1}{da_i/dN}\right) * (a_i - a_0)$$

Following the evaluation of the numerical integration, the resultant value of crack length is set as the new initial crack length, the increment is increased, and the number of cycles is estimated for the next increment. The total number of cycles to failure is then calculated as:

$$N_f = \Sigma N_i$$

To facilitate this estimate, values of the crack growth rate must be determined for the initial and incremented crack growth length. This is completed by first calculating the stress intensity range at the initial crack length using the information of the geometry and loads.

$$\Delta K = \varphi_N F_N \Delta\sigma\sqrt{\pi a}$$

$$\varphi_N = \frac{0.6865}{\left(0.2772 + \frac{a}{r}\right)} + 0.9439$$

$$\varphi_N = \frac{0.6865}{\left(0.2772 + \frac{0.5\ mm}{3\ mm}\right)} + 0.9439$$

$$\varphi_N = 2.491$$

$$F_N = \sqrt{\sec\left[\left(\frac{\pi}{2}\right) * \left(\frac{r+a}{W/2}\right)\right]} * \sqrt{\sec\left[\left(\frac{\pi}{2}\right) * \left(\frac{2r}{W}\right)\right]}$$

$$F_N = \sqrt{\sec\left[1.571 * \left(\frac{3\ mm + 0.5\ mm}{30\ mm/2}\right)\right]} * \sqrt{\sec\left[(1.571) * \left(\frac{2 * 3\ mm}{30\ mm}\right)\right]}$$

$$F_N = 1.061$$

$$\Delta K = 2.491 * 1.061 * 270\ MPa \sqrt{\pi * \left(0.5\ mm * \frac{1\ m}{1000\ mm}\right)}$$

$$\Delta K = 28.3\ MPa\sqrt{m}$$

Using the calculated stress intensity range the crack growth rate for the ungraded HARD material is found by reading the values on the graph, or in the case of a computer algorithm, by interpolation between points on the crack growth curve. Similarly, the crack growth rate of the GRADED material is found by looking up the values of the crack growth rate for the HARD and SOFT materials, determining the value of the potential function P, multiplying the value of the potential function by the difference in crack growth rate between the HARD and SOFT materials and then adding that value to the value for the SOFT material. Using Figure 15 for the HARD and SOFT material crack growth rates at $\Delta K = 28.4\ MPa\sqrt{m}$:

$$\frac{da}{dN_{HARD}} = 1.10 * 10^{-4}\frac{mm}{cycle}$$

$$\frac{da}{dN_{SOFT}} = 2.92 * 10^{-5}\frac{mm}{cycle}$$

$$P = 10^{-9(0)} = 1$$

$$\frac{da}{dN_{GRADED}} = \frac{da}{dN_{SOFT}} + \left(\frac{da}{dN_{HARD}} - \frac{da}{dN_{SOFT}}\right) * P$$

$$\frac{da}{dN_{GRADED}} = \left[2.92 * 10^{-5} + \left((1.10 * 10^{-4}) - (2.92 * 10^{-5})\right) * 1\right]\frac{mm}{cycle}$$

$$\frac{da}{dN_{GRADED}} = 1.10 * 10^{-4}\frac{mm}{cycle}$$

The crack growth rate of the GRADED specimen matches that of the ungraded HARD specimen since the value of the potential function is 1 at the initial crack length. Since the crack has not yet grown, the number of cycles N is set to zero for the first round of calculation. To estimate the number of cycles between the initial crack and the first increment of crack growth of 0.01 mm the same process is applied to calculate the stress intensity range and crack growth rates. A summary of the resultant calculated values for $a = 0.51\ mm$ is as follows:

$$\varphi_N = 2.479$$

$$F_N = 1.061$$

$$\Delta K = 28.4\ MPa\sqrt{m}$$

$$\frac{da}{dN_{HARD}} = 1.12 * 10^{-4}\frac{mm}{cycle}$$

$$\frac{da}{dN_{SOFT}} = 2.96 * 10^{-5}\frac{mm}{cycle}$$

The value of the potential function is determined by observing that the current crack length is some percentage distance from the initial crack length and the end of the grading at the edge of the specimen at length L. By inspection, the length of the grading extends from the initial crack a_0 to the specimen edge 15 mm from the centerline. The total length the crack can grow is therefore:

$$L = \frac{W}{2} - r - a_0$$

$$L = \frac{30\ mm}{2} - 3\ mm - 0.5\ mm$$

$$L = 11.5\ mm$$

Normalizing the length vector L between zero and one:

$$L(0) = a_0 = 0.5\ mm \qquad L(1) = 11.5m\ m$$

The normalized value of L for the current crack length a can, therefore, be calculated by the following relationship:

$$L(a) = \frac{a - a_0}{L(1) - a_0}$$

$$L(0.51) = \frac{0.51 - 0.50}{11.5 - 0.50}$$

$$L(0.51) = 0.00091\ or\ 0.091\%$$

The value of the potential function for the first increment of crack growth is therefore:

$$P = 10^{-9(0.00091)} = 0.98$$

The same method as before can now be applied to estimate the crack growth rate of the GRADED specimens when $a = 0.51\ mm$:

$$\frac{da}{dN}_{GRADED} = \left[2.96 * 10^{-5} + \left((1.12 * 10^{-4}) - (2.96 * 10^{-5})\right) * 0.98\right] \frac{mm}{cycle}$$

$$\frac{da}{dN}_{GRADED} = 1.10 * 10^{-4}\ \frac{mm}{cycle}$$

Observe that the crack growth rate was not affected by the increment of crack growth. This is understandable given that over such a small increment of crack growth the grading defined by the potential function did not change significantly. However, as the potential function defines a decay from the HARD to SOFT material, it can be expected the crack

growth rate will decay accordingly in further iterations. Now that there are at least two values of crack growth length and crack growth rate for the HARD and GRADED specimens numerical integration is used to estimate the number of cycles the specimen experienced to grow the crack over the increment:

$$N_{HARD} = \frac{1}{2}\left(\frac{1}{1.10 * 10^{-4}} + \frac{1}{1.12 * 10^{-4}}\right)\frac{cycles}{mm} * (0.51 - 0.50)\, mm$$

$$N_{HARD} = \frac{1}{2}(9091 + 8929)\frac{cycles}{mm} * (0.01)\, mm$$

$$N_{HARD} = 90\, cycles$$

$$N_{GRADED} = \frac{1}{2}\left(\frac{1}{1.10 * 10^{-4}} + \frac{1}{1.10 * 10^{-4}}\right)\frac{cycles}{mm} * (0.51 - 0.50)\, mm$$

$$N_{GRADED} = \frac{1}{2}(9091 + 9091)\frac{cycles}{mm} * (0.51 - 0.50)\, mm$$

$$N_{GRADED} = 91\, cycles$$

From the first increment of crack growth, it is notable that the GRADED specimen achieved one more cycle than the HARD specimen. As the influence of the softer material increases it can be expected that this trend will continue. It is the continually decreasing crack growth rate as a function of the grading that results in an extended crack growth life. This example demonstrates results for the manual approach to estimating crack growth in a functionally graded specimen. Using the same methodology programmed into the Total Fatigue Life Analysis Matlab application the fatigue crack growth life was calculated for the specimen for five values of maximum gross stress using the HARD and GRADED E-PBF Ti-6Al-4V materials. The values of maximum gross stress were initially estimated by calculating crack growth for maximum stresses between 30-50% of the material yield stress (approximately 300-500 MPa). Values of maximum gross stress were then further refined by setting the goal of achieving between 10^3 and 10^7 cycles during crack growth. This resulted in maximum loads between 200-400 MPa for the given specimen geometry and material. A comparison of the crack growth life with the HARD material as the baseline is shown in Figure 33 for five maximum gross stresses. The percentages affixed to the GRADED material are percent increase in number of cycles compared to the HARD material. From this comparison the crack growth life was improved for all cases by functional grading of the alpha lath size using the defined potential function.

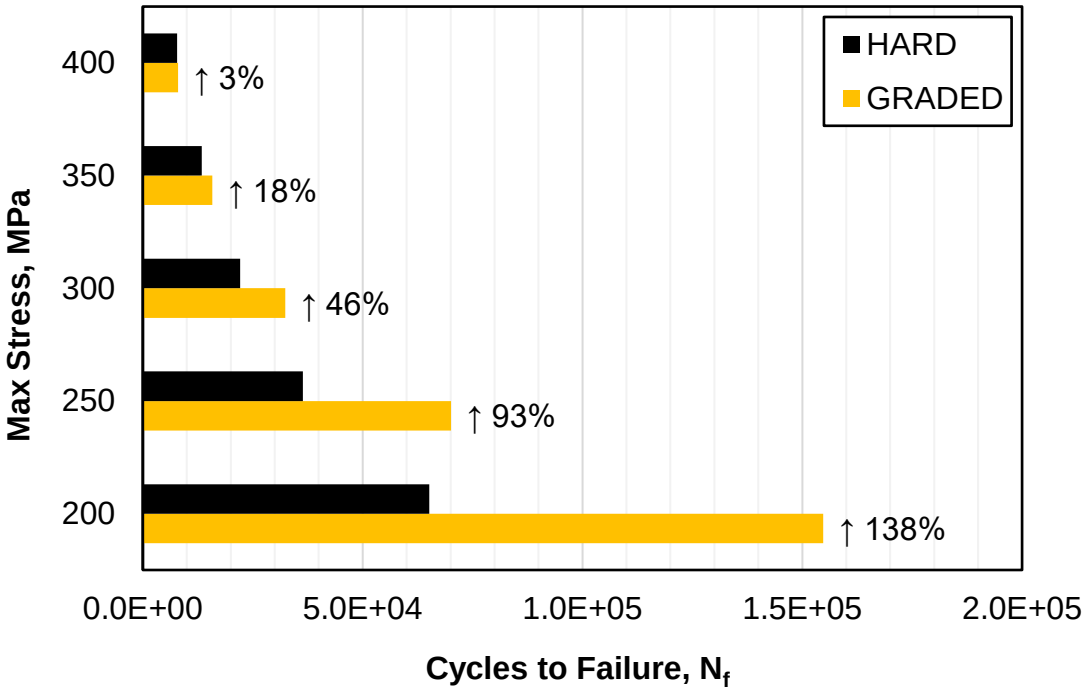

Figure 33. Crack growth life comparison for ungraded and graded E-PBF Ti-6Al-4V materials.

4.2. Graded Material Composition Case

From observation of the results of the first case it is plausible that further improvements in fatigue life could be realized by taking advantage of the significant life that occurs in the crack initiation phase. An alternative to functional grading by grain morphology is to grade by material composition. Table 3 highlighted that most functional grading examples in the literature using Ti-6Al-4V feedstock employed mixtures of different material compositions and DED AM. The key advantage of DED is that the chemical composition of the melt pool can be controlled by precise mixture of two metal feedstocks according to a functional grading. This control of the mixture is an opportunity for specifying graded material properties that improve both crack initiation and crack growth phases of total fatigue life.

A grading of material composition that improves both crack initiation and growth could be advantageous in replacing legacy aircraft components with ones of improved, engineered design. In the RCAF there remains a multitude of aircraft of primarily aluminium construction, as was popular when the aircraft were procured. Due to the age and condition of several aircraft fleets there exists a long history of structural integrity monitoring and, therefore, the critical aircraft components with known failure modes are relatively easy to identify. If a component is identified as suitable for AM, a preliminary viewpoint could be to seek a replacement using AM using the same or similar aluminium alloy. In the case of legacy parts this option may be cheaper or faster than contracting a new production line for a small run of components. While this could solve the issue it does

not take advantage of the opportunities afforded by AM. Another possibility is to replace the component with one of greater strength, say using Ti-6Al-4V. This is an undesirable solution as the difference in the material properties between the replacement component and the surrounding aluminum structure would likely cause new failures in the weaker aluminium material.

The example aerospace component from Figure 24 is made from 7075-T6 aluminum. The 7000 series aluminum alloys are known for their high strength but are less suitable for damage tolerant designs compared to other aluminum alloys. As an example case, it was decided to strengthen the hole of the custom specimen using Ti-6Al-4V and grade to 7075-T6 material to improve total fatigue life using DED AM. It is hypothesized that functionally grading the component with the harder and stronger Ti-6Al-4V close to the region of stress concentration will significantly improve the crack initiation life compared to the ungraded 7075-T6 component. The bulk of the component will consist of 7075-T6 material, therefore, the mismatch of material properties with the surrounding aluminium structure is minimized.

For this case it is assumed that mixing of the powders is fully controllable during processing and that any composition of the two materials will result in fully dense parts with material compatibility. The compatibility assumption is supported by the previous observation by Reichardt et al. [54] that Ti-6Al-4V is the most compatible metal feedstock for mixing with other metals available for DED AM, including when mixing with aluminium alloys. The same geometry from Figure 25, stress ratio of R = 0.1, and grading defined by the potential function of $P = 10^{-9L}$ as the previous case are used. The applied loading, however, is adjusted to be suitable for the 7075-T6 material using a similar logic as before: By testing values between 20-50% of max stress of the 7075-T6 material. Using the Total Fatigue Life application and 7075-T6 material data from AFGROW the range of maximum stresses was determined to be between 100-300 MPa. The crack initiation life is determined by applying Neuber's rule [30] to find the maximum notch stress-strain response assuming the E-PBF Ti-6Al-4V material properties are like those of DED Ti-6Al-4V. Recall that for E-PBF Ti-6Al-4V it was estimated that notch sensitivity $q = 0.4$.

$$K_f = 1 + q(K_t - 1)$$

$$K_t = 2 + 0.284\left(1 - \frac{d}{W}\right) - 0.600\left(1 - \frac{d}{W}\right)^2 + 1.32\left(1 - \frac{d}{W}\right)^3$$

$$\frac{d}{W} = \frac{6\ mm}{30\ mm} = 0.2$$

$$K_t = 2 + 0.284(1 - 0.2) - 0.600(1 - 0.2)^2 + 1.32(1 - 0.2)^3$$

$$K_t = 2.52$$

$$K_f = 1 + 0.4(2.52 - 1)$$

$$K_f = 1.6$$

Using 200 MPa maximum gross stress as an example, the notch stress-strain repsonse is calculated using material properties and by iteration of the max-stress:

$$\sigma\left[\frac{\sigma}{E}+\left(\frac{\sigma}{K'}\right)^{1/n'}\right]=\frac{\left(K_f S\right)^2}{E}$$

$$\sigma\left[\frac{\sigma}{108800\ MPa}+\left(\frac{\sigma}{1710\ MPa}\right)^{1/0.11}\right]=\frac{(1.6*200\ MPa)^2}{108800\ MPa}$$

$$\sigma\left[\frac{\sigma}{108800\ MPa}+\left(\frac{\sigma}{1710\ MPa}\right)^{1/0.11}\right]=0.941\ MPa$$

$$guess\ \sigma=250\ MPa$$

$$250\ MPa\left[\frac{250\ MPa}{108800\ MPa}+\left(\frac{250\ MPa}{1710\ MPa}\right)^{1/0.11}\right]=0.941\ MPa$$

$$250\ MPa[0.00230+2.6*10^{-8}]=0.941\ MPa$$

$$0.575\ \neq 0.941$$

$$guess\ \sigma=300\ MPa$$

$$300\left[\frac{300}{108800}+\left(\frac{300}{1710}\right)^{1/0.11}\right]=0.941$$

$$0.827\ \neq 0.941$$

$$guess\ \sigma=320\ MPa$$

$$320\left[\frac{320}{108800}+\left(\frac{320}{1710}\right)^{1/0.11}\right]=0.941$$

$$0.941=0.941$$

The maximum notch stress is therefore 320 MPa. The same analysis can be completed to determine the minimum notch stress and notch stress amplitude. The stress amplitude is required so that the notch strain amplitude can be determined.

$$\sigma_a=\frac{\sigma_{max}-\sigma_{\min}}{2}=\frac{\sigma_{max}-(\sigma_{max}*R)}{2}$$

$$\sigma_a=\frac{200\ MPa-(200\ MPa*0.1)}{2}$$

$$\sigma_a = 90\ MPa$$

$$guess\ \sigma = 144\ MPa$$

$$145\left[\frac{145}{108800} + \left(\frac{145}{1710}\right)^{9.09}\right] = \frac{(1.6 * 90\ MPa)^2}{108800\ MPa}$$

$$0.191 = 0.191$$

The stress amplitude at the notch is therefore 144 MPa. The determination of the notch strain amplitude is accomplished by recognizing the total strain can be expressed in terms of stress:

$$\varepsilon = \frac{\sigma}{E} + \left(\frac{\sigma}{K'}\right)^{1/n'}$$

$$\varepsilon = \frac{144\ MPa}{108800\ MPa} + \left(\frac{144\ MPa}{1710\ MPa}\right)^{1/0.11}$$

$$\varepsilon = 0.0013$$

The number of cycles to crack initiation is then estimated using the SWT variant of the strain-life equation [30] using the maximum stress and strain amplitude at the notch. The SWT strain-life equation is solved by iteration of the number of reversals. The number of cycles to crack initiation is then half the number of reversals.

$$\sigma_{max}\varepsilon_a = \frac{\left(\sigma_f'\right)^2}{E}\left(2N_f\right)^{2b} + \sigma_f'\varepsilon_f'\left(2N_f\right)^{b+c}$$

$$320MPa * 0.0013 = \frac{(1935\ MPa)^2}{108800\ MPa}\left(2N_f\right)^{2(-0.087)} + 1935\ MPa * 0.13\left(2N_f\right)^{-0.087-0.546}$$

$$0.42 = 34.4\left(2N_f\right)^{-0.174} + 252\left(2N_f\right)^{-0.633}$$

$$2N_f\ guess = 10^6$$

$$0.42 = 34.4(10^6)^{-0.174} + 252(10^6)^{-0.633}$$

$$0.416 \neq 3.1$$

$$2N_f\ guess = 10^9$$

$$0.42 = 34.4(10^9)^{-0.174} + 252(10^9)^{-0.633}$$

$$0.416 \neq 0.93$$

$$2N_f\ guess = 10^{11}$$

$$0.42 = 34.4(10^{11})^{-0.174} + 252(10^{11})^{-0.633}$$

$$0.42 = 0.42$$

$$N_f = \frac{10^{11}}{2} = 5 * 10^{10}\ cycles$$

This process is repeated for any applied gross stress and material given that the material specific parameters are known. The calculation of crack growth is the same as was presented in the previous example except that the grading is applied between the Ti-6Al-4V and 7075-T6 materials. Crack initiation and growth data for 7075-T6 was taken from the AFGROW repository AFMAT. The data was implemented into the Total Fatigue Life Analysis application to help with iterations of analysis. A comparison of the specimen total life using 7075-T6 material and specimen using a graded Ti-6Al-4V to 7075-T6 material is shown in Figure 34 for various values of applied maximum gross stress. The simulations were completed using the Total Fatigue Life Analysis application.

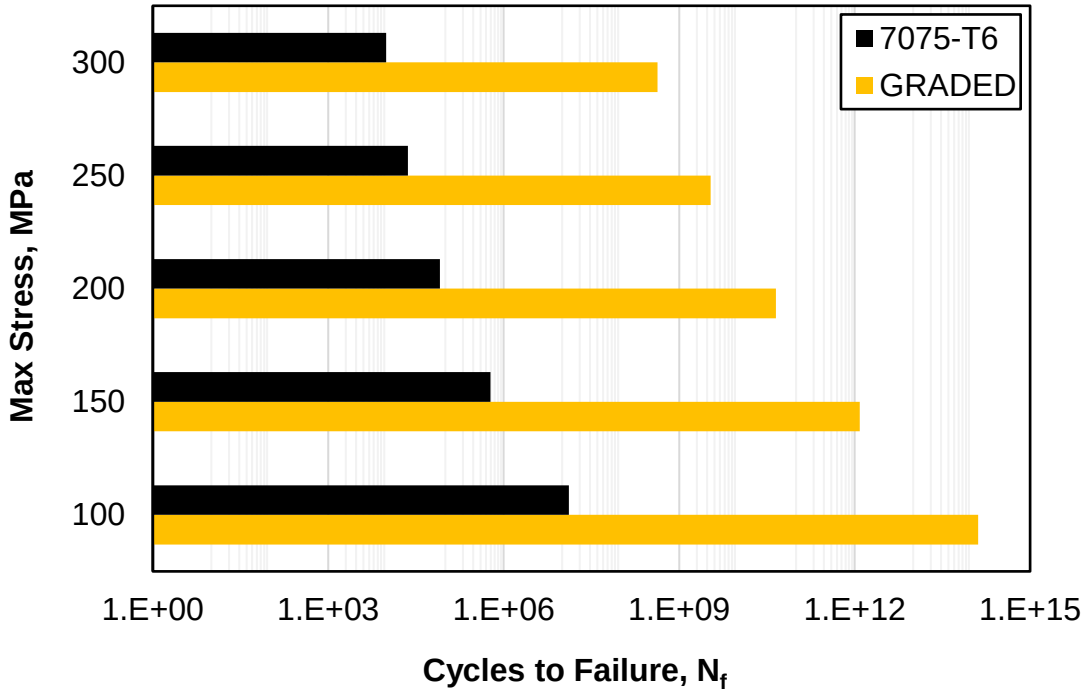

Figure 34. Crack growth life comparison for ungraded 7075-T6 material and graded Ti-6Al-4V to 7075-T6 using DED AM.

5. Discussion

5.1. Input Data and the PSPP Framework

Unlike conventionally manufactured materials there are no openly accessible repositories of material fatigue data for AM materials. For this reason, this research required significant effort to locate and analyze material data. The most comprehensive open repository of material data is the Senvol Database of Additive Manufacturing Machines & Materials [108]. This database lacks information on material fatigue properties, which significantly limits the usefulness when analyzing fatigue. The AFMAT Fracture Mechanics Database [109] included with a subscription to AFGROW is another repository that includes data like fracture toughness and crack growth rates for a small number of tests on some metal AM materials. In both cases the usefulness of the information is limited because the machine parameters and microstructure are not provided with the material performance information. It is likely that repositories of AM data exist but are either blocked by a payment requirement or are being held as intellectual property by the organization that generated the information. This is an unfortunate current reality as it slows the progress of research in the field of additive manufacturing. Regardless, the general lack of AM data related to fatigue is what necessitated a deep review of the literature for this research.

A review of available literature revealed there did not exist studies using a single batch of material with a single AM machine linking all parts of the PSPP framework. This thesis is an attempt to do so with the information available. The effort facilitated the development of a fatigue model for estimating total fatigue life of FGMs, while also revealing what future work would be necessary to improve fatigue life estimates of FGMs. Estimating the E-PBF Ti-6Al-4V microstructure from a given set of process parameters provides an example of the required effort; approximately fifty studies were analyzed to make an estimate. Even with this bulk of information, it was determined that it in most cases it was not possible to directly link process parameters to microstructure due to the use of proprietary algorithms used by E-PBF machines that mask the process parameters during the build. Manual extraction and analysis of micrographs from the studies resulted in an estimate of the Hall-Petch relationship. Although this was completed successfully, the strength of the relationship is weak with an R-squared value of only 0.23. Part of this weakness is attributed to the inconsistency of micrograph image quality, the relatively low number of sample points, and missing process parameter information in the literature like the focus offset. Similarly, a relationship between Vickers hardness and alpha lath size was found, but only in one a few references and for a limited number of runs. At best the determined Hall-Petch and hardness versus alpha lath relationships are rough estimates. This information, however, can be used to cross reference material strength or hardness with the process parameters or fatigue properties from other references which, would not have been possible without the literature review in this work. The key point is that the requirement for many assumptions in this thesis was driven by a lack of material information spanning the PSPP framework.

To address the challenges with AM data that transcend all parts of the PSPP framework, a single batch of bulk feedstock material on a single AM machine would be required with all specimens being manufactured and tested to the same standards. Using this thesis as

an example, a design of experiments approach like the Taguchi method could be used to specify the minimum number of specimens required to determine the statistical significance between machine process parameter settings and material properties. From a simplified perspective, the minimum number of specimens required to define a single material property is typically three (although each testing standard provides the exact minimum). Due to the scatter in material properties identified in the literature and the current lack of AM specific standards, it is expected that this minimum is insufficient. To achieve greater confidence in the experimental data a minimum of five specimens is suggested. Additionally, since multiple specimens are manufactured within an AM machine during a build, to ensure no errors have occurred at least two separate runs should be completed. From this breakdown, it is suggested that for any individual setup of the machine process parameters a minimum of two runs of five specimens is required to obtain reliable results. In reviewing the number of specimens required for this thesis, the testing effort would be a substantial undertaking.

5.2. Characteristics of the developed model

The work in this thesis exists at an intersection of several areas of research, which is highly interesting but also complicates the effort. A Venn diagram of the required prerequisite knowledge is shown in Figure 35. At the intersection of the three circles exists this work. The reality of this multidisciplinary relationship is that locating and comparing previous studies related to this research was difficult. It also complicates the selection of search terms when finding literature in a repository. Analyzing each of the intersecting research areas, there was a significant amount of research available on metal AM particularly E-PBF Ti-6Al-4V. Of these studies there were some focussed on functional grading and there were others focussed on fatigue properties but none could be found that included all three research areas. Expanding the search revealed studies of additively manufactured FGMs and studies on the fatigue properties of FGMs, by AM or other means. Of these works only one could be found on fatigue properties of an AM FGM. This is an important observation because it highlights the novelty of AM and the work that remains to understand AM material properties when considering the design of new engineered components.

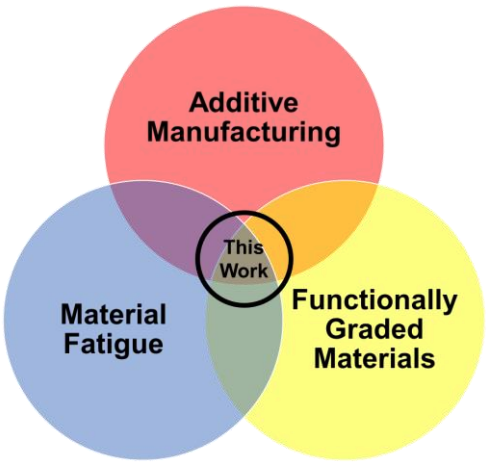

Figure 35. Venn diagram of required knowledge for this study.

In relation to the developed fatigue model, the results indicate potential for significant improvement in total fatigue life when considering the three research areas simultaneously. The strength of the proposed model is in the simplicity of analysis. There is currently no FEA modelling method that permits analysis of FGMs without adapting the software with additional coding. The proposed model, however, uses no adaptations other than setting up the analysis in a common software suite like MS Excel. Once this is completed the remaining challenge becomes accessing reliable data to input into the model. This should serve as motivation for future researchers to increase material testing to permit refinements of the fatigue life estimates calculated using the model.

5.3. Consideration of Initial Assumptions

The total fatigue life model for FGMs and the Total Fatigue Life Analysis Matlab application were created with the intent of demonstrating that the fatigue life of functionally graded components could be estimated without requiring custom scripting in FEA software. Passing forward and backwards through the PSPP framework numerous assumptions were required to permit estimates of total fatigue life of FGM components. To frame the results of this thesis, a review of the necessary assumptions is required.

Firstly, it was assumed that the functional grading of alpha lath size was completely controllable. This assumption was necessary to permit a mapping of a potential function to the crack growth rates of the two materials. While reference work was presented demonstrating that discrete grading is possible, no specific examples were found in the literature of continuously graded E-PBF Ti-6Al-4V. During informal conversations with AM experts at Waterloo U it was identified that there were no physical limitations preventing continuous updating of process parameters on an Arcam EBM machine. There were, however, software and training limitations on how to achieve this in practice. The implication is that there may be unknown limitations of the AM machine or the physics of the manufacturing process that prevent a truly continuous functional grading. To verify this assumption more testing is required.

Secondly, it was assumed that the material data gathered from the literature could be linked across the PSPP framework. This assumption was necessary to permit any analysis or development of a model due to the lack of available data. It is likely that real specimens tested in the lab for various alpha lath sizes from the same batch of material on a single AM machine will result in crack initiation and crack growth data different from what could be interpreted from the literature. The initial assumptions about harder and softer materials should, however, hold true since they are based on conventional knowledge on fatigue of metals and were supported by estimating the impact of Hall-Petch, material hardness, strain-life, and crack growth on the total fatigue life of E-PBF Ti-6Al-4V. Nonetheless the strain-life and crack growth data for the HARD and SOFT materials are not linked directly or supported by experimentation. Results should therefore be interpreted as potential improvements in total fatigue life rather than specific magnitudes of improvement.

A remaining critical assumption is that the functionally graded crack growth curve defined by the potential function accurately describes the responses of the graded material. When the material is graded using a potential function it is an interpolation that has not been

verified by testing of graded specimens. It is plausible that the rate of change of the potential function may reveal interaction effects at the microstructural level of the material. One example could be that when a grading with an aggressive rate is applied the crack is deflected as it approaches the change in material properties. This effect in fatigue specimens has been shown when a notch is present at some distance and angle to the current path of the crack. In these cases the crack will tend to deflect towards the notch as it is the nearest location of a stress concentration. This effect might also be experienced when an abrupt change in material properties from a grading is applied. Depending on how the material is graded, crack deflection could either improve or diminish the total life of a specimen. There may also exist a leading or lagging of crack growth in an actual material from what would be interpolated directly using the potential function. In this case, an empirical fit might be required to adjust the crack growth rate to improve the relationship between the potential function mapping and the performance of an actual specimen. These observations justify the need for further research using a single AM machine and batch of material to gather all data as inputs into the model and link the parts of the PSPP framework.

5.4. Application of Fatigue Model to Other Cases

The applied loading will be linked to the estimate of total fatigue life for a component. All variables remaining the same, a fully reversed loading would likely decrease the total fatigue life of any component, graded or not. Additionally, the application of a variable amplitude loading, which would most likely represent actual loading experienced during the life of a component, would require an optimization of the functional grading targeting a specific range of cycles identified by rainflow-counting. It is argued that this is a problem of optimization that could still be accounted for using the model developed in this thesis. The model applies conventional fatigue analysis except in the definition of the functional grading with a potential function. If stress effects are accounted for in the input data and the method of calculation does not change then the model can still be used.

The selection of a single geometry can be viewed similarly. The most significant impact of the selection of a is in determining the geometry parameter used to calculate the stress intensity. Although the Matlab application presents a graphic of the selected specimen, any specimen geometry can be used if there is a known solution for the geometry parameter. This limits applicability of the Matlab application, as currently developed, to simplified geometries. It is argued, however, that this is a common engineering practice in conventional fatigue analysis. If there is the desire to extend modelling of components of greater geometric complexity then finding a solution for a specific geometry could be completed by FEA, although this goes somewhat against the original intent of avoiding FEA. In this context, since the results could be reusable, this may be a desirable trade-off. The current model does, however, allow optimization studies to be completed on the effects of geometry like increasing the material thickness or increasing the specimen width to allow more room for crack growth. These studies were not undertaken in this work as a single potential function was applied, although they could also have been analyzed.

For this study, only one potential function was selected based on an intuitive understanding of the factors affecting fatigue using the given geometry. There is nothing in the fatigue model preventing analysis using a different curve as potential functions are

normalized and only require consistent start and end points for grading. This provides opportunities for studies into optimization of FGMs by optimization of the potential function for a given geometry, material, and loads. In many cases no alteration of the developed model is required, only different inputs.

In this work, the goal was to design a functional grading to improve the fatigue life of a representative component. This was achieved either by locally specifying the material hardness within the component or by varying the material composition. In the example changing material composition using DED, a secondary consequence is a change in the material stiffness; Ti-6Al-4V is stiffer than 7075-T6. This mismatch in stiffness could result in damage to the surrounding aluminum structure if the component were to be manufactured of only Ti-6Al-4V. To mitigate the impacts of a mismatch in stiffness, Ti-6Al-4V was only graded close to the hole. This results in a component that is likely similar in stiffness to the adjacent aluminum structure while still improving the fatigue life of the component. A similar approach could be used to enhance properties of a material and achieve a different design goal than extending fatigue life. One example would be to locally define the stiffness of a material to either prevent exceedance of a maximum deflection of a component feature or to locally tune the deflection to achieve a desired deflection of the component. In this example, the potential function would be optimized according to material stiffness instead of for crack growth rate.

On the hypothesis that crack growth can be controlled by deflection of the crack through manipulation of local material properties, there is the possibility for further improvements in fatigue life by functional grading. For many simple geometries the crack path is known because the stress concentration is well understood. In these cases, functional grading in the region of the crack path could increase the travel distance by deflecting the crack. This would permit the crack to grow longer without a reduction in net section yielding, effectively reducing the crack growth rate. Mathematically, crack growth curves could be adjusted according to an effective crack growth rate and analysis of the FGM could still be completed using the developed model.

6. Future Work

There are several upgrades that can be made to the Total Fatigue Life Analysis application. Currently, the model only supports one geometry and potential function, a decision that was made to reduce development time in support of this thesis. However, many solutions for the geometry parameter and stress concentration are available, which could permit expansion of the application for other common two-dimensional geometries. Additionally, the potential function was input as an equation in the program back-end and not made available to the user. While it is possible this could be implemented in the current user interface the programming required to accept and check all input equations would be significant. A better option would be to provide an interactive potential function curve whereby users drag a set of points on a graph connected by a spline to create any desirable potential function. The data could then be interpolated for values of the potential function. Since the values are normalized the live updating of the potential function could be linked to a coloured image, like the one presented in Figure 26, providing intuitive feedback to the user on the selected grading.

The developed Total Fatigue Life Analysis application was limited to accepting only constant amplitude loading. This restriction reduces the applicability of results outside many real-world applications. Implementing a way to accept a loading spectrum and to conduct rainflow counting is feasible but unnecessary as numerous available rainflow counting solutions exist. What would be preferable is to allow a user to input the rainflow-counted cycles as this would significantly reduce the application programming requirements. The user can then run simulations of different potential functions to best improve total fatigue life.

A task requiring significant effort would be to permit an analysis of three-dimensional crack growth using a three-dimensional potential function. From a programming standpoint using Matlab, it would be relatively straightforward. The greater challenge would be to verify that the potential functions and resultant crack growth rates in two crack growth directions match those determined by experiment.

Finally, there are future material optimizations that could be made. If indeed the model can predict improvements in fatigue life from functional grading, then a foreseeable improvement would be to improve a component by both topology optimization and voxel level material control, simultaneously. This would take advantage of the afforded complexity of additive manufacturing in tailoring both the location specific geometry and material properties. Significant research would have to be completed to understand how to optimize the balance between removal of material or optimization of material properties to meet a desired design goal.

7. Conclusions

From the effort required to link process-structure-properties-performance, it is concluded that investment in a repository of additive manufacturing material data from tested samples would be beneficial to the international community of engineers and designers applying AM. A source like the Metallic Materials Properties Development and Standardization (MMPDS) developed by the FAA, but for additive manufactured materials at various process settings, would limit reliance on manual extraction of data from the literature and provide standardization in how the data is obtained and analyzed. This coincides with the efforts by the ASTM Committee F42 on Additive Manufacturing Technologies in trying to standardize the industry. In doing so, improvements in estimated fatigue life from the developed model could be realized as the reliability of input information would be verified.

A custom specimen was designed to model a common feature found in aerospace components. Using the developed fatigue life model it was estimated that the crack growth life of a custom specimen under constant amplitude cyclic load, a stress ratio of R = 0.1, and a grading of E-PBF Ti-6Al-4V crack growth rates defined by the potential function of $P = 10^{-9L}$ could be increased by 3% at a maximum gross stress of 400 MPa, by 18% at a maximum gross stress of 350 MPa, by 46% at a maximum gross stress of 300 MPa, by 93% at a maximum gross stress of 250 MPa, and by 138% at a maximum gross stress of 200 MPa. The predicted improvements in fatigue crack growth life were achieved by strengthening the material in the region of a stress concentration, with material of small alpha lath size, and specifying an increasing alpha lath size away from the notch to reduce crack growth once a crack is initiated. The estimated values are based on assumptions about material properties found in the literature and interpolation of crack growth rates between two graded materials.

The developed fatigue model was also used to analyze the same custom specimen under a constant amplitude loading, a stress ratio of R = 0.1, and a grading between Ti-6Al-4V and 7075-T6 materials defined by the potential function $P = 10^{-9L}$ using DED. The engineered specimen was compared to an ungraded 7075-T6 to mimic installation of a replacement component. It was estimated that the total fatigue life could be increased by approximately two to three orders of magnitude for a range of maximum gross stresses between 100-300 MPa. This was achieved by strengthening the hole in the specimen with the much stronger Ti-6Al-4V material and grading to the 7075-T6 material away from the hole. Applying this strategy, the original component could be replaced by the engineered component with comparable stiffness, hardness, and static strength. The estimated values assume that E-PBF Ti-6Al-4V material properties and conventional 7075-T6 properties are like those achieved by DED AM.

References

[1] NIINO, M., HIRAI, T., and WATANABE, R. “Functionally Gradient Materials. In Pursuit of Super Heat Resisting Materials for Spacecraft.” *Journal of the Japan Society for Composite Materials*, Vol. 13, No. 6, 1987, pp. 257–264. https://doi.org/10.6089/JSCM.13.257.

[2] Hartford Civic Center | Failure Case Studies. https://eng-resources.charlotte.edu/failurecasestudies/building-failure-cases/hartford-civic-center/. Accessed Mar. 17, 2023.

[3] Ashirbekov, A., Abilgaziyev, A., Kurokawa, S., and Hazrat Ali, Md. “(PDF) MODELLING OF FUNCTIONALLY GRADED MATERIALS USING THERMAL LOADS.”

[4] Canada. Department of National Defence., Canada. Royal Canadian Air Force., and Canadian Forces Aerospace Warfare Centre. “Royal Canadian Air Force Doctrine.” 2016, p. 62.

[5] ISO - ISO/ASTM 52900:2021 - Additive Manufacturing — General Principles — Fundamentals and Vocabulary. https://www.iso.org/standard/74514.html. Accessed Feb. 20, 2023.

[6] Committee F42 on Additive Manufacturing Technologies. https://www.astm.org/get-involved/technical-committees/committee-f42. Accessed Mar. 6, 2023.

[7] EBM Technology | GE Additive. https://www.ge.com/additive/ebm. Accessed Mar. 8, 2023.

[8] File:Arcam A2.Jpg - Wikimedia Commons. https://commons.wikimedia.org/wiki/File:Arcam_A2.jpg. Accessed Mar. 7, 2023.

[9] WebPlotDigitizer - Extract Data from Plots, Images, and Maps. https://automeris.io/WebPlotDigitizer/. Accessed Dec. 11, 2022.

[10] Kirchner, A., Klöden, B., Luft, J., Weißgärber, T., and Kieback, B. “Process Window for Electron Beam Melting of Ti-6Al-4V.” *https://doi.org/10.1179/0032589915Z.000000000244*, Vol. 58, No. 4, 2015, pp. 246–249. https://doi.org/10.1179/0032589915Z.000000000244.

[11] Pobel, C. R., Arnold, C., Osmanlic, F., Fu, Z., and Körner, C. “Immediate Development of Processing Windows for Selective Electron Beam Melting Using Layerwise Monitoring via Backscattered Electron Detection.” *Materials Letters*, Vol. 249, 2019. https://doi.org/10.1016/j.matlet.2019.03.048.

[12] Expansion of the Capability of SEBM by Improved Electron Beam Technology › Chair of Materials Science and Engineering for Metals. https://www.wtm.tf.fau.eu/forschung/additive-fertigung/expansion-of-the-capability-of-sebm-by-improved-electron-beam-technology/. Accessed Mar. 8, 2023.

[13] Scharowsky, T., Juechter, V., Singer, R. F., and Körner, C. “Influence of the Scanning Strategy on the Microstructure and Mechanical Properties in Selective Electron Beam Melting of Ti–6Al–4V.” *Advanced Engineering Materials*, Vol. 17, No. 11, 2015, pp. 1573–1578. https://doi.org/10.1002/ADEM.201400542.

[14] Image Analysis Software | Scientific Image Analysis | Processing. https://www.mipar.us/. Accessed Mar. 13, 2023.

[15] Sharma, H., Parfitt, D., Syed, A. K., Wimpenny, D., Muzangaza, E., Baxter, G., and Chen, B. “A Critical Evaluation of the Microstructural Gradient along the Build Direction in Electron Beam Melted Ti-6Al-4V Alloy.” 2018. https://doi.org/10.1016/j.msea.2018.12.016.

[16] Wanjara, P., Backman, D., Sikan, F., Gholipour, J., Amos, R., Patnaik, P., and Brochu, M. “Microstructure and Mechanical Properties of Ti-6Al-4V Additively Manufactured by Electron Beam Melting with 3D Part Nesting and Powder Reuse Influences.” *Journal of Manufacturing and Materials Processing 2022, Vol. 6, Page 21*, Vol. 6, No. 1, 2022, p. 21. https://doi.org/10.3390/JMMP6010021.

[17] Ran, J., Jiang, F., Sun, X., Chen, Z., Tian, C., and Zhao, H. “Microstructure and Mechanical Properties of Ti-6Al-4V Fabricated by Electron Beam Melting.” *Crystals 2020, Vol. 10, Page 972*, Vol. 10, No. 11, 2020, p. 972. https://doi.org/10.3390/CRYST10110972.

[18] Pasang, T., Tavlovich, B., Yannay, O., Jakson, B., Fry, M., Tao, Y., Turangi, C., Wang, J. C., Jiang, C. P., Sato, Y., Tsukamoto, M., and Misiolek, W. “Directionally-Dependent Mechanical Properties of Ti6Al4V Manufactured by Electron Beam Melting (EBM) and Selective Laser Melting (SLM).” *Materials (Basel, Switzerland)*, Vol. 14, No. 13, 2021. https://doi.org/10.3390/MA14133603.

[19] Koike, M., Greer, P., Owen, K., Lilly, G., Murr, L. E., Gaytan, S. M., Martinez, E., and Okabe, T. “Evaluation of Titanium Alloys Fabricated Using Rapid Prototyping Technologies-Electron Beam Melting and Laser Beam Melting.” *Materials*, Vol. 4, 2011, pp. 1776–1792. https://doi.org/10.3390/ma4101776.

[20] Edwards, P., O’Conner, A., and Ramulu, M. “Electron Beam Additive Manufacturing of Titanium Components: Properties and Performance.” *Journal of Manufacturing Science and Engineering*, Vol. 135, No. 6, 2013. https://doi.org/10.1115/1.4025773.

[21] Wysocki, B., Maj, P., Sitek, R., Buhagiar, J., Kurzydłowski, K. J., and Świeszkowski, W. “Laser and Electron Beam Additive Manufacturing Methods of Fabricating Titanium Bone Implants.” *Applied Sciences (Switzerland)*, Vol. 7, No. 7, 2017. https://doi.org/10.3390/app7070657.

[22] Zhai, Y., Galarraga, H., and Lados, D. A. “Microstructure, Static Properties, and Fatigue Crack Growth Mechanisms in Ti-6Al-4V Fabricated by Additive Manufacturing: LENS and EBM.” *Engineering Failure Analysis*, Vol. 69, 2016. https://doi.org/10.1016/j.engfailanal.2016.05.036.

[23] Rafi, H. K., Karthik, N. V, Gong, H., Starr, T. L., and Stucker, B. E. “Microstructures and Mechanical Properties of Ti6Al4V Parts Fabricated by Selective Laser Melting and Electron Beam Melting.” https://doi.org/10.1007/s11665-013-0658-0.

[24] Mohammadhosseini, A., Fraser, D., Masood, S. H., and Jahedi, M. Microstructure and Mechanical Properties of Ti-6Al-4V Manufactured by Electron Beam Melting Process. No. 17, 2013.

[25] Rafi, K. H., Starr, T. L., and Stucker, B. E. “Mechanical Property Evaluation of Ti-6Al-4V Parts Made Using Electron Beam Melting.”

[26] Syed, A. K., Awd, M., Walther, F., and Zhang, X. “Microstructure and Mechanical Properties of As-Built and Heat-Treated Electron Beam Melted Ti–6Al–4V.” *Materials Science and Technology (United Kingdom)*, Vol. 35, No. 6, 2019, pp. 653–660. https://doi.org/10.1080/02670836.2019.1580434.

[27] Zhao, X., Li, S., Zhang, M., Liu, Y., Sercombe, T. B., Wang, S., Hao, Y., Yang, R., and Murr, L. E. “Comparison of the Microstructures and Mechanical Properties of

Ti–6Al–4V Fabricated by Selective Laser Melting and Electron Beam Melting." *Materials & Design*, Vol. 95, 2016, pp. 21–31. https://doi.org/10.1016/J.MATDES.2015.12.135.

[28] Gong, H., Rafi, K., Gu, H., Ram, G. D. J., Starr, T., and Stucker, B. "Influence of Defects on Mechanical Properties of Ti-6Al-4 V Components Produced by Selective Laser Melting and Electron Beam Melting." 2015. https://doi.org/10.1016/j.matdes.2015.07.147.

[29] Camilleri, C., and Rochman, A. "Defect Formation in EBM Parts Built at Different Orienta-Tion." *Journal of Advances in Technology and Engineering Research JATER*, Vol. 2019, No. 3, 2019, pp. 125–134. https://doi.org/10.20474/jater-5.3.3.

[30] Bannantine, J. A., Comer, J. J., and Handrock, J. L. "Fundamentals of Metal Fatigue Analysis." 1990, p. 273.

[31] DTIC AD0227788: PROCEEDINGS OF THE SYMPOSIUM ON FATIGUE OF AIRCRAFT STRUCTURES, 11-13 AUGUST 1959 : Defense Technical Information Center : Free Download, Borrow, and Streaming : Internet Archive. https://archive.org/details/DTIC_AD0227788/page/n7/mode/2up. Accessed Feb. 27, 2023.

[32] Razavi, S. M. J., Van Hooreweder, B., and Berto, F. "Effect of Build Thickness and Geometry on Quasi-Static and Fatigue Behavior of Ti-6Al-4V Produced by Electron Beam Melting." *Additive Manufacturing*, Vol. 36, 2020, p. 101426. https://doi.org/10.1016/J.ADDMA.2020.101426.

[33] Haritos, G. K., Nicholas, T., and Lanning, D. B. "Notch Size Effects in HCF Behavior of Ti–6Al–4V." *International Journal of Fatigue*, Vol. 21, No. 7, 1999, pp. 643–652. https://doi.org/10.1016/S0142-1123(99)00023-7.

[34] Sun, T., Liu, Y., Li, S. J., and Li, J. P. "Effect of HIP Treatment on Fatigue Notch Sensitivity of Ti–6Al–4V Alloy Fabricated by Electron Beam Melting." *Acta Metallurgica Sinica (English Letters)*, Vol. 32, No. 7, 2019, pp. 869–875. https://doi.org/10.1007/S40195-018-0850-1.

[35] Kahlin, M., Ansell, H., and Moverare, J. J. "Fatigue Behaviour of Notched Additive Manufactured Ti6Al4V with As-Built Surfaces." *International Journal of Fatigue*, Vol. 101, 2017, pp. 51–60. https://doi.org/10.1016/J.IJFATIGUE.2017.04.009.

[36] Radlof, W., Benz, C., Heyer, H., and Sander, M. "Monotonic and Fatigue Behavior of EBM Manufactured Ti-6Al-4V Solid Samples: Experimental, Analytical and Numerical Investigations." *Materials 2020, Vol. 13, Page 4642*, Vol. 13, No. 20, 2020, p. 4642. https://doi.org/10.3390/MA13204642.

[37] Zhang, Y., Fang, X., Wang, H., Zong, R., Zhao, E., Han, J., Dong, Z., and Zhang, Z. "Microstructure and Low-Cycle Fatigue Performance of Selective Electron Beam Melted Ti6Al4V Alloy." *International Journal of Fatigue*, Vol. 163, 2022, p. 107017. https://doi.org/10.1016/J.IJFATIGUE.2022.107017.

[38] Zhang, Y., Chen, Z., Qu, S., Feng, A., Mi, G., Shen, J., Huang, X., and Chen, D. "Multiple Sub-Variants and Anisotropic Mechanical Properties of an Additively-Manufactured Ti-6Al-4V Alloy." *Journal of Materials Science & Technology*, Vol. 70, 2021, pp. 113–124. https://doi.org/10.1016/j.jmst.2020.06.039.

[39] Zhang, Y. L., Chen, Z., Qu, S. J., Feng, A. H., Mi, G. B., Shen, J., Huang, X., and Chen, D. L. "Microstructure and Cyclic Deformation Behavior of a 3D-Printed Ti–6Al–4V Alloy." *Journal of Alloys and Compounds*, Vol. 825, 2020, p. 153971. https://doi.org/10.1016/J.JALLCOM.2020.153971.

[40] Bai, C., Lan, L., Xin, R., Gao, S., and He, B. “Microstructure Evolution and Cyclic Deformation Behavior of Ti-6Al-4 V Alloy via Electron Beam Melting during Low Cycle Fatigue.” *International Journal of Fatigue*, Vol. 159, 2022, p. 106784. https://doi.org/10.1016/J.IJFATIGUE.2022.106784.

[41] Smith, R. A., and Miller, K. J. “Fatigue Cracks at Notches.” *International Journal of Mechanical Sciences*, Vol. 19, No. 1, 1977, pp. 11–22. https://doi.org/10.1016/0020-7403(77)90011-X.

[42] Galarraga, H., Warren, R. J., Lados, D. A., Dehoff, R. R., and Kirka, M. M. “Fatigue Crack Growth Mechanisms at the Microstructure Scale in As-Fabricated and Heat Treated Ti-6Al-4V ELI Manufactured by Electron Beam Melting (EBM).” 2017. https://doi.org/10.1016/j.engfracmech.2017.03.024.

[43] Seifi, M., Salem, A., Satko, D., Shaffer, J., and Lewandowski, J. J. “Defect Distribution and Microstructure Heterogeneity Effects on Fracture Resistance and Fatigue Behavior of EBM Ti–6Al–4V.” *International Journal of Fatigue*, Vol. 94, 2017, pp. 263–287. https://doi.org/10.1016/J.IJFATIGUE.2016.06.001.

[44] Draper, S., Lerch, B., Rogers, R., Martin, R., Locci, I., and Garg, A. “Materials Characterization of Electron Beam Melted Ti-6Al-4V.” *Proceedings of the 13th World Conference on Titanium*, 2016, pp. 1433–1440. https://doi.org/10.1002/9781119296126.CH242.

[45] Zhang, N., Khan, T., Guo, H., Shi, S., Zhong, W., and Zhang, W. “Functionally Graded Materials: An Overview of Stability, Buckling, and Free Vibration Analysis.” *Advances in Materials Science and Engineering*, Vol. 2019, 2019. https://doi.org/10.1155/2019/1354150.

[46] Liu, Z., Meyers, M. A., Zhang, Z., and Ritchie, R. O. “Functional Gradients and Heterogeneities in Biological Materials: Design Principles, Functions, and Bioinspired Applications.” *Progress in Materials Science*, Vol. 88, 2017, pp. 467–498. https://doi.org/10.1016/J.PMATSCI.2017.04.013.

[47] Foley, J. D., Van Dam, A., Feiner, S. K., and Hughes, J. F. *Computer Graphics: Principles and Practice*.

[48] Zhang, C., Chen, F., Huang, Z., Jia, M., Chen, G., Ye, Y., Lin, Y., Liu, W., Chen, B., Shen, Q., Zhang, L., and Lavernia, E. J. “Additive Manufacturing of Functionally Graded Materials: A Review.” *Materials Science and Engineering A*, Vol. 764, 2019. https://doi.org/10.1016/j.msea.2019.138209.

[49] Tyagi, S. A., and Manjaiah, M. “Laser Additive Manufacturing of Titanium-Based Functionally Graded Materials: A Review.” https://doi.org/10.1007/s11665-022-07149-w.

[50] El-Galy, I. M., Saleh, B. I., and Ahmed, M. H. “Functionally Graded Materials Classifications and Development Trends from Industrial Point of View.” *SN Applied Sciences 2019 1:11*, Vol. 1, No. 11, 2019, pp. 1–23. https://doi.org/10.1007/S42452-019-1413-4.

[51] Li, Y., Feng, Z., Hao, L., Huang, L., Xin, C., Wang, Y., Bilotti, E., Essa, K., Zhang, H., Li, Z., Yan, F., and Peijs, T. “A Review on Functionally Graded Materials and Structures via Additive Manufacturing: From Multi-Scale Design to Versatile Functional Properties.” *Advanced Materials Technologies*, Vol. 5, No. 6, 2020, p. 1900981. https://doi.org/10.1002/ADMT.201900981.

[52] Gupta, V., and Tandon, P. “Heterogeneous Object Modeling with Material Convolution Surfaces.” *Computer-Aided Design*, Vol. 62, 2015, pp. 236–247. https://doi.org/10.1016/J.CAD.2014.12.005.

[53] Saleh, B., Jiang, J., Fathi, R., Al-hababi, T., Xu, Q., Wang, L., Song, D., and Ma, A. “30 Years of Functionally Graded Materials: An Overview of Manufacturing Methods, Applications and Future Challenges.” *Composites Part B: Engineering*, Vol. 201, 2020, p. 108376. https://doi.org/10.1016/J.COMPOSITESB.2020.108376.

[54] Reichardt, A., Shapiro, A. A., Otis, R., Dillon, R. P., Borgonia, J. P., McEnerney, B. W., Hosemann, P., and Beese, A. M. “Advances in Additive Manufacturing of Metal-Based Functionally Graded Materials.” *https://doi.org/10.1080/09506608.2019.1709354*, Vol. 66, No. 1, 2020, pp. 1–29. https://doi.org/10.1080/09506608.2019.1709354.

[55] Yan, L., Chen, Y., and Liou, F. “Additive Manufacturing of Functionally Graded Metallic Materials Using Laser Metal Deposition.” *Additive Manufacturing*, Vol. 31, 2020, p. 100901. https://doi.org/10.1016/J.ADDMA.2019.100901.

[56] Ghanavati, R., and Naffakh-Moosavy, H. “Additive Manufacturing of Functionally Graded Metallic Materials: A Review of Experimental and Numerical Studies.” *Journal of Materials Research and Technology*, Vol. 13, 2021, pp. 1628–1664. https://doi.org/10.1016/J.JMRT.2021.05.022.

[57] Tyagi, S. A., and Manjaiah, M. “Laser Additive Manufacturing of Titanium-Based Functionally Graded Materials: A Review.” https://doi.org/10.1007/s11665-022-07149-w.

[58] Hasanov, S., Alkunte, S., Rajeshirke, M., Gupta, A., Huseynov, O., Fidan, I., Alifui-Segbaya, F., and Rennie, A. “Review on Additive Manufacturing of Multi-Material Parts: Progress and Challenges.” *Journal of Manufacturing and Materials Processing 2022, Vol. 6, Page 4*, Vol. 6, No. 1, 2021, p. 4. https://doi.org/10.3390/JMMP6010004.

[59] Popovich, V. A., Borisov, E. V., Sufiyarov, V. S., and Popovich, A. A. “Tailoring the Properties in Functionally Graded Alloy Inconel 718 Using Additive Technologies.” *Metal Science and Heat Treatment 2019 60:11*, Vol. 60, No. 11, 2019, pp. 701–709. https://doi.org/10.1007/S11041-019-00343-Z.

[60] Popovich, V. A., Borisov, E. V., Popovich, A. A., Sufiiarov, V. S., Masaylo, D. V., and Alzina, L. “Functionally Graded Inconel 718 Processed by Additive Manufacturing: Crystallographic Texture, Anisotropy of Microstructure and Mechanical Properties.” *Materials & Design*, Vol. 114, 2017, pp. 441–449. https://doi.org/10.1016/J.MATDES.2016.10.075.

[61] Ghorbanpour, S., Sahu, S., Deshmukh, K., Borisov, E., Riemslag, T., Reinton, E., Bertolo, V., Jiang, Q., Popovich, A., Shamshurin, A., Knezevic, M., and Popovich, V. “Effect of Microstructure Induced Anisotropy on Fatigue Behaviour of Functionally Graded Inconel 718 Fabricated by Additive Manufacturing.” *Materials Characterization*, Vol. 179, 2021, p. 111350. https://doi.org/10.1016/J.MATCHAR.2021.111350.

[62] Domack, M. S., and Baughman, J. M. “Development of Nickel-Titanium Graded Composition Components.” *Rapid Prototyping Journal*, Vol. 11, No. 1, 2005, pp. 41–51. https://doi.org/10.1108/13552540510573383/FULL/XML.

[63] Vamsi Krishna, B., Xue, W., Bose, S., and Bandyopadhyay, A. “Functionally Graded Co–Cr–Mo Coating on Ti–6Al–4V Alloy Structures.” *Acta Biomaterialia*, Vol. 4, No. 3, 2008, pp. 697–706. https://doi.org/10.1016/J.ACTBIO.2007.10.005.

[64] Shah, K. “Laser Direct Metal Deposition of Dissimilar and Functionally Graded Alloys.” 2011.

[65] Al-Bermani, S. S. “An Investigation into Microstructure and Microstructural Control of Additive Layer Manufactured Ti-6Al-4V by Electron Beam Melting.” 2011.
[66] Shishkovsky, I., Missemer, F., and Smurov, I. “Direct Metal Deposition of Functional Graded Structures in Ti- Al System.” *Physics Procedia*, Vol. 39, 2012, pp. 382–391. https://doi.org/10.1016/J.PHPRO.2012.10.052.
[67] Ren, H. S., Liu, D., Tang, H. B., Tian, X. J., Zhu, Y. Y., and Wang, H. M. “Microstructure and Mechanical Properties of a Graded Structural Material.” *Materials Science and Engineering: A*, Vol. 611, 2014, pp. 362–369. https://doi.org/10.1016/J.MSEA.2014.06.016.
[68] Zhang, J., Zhang, Y., Liou, F., Newkirk, J., Taminger, K. B., and Seufzer, W. “A Microstructure and Hardness Study of Functionally Graded Materials Ti6Al4V/TiC by Laser Metal Deposition.” *Proceedings of the 26th Annual International Solid Freeform Fabrication Symposium (2015, Austin, TX)*, 2015.
[69] Mahamood, R. M., and Akinlabi, E. T. “Laser Metal Deposition of Functionally Graded Ti6Al4V/TiC.” *Materials & Design*, Vol. 84, 2015, pp. 402–410. https://doi.org/10.1016/J.MATDES.2015.06.135.
[70] Ge, W., Lin, F., and Guo, C. “Functional Gradient Material of Ti-6Al-4V and γ-TiAl Fabricated by Electron Beam Selective Melting.” 2015.
[71] Sahasrabudhe, H., Harrison, R., Carpenter, C., and Bandyopadhyay, A. “Stainless Steel to Titanium Bimetallic Structure Using LENS™.” *Additive Manufacturing*, Vol. 5, 2015, pp. 1–8. https://doi.org/10.1016/J.ADDMA.2014.10.002.
[72] Tan, X., Kok, Y., Tan, Y. J., Descoins, M., Mangelinck, D., Tor, S. B., Leong, K. F., and Chua, C. K. “Graded Microstructure and Mechanical Properties of Additive Manufactured Ti–6Al–4V via Electron Beam Melting.” *Acta Materialia*, Vol. 97, 2015, pp. 1–16. https://doi.org/10.1016/J.ACTAMAT.2015.06.036.
[73] Reichardt, A., Dillon, R. P., Borgonia, J. P., Shapiro, A. A., McEnerney, B. W., Momose, T., and Hosemann, P. “Development and Characterization of Ti-6Al-4V to 304L Stainless Steel Gradient Components Fabricated with Laser Deposition Additive Manufacturing.” *Materials & Design*, Vol. 104, 2016, pp. 404–413. https://doi.org/10.1016/J.MATDES.2016.05.016.
[74] Bobbio, L. D., Otis, R. A., Borgonia, J. P., Dillon, R. P., Shapiro, A. A., Liu, Z. K., and Beese, A. M. “Additive Manufacturing of a Functionally Graded Material from Ti-6Al-4V to Invar: Experimental Characterization and Thermodynamic Calculations.” *Acta Materialia*, Vol. 127, 2017, pp. 133–142. https://doi.org/10.1016/J.ACTAMAT.2016.12.070.
[75] Li, W., Karnati, S., Kriewall, C., Liou, F., Newkirk, J., Brown Taminger, K. M., and Seufzer, W. J. “Fabrication and Characterization of a Functionally Graded Material from Ti-6Al-4V to SS316 by Laser Metal Deposition.” *Additive Manufacturing*, Vol. 14, 2017, pp. 95–104. https://doi.org/10.1016/J.ADDMA.2016.12.006.
[76] Li, L., Wang, J., Lin, P., and Liu, H. “Microstructure and Mechanical Properties of Functionally Graded TiCp/Ti6Al4V Composite Fabricated by Laser Melting Deposition.” *Ceramics International*, Vol. 43, No. 18, 2017, pp. 16638–16651. https://doi.org/10.1016/J.CERAMINT.2017.09.054.
[77] Liu, Y., Liu, C., Liu, W., Ma, Y., Zhang, C., Cai, Q., and Liu, B. “Microstructure and Properties of Ti/Al Lightweight Graded Material by Direct Laser Deposition.” *https://doi.org/10.1080/02670836.2017.1412042*, Vol. 34, No. 8, 2017, pp. 945–951. https://doi.org/10.1080/02670836.2017.1412042.

[78] Schneider-Maunoury, C., Weiss, L., Acquier, P., Boisselier, D., and Laheurte, P. “Functionally Graded Ti6Al4V-Mo Alloy Manufactured with DED-CLAD® Process.” *Additive Manufacturing*, Vol. 17, 2017, pp. 55–66. https://doi.org/10.1016/J.ADDMA.2017.07.008.

[79] Bobbio, L. D., Bocklund, B., Otis, R., Borgonia, J. P., Dillon, R. P., Shapiro, A. A., McEnerney, B., Liu, Z. K., and Beese, A. M. “Characterization of a Functionally Graded Material of Ti-6Al-4V to 304L Stainless Steel with an Intermediate V Section.” *Journal of Alloys and Compounds*, Vol. 742, 2018, pp. 1031–1036. https://doi.org/10.1016/J.JALLCOM.2018.01.156.

[80] Zhang, Y., and Bandyopadhyay, A. “Direct Fabrication of Compositionally Graded Ti-Al2O3 Multi-Material Structures Using Laser Engineered Net Shaping.” *Additive Manufacturing*, Vol. 21, 2018, pp. 104–111. https://doi.org/10.1016/J.ADDMA.2018.03.001.

[81] Yang, J., Yang, H., Yu, H., Wang, Z., Wang, H., and Zeng, X. “A Novel Approach to In-Situ Fabricate Ti-6Al-4V Alloy with Graded Microstructure and Property by Selective Laser Melting.” *Materials Letters*, Vol. 215, 2018, pp. 246–249. https://doi.org/10.1016/J.MATLET.2017.12.098.

[82] Narra, S. P., Cunningham, R., Beuth, J., and Rollett, A. D. “Location Specific Solidification Microstructure Control in Electron Beam Melting of Ti-6Al-4V.” *Additive Manufacturing*, Vol. 19, 2018, pp. 160–166. https://doi.org/10.1016/J.ADDMA.2017.10.003.

[83] Adomako, N. K., Noh, S., Oh, C. S., Yang, S., and Kim, J. H. “Laser Deposition Additive Manufacturing of 17-4PH Stainless Steel on Ti-6Al-4V Using V Interlayer.” *http://mc.manuscriptcentral.com/tmrl*, Vol. 7, No. 7, 2019, pp. 259–266. https://doi.org/10.1080/21663831.2019.1596989.

[84] Meng, W., Zhang, W., Zhang, W., Yin, X., Guo, L., and Cui, B. “Additive Fabrication of 316L/Inconel625/Ti6Al4V Functionally Graded Materials by Laser Synchronous Preheating.” *International Journal of Advanced Manufacturing Technology*, Vol. 104, Nos. 5–8, 2019, pp. 2525–2538. https://doi.org/10.1007/S00170-019-04061-X/METRICS.

[85] Meng, W., Xiaohui, Y., Zhang, W., Junfei, F., Lijie, G., Qunshuang, M., and Bing, C. “Additive Manufacturing of a Functionally Graded Material from Inconel625 to Ti6Al4V by Laser Synchronous Preheating.” *Journal of Materials Processing Technology*, Vol. 275, 2020, p. 116368. https://doi.org/10.1016/J.JMATPROTEC.2019.116368.

[86] Ji, S., Sun, Z., Zhang, W., Chen, X., Xie, G., and Chang, H. “Microstructural Evolution and High Temperature Resistance of Functionally Graded Material Ti-6Al-4V/Inconel 718 Coated by Directed Energy Deposition-Laser.” *Journal of Alloys and Compounds*, Vol. 848, 2020, p. 156255. https://doi.org/10.1016/J.JALLCOM.2020.156255.

[87] Zhao, K., Zhang, G., Ma, G., Shen, C., and Wu, D. “Microstructure and Mechanical Properties of Titanium Alloy / Zirconia Functionally Graded Materials Prepared by Laser Additive Manufacturing.” *Journal of Manufacturing Processes*, Vol. 56, 2020, pp. 616–622. https://doi.org/10.1016/J.JMAPRO.2020.05.044.

[88] Hsu, T. I., Jhong, Y. T., and Tsai, M. H. “Effect of Gradient Energy Density on the Microstructure and Mechanical Properties of Ti6Al4V Fabricated by Selective Electron Beam Additive Manufacture.” *Materials (Basel, Switzerland)*, Vol. 13, No. 7, 2020. https://doi.org/10.3390/MA13071509.

[89] Geng, Y. “Microstructural Functionally Graded Ti-6Al-4V via Advanced Laser-Based Technologies Laser Surface Modification of Ti6Al4V View Project NUI Galway Final Year Project (Undergraduate) View Project.”
[90] Zhai, W., Wang, P., Ng, F. L., Zhou, W., Nai, S. M. L., and Wei, J. “Hybrid Manufacturing of γ-TiAl and Ti–6Al–4V Bimetal Component with Enhanced Strength Using Electron Beam Melting.” *Composites Part B: Engineering*, Vol. 207, 2021, p. 108587. https://doi.org/10.1016/J.COMPOSITESB.2020.108587.
[91] Han, J., Lu, L., Xin, Y., Chen, X., Zhang, G., Cai, Y., and Tian, Y. “Microstructure and Mechanical Properties of a Novel Functionally Graded Material from Ti6Al4V to Inconel 625 Fabricated by Dual Wire + Arc Additive Manufacturing.” *Journal of Alloys and Compounds*, Vol. 903, 2022, p. 163981. https://doi.org/10.1016/J.JALLCOM.2022.163981.
[92] AFGROW (Air Force Growth) Fracture Mechanics and Fatigue Crack Growth Analysis Software - Home Page. https://www.afgrow.net/. Accessed Mar. 7, 2023.
[93] Ansys Mechanical | Structural FEA Analysis Software. https://www.ansys.com/products/structures/ansys-mechanical. Accessed Mar. 7, 2023.
[94] AFGROW History. https://www.afgrow.net/about/history.aspx. Accessed Mar. 12, 2023.
[95] Ansys Inc. “White Paper / SMART Fracture.” 2020.
[96] Birman, V., and Byrd, L. W. “Modeling and Analysis of Functionally Graded Materials and Structures.” *Applied Mechanics Reviews*, Vol. 60, No. 5, 2007, pp. 195–216. https://doi.org/10.1115/1.2777164.
[97] Kanu, N. J., Vates, U. K., Singh, G. K., and Chavan, S. “Fracture Problems, Vibration, Buckling, and Bending Analyses of Functionally Graded Materials: A State-of-the-Art Review Including Smart FGMS.” *https://doi.org/10.1080/02726351.2017.1410265*, Vol. 37, No. 5, 2018, pp. 579–604. https://doi.org/10.1080/02726351.2017.1410265.
[98] Mo Es, N., Dolbow, J., and Belytschko, T. “A FINITE ELEMENT METHOD FOR CRACK GROWTH WITHOUT REMESHING.”
[99] Verma, R., Kumar, P., Jayaganthan, R., and Pathak, H. “Extended Finite Element Simulation on Tensile, Fracture Toughness and Fatigue Crack Growth Behaviour of Additively Manufactured Ti6Al4V Alloy.” *Theoretical and Applied Fracture Mechanics*, Vol. 117, 2022, p. 103163. https://doi.org/10.1016/J.TAFMEC.2021.103163.
[100] Standard Test Methods for Tension Testing of Metallic Materials. https://www.astm.org/e0008_e0008m-22.html. Accessed Apr. 2, 2023.
[101] Standard Test Method for Strain-Controlled Fatigue Testing. https://www.astm.org/e0606_e0606m-21.html. Accessed Apr. 2, 2023.
[102] Dass, A., and Moridi, A. “State of the Art in Directed Energy Deposition: From Additive Manufacturing to Materials Design.” *Coatings 2019, Vol. 9, Page 418*, Vol. 9, No. 7, 2019, p. 418. https://doi.org/10.3390/COATINGS9070418.
[103] Takase, A., Ishimoto, T., Morita, N., Ikeo, N., and Nakano, T. “Comparison of Phase Characteristics and Residual Stresses in Ti-6Al-4V Alloy Manufactured by Laser Powder Bed Fusion (L-PBF) and Electron Beam Powder Bed Fusion (EB-PBF) Techniques.” *Crystals 2021, Vol. 11, Page 796*, Vol. 11, No. 7, 2021, p. 796. https://doi.org/10.3390/CRYST11070796.
[104] Pilkey, W. D., and Pilkey, D. F. *Peterson’s Stress Concentration Factors*. 2008.

[105] Lampman, S. R. “ASM Handbook: Volume 19, Fatigue and Fracture.” *ASM International*, Vol. 19, No. 9, 1996, pp. 557–565.
[106] Tammas-Williams, S., Zhao, H., Léonard, F., Derguti, F., Todd, I., and Prangnell, P. B. “XCT Analysis of the Influence of Melt Strategies on Defect Population in Ti–6Al–4V Components Manufactured by Selective Electron Beam Melting.” *Materials Characterization*, Vol. 102, 2015, pp. 47–61. https://doi.org/10.1016/J.MATCHAR.2015.02.008.
[107] Use Goal Seek to Find the Result You Want by Adjusting an Input Value - Microsoft Support. https://support.microsoft.com/en-us/office/use-goal-seek-to-find-the-result-you-want-by-adjusting-an-input-value-320cb99e-f4a4-417f-b1c3-4f369d6e66c7. Accessed Mar. 12, 2023.
[108] Database of Additive Manufacturing Machines & Materials | Senvol. http://senvol.com/database/. Accessed Mar. 30, 2023.
[109] AFMAT – Fracture Mechanics Database. https://www.afgrow.net/afmat.aspx. Accessed Mar. 30, 2023.